Allman

SE-PB-84-058

RAFT RIVER FRACTURE CHARACTERIZATION AND RESERVOIR SIMULATION

J. D. Miller
D. W. Allman
D. Wulf

Earth and Life Sciences Branch
Geosciences Section

TABLE OF CONTENTS

FIGURES

EXECUTIVE SUMMARY

RAFT RIVER FRACTURE CHARACTERIZATION AND RESERVOIR SIMULATION

TABLES

EXECUTIVE SUMMARY
RAFT RIVER FRACTURE CHARACTERIZATION AND RESERVOIR SIMULATION

Raft River Well RRGP-5BF was tested in September through November of 1982 as part of an effort to develop and refine new techniques for reservoir analysis when simultaneous injection and production are planned. The use of tracers in single well injection and recovery tests is an integral part of the technique under study. The Raft River Geothermal Field was selected as the site for the initial field testing in this program because the field was immediately available with excellent facilities and because the moderate formation temperatures provided an ideal testing environment. The Raft River Reservoir is highly fractured and it is a program objective to develop techniques for fractured reservoir analysis.

During the interim since the tests were completed, a significant effort has been expended in developing analytic, physical and numerical methods for analyzing flow and dispersion in fractured media. The initial objective of this effort is to correlate the data collected in the Raft River tests. The FY-84 physical model development work is presented in a separate report. This document presents the numerical modeling work and the fracture characterization research conducted to provide the required description of fractured media characteristics. The characterization work consisted of a survey of generic fracture literature, an analysis of borehole data leading to a partial description of the local fracture system and the synthesis of a stochastic fracture system in the vicinity of the borehole. The numerical modeling effort involved the development of a fractured media simulation code, the evolution of two numerical models and a scoping analysis using one of the models.

The generic fracture characterization study included the complete range of scale from microcracks to major faults. The distinction was made between the three categories of void space which together represent all of the water in a fractured formation. The first, flow porosity, is the void space in which flow is the dominant transport mechanism. The second, diffusion porosity, include voids and small channels in which molecular diffusion is the dominant process. The third, residual porosity, includes the isolated voids which do not communicate with the others and are therefore not of interest.

The need for an understanding of the nature of a fracture system in terms of its geologic evolution is clear from the literature and from the existence of fracture patterns. The genesis of a fractured formation may include pluton emplacement and crystallization, tectonic cycles resulting in folding, fracturing and faulting and, finally, mineral and chemical alteration.

The geometric fracture characteristics described in detail include orientation, persistence (length), spacing and aperture.

Fracture orientation is measured from surface outcrops or from boreholes or tunnels. A statistically significant number of fractures and a variety of orientations of boreholes or exposed surfaces is desirable. A correction is available for the effect of non-random borehole orientations on the number of fractures of a given orientation. Bivariate normal and spherical normal distributions have been used to describe orientation sets. There are usually three or four and as many as six orientation sets in a rock mass.

The persistence or length of discontinuities has been defined using log normal, exponential and power law distributions. The effect of censored (one or both ends not visible) and truncated (small fractures not observed) data must be considered in developing length distributions.

The spacing of fractures within an orientation set has been observed to conform to negative exponential and log normal frequency distributions.

Fracture apertures are poorly defined because of spatial and stress induced variations. Microfracture apertures have been quantified using scanning electron microscopes.

Fractures are frequently partially or completely filled with minerals which affect the permeability, porosity and chemical reactions between fluids and the host rock. The minerology can be used to correlate fractures and to help determine emplacement and tectonic history.

Flow through individual fractures has been shown to be a function of normal stress, shear stress and fracture surface characteristics. Effective aperture is commonly measured in terms of a measured flow which is proportional to the

cube of the effective aperture. The effect of variation of aperture in the transverse direction has been studied in the laboratory.

The Raft River characterization included driller's logs, borehole geophysical logs including acoustic televiewer surveys and borehole logging conducted during the test series. This data was analyzed to determine fracture orientation, spacing, correlation with producing/receiving zones and apertures.

Figure 1 shows the geology of the Raft River KGRA and sectional view of the wells in the field. Test well RRGP-5BF had a long and involved completion history. An initial leg produced 1000 gpm of fluid at 275°F. Drilling continued in an effort to locate a higher temperature aquifer. The drill stem twisted off and the leg was completed with salt and cement. Leg B was drilled at an offset and was cased to a depth below the major aquifer in leg A. The well was hydrofractured and propped with sand. Figure 2 shows a completion drawing.

An acoustic televiewer survey was made by the United States Geological Survey for a 495 foot borehole interval prior to well completion. A second survey was made of the production interval after the liner was installed and the well was hydrofractured. There were no discernible differences in the common interval attributable to the hydrofracture. The log providing the highest quality data was used in the open interval and the precompletion log was used to provide additional data for the upper interval.

Only 35 well-defined discontinuities and 12 additional apparent discontinuities were observed. The well-defined discontinuities were grouped into five orientation sets based on the stereonet contouring shown in Figure 3. This is a southern hemisphere projection in which a normal to the fracture plane is extended until it pierces the surface of the hemisphere. The fracture is represented by that point. The data was corrected for magnetic declination, borehole inclination and, using the Terzaghi correction, for orientation frequency.

Sets 2, 4 and 5 form a band on the stereonet where the strike is approximately N9°W. The dip ranges along this band from 75°W to 36°NE, assuring that these discontinuities will intersect. Sets 1 and 3 bracket set 2.

Figure 4 is a vertical profile showing the lithologic log, the fracture orientation, the discontinuity density and the cumulative discontinuity occurrence. The strike (azimuth of the intersection of the fracture plane with a horizontal plane) is indicated by the lateral position on the scale and the dip (steepest angle between the horizontal plane and the fracture plane) by the inclination from the horizontal of the tail.

After grouping the very closely spaced discontinuities of common orientation as a single feature, the borehole separations for the various sets were evaluated as follows:

Set	Maximum Density		Number	Separation Along Borehole - ft		
	Strike	Dip		logarithm of mean	logarithm of std dev	mean distance
1	N46°E	74°NW	6	1.768	.481	58.6
2	N	77°W	10	1.674	.298	47.2
3	N46°W	78°SW	5	2.154	.332	142.6
4	N5°W	18°W	12	2.137	.340	137.1
5	N23°W	41°E	2	-	-	319.

Apparent apertures, those inferred from the acoustic televiewer log, were classified in 0.5 inch intervals. The majority of apparent apertures range in width from 0.5 to 1.5 inch. Effective aperture, or even the existence of permeability, is much more difficult to determine. Figure 5 shows a correlation between the discontinuity locations and the production zones as shown by the spinner log. Within the resolution of the spinner log, all of the observed discontinuities appear to be flowing.

Computer models implementing these characteristics were developed using the FRACSL (FRactured media - Advanced Continuous Simulation Language) reservoir simulation code. This code has been developed at EG&G to specifically address flow and dispersion in fractured media. Mathematical models of the flow and dispersion processes have been developed and coded using algebraic and first order differential equations. The commercial ACSL software supplies the utilities to implement the model, namely input, integration, interpolation, output, etc. Integration has been accomplished using the Gear stiff system algorithm, which is extremely efficient for those systems having a wide range of eigenvalues

or characteristic frequencies. Another capability used extensively is a direct steady state by Newton-Raphson iteration rather than integration.

FRACSL is a two-dimensional simulation of isothermal flow and solute transport in fractured porous media. Fractures are superimposed on the edges or diagonals of rectangular matrix blocks. Nodes are defined at the intersection of vertical and horizontal grid lines. Head is calculated at the grid nodes based on the matrix and fracture flows and using the conservation of mass relationship. A continuative boundary condition "continues" the fracture or matrix flow at the same conductivity through a specified distance to a zero head point.

After the matrix and fracture velocity distribution is found, the transport of solute is simulated by moving imaginary marker particles, each tagged with a mass of tracer. The particles are moved under the influence of the local velocity and the random movements due to molecular diffusion. A random dispersive movement is added to particle motion in the matrix.

Two FRACSL models of the reservoir near RRGP-5BF have been developed. The smaller of the two is a vertical section centered on the hydrofracture and extending in an approximate E-W direction. This model is 189 feet high by 77 feet wide and includes the hydrofracture, the fractures observed in the production interval and the major aquifer observed in leg A of the well. The second model is 500 feet high by 500 feet wide, similarly located, and includes a stochastic fracture system synthesized on the basis of the fracture characterization studies.

The orientation of the two models is parallel to the band shown on the stereonet for fractures with a strike of N9°W. This model plane therefore displays the intersections of the three fracture sets in the band. The other two fracture sets bracket this band and have the same apparent 79°W dip as set 2 which lies in the band.

The effective thickness of the area modeled must be chosen in order to determine the average flow rate across the thickness. This value is then used as the input from the well to the one foot thick "typical section" modeled. The effective thickness requires an approximation to the fracture distribution in the third dimension. The effect of flow into the thickness dimension cannot

be included in this simulation, but tends to be small because of the selected model orientation. Effective thicknesses of 160 and 263 feet were chosen for the small and large models, respectively.

Simulation was conducted with the smaller model in an attempt to scope the range of effective apertures in the fracture system. The actual fracture system and the computer approximations are shown in Figures 6 and 7, respectively. The locations of the various fractures are those given by the acoustic televiewer. Each is assumed to extend to the model boundaries. The apertures of the hydrofracture and the upper aquifer fracture were set at .025 feet since the maximum apparent hydrofracture aperture was given as .05 feet. The apertures of the other fractures were adjusted to match the flow distribution given by the spinner log. The resulting values, moving down from the bottom of the well liner are .0095, .0095, .018, .018 and .025 feet. The distance to the zero head remote boundary was arbitrarily chosen as 1000 feet. The resulting head at the injection node, corresponding to 150 gpm injection, was .036 feet. This is approximately 3 orders of magnitude lower than the measured value of 49 feet, after allowing for turbulent losses which are not modeled.

The selection of the distance to the remote boundary only affects the computed head by about a factor of three. A second case was therefore run to address the more sensitive aperture parameter. A reduction of all apertures by a factor of 10 yielded a head at the injection mode of 34.6 feet. These apertures are apparently closer to those expected in the real aquifer.

A final simulation performed with this model was an attempt to match the transient pressure response correlated in a series of withdrawal tests at a range of flow rates. A specific storage value of 1.E-7 per foot, which is reasonable in view of data in the literature, was found to give the best match.

The fracture system for the 500 feet by 500 feet model was synthesized using the method given by Andersson (1984). The procedure incorporates the following elements as applied independently to each of the five fracture sets:

1) Fracture traces lie on infinite lines at equally probable locations on a scanline through the center of the model. Each of these lines has a dip equal to the mean of the appropriate set.

2) Length is selected from a log normal distribution with a mean equal to 3.5 times the mean perpendicular spacing as determined from the borehole survey. A range of 3-4 for this factor was given by Gale (1982).
3) The center of the fracture is equally probable over the interval encompassing all fractures of the specified length which intersect the model.
4) Fractures are synthesized until the total number intersecting the scanline corresponds to the mean spacing measured in the RRGP-5 borehole.

A total of 15 fractures were synthesized for set 4 and 5 fractures for set 5. A total of 778 fractures were synthesized for sets 1, 2 and 3 combined. Figure 8 shows the synthesized system with only the largest of the fractures from sets 1, 2 and 3 shown. The vertical has been rotated 11°CW to align the steeply dipping fractures from sets 1, 2 and 3 with the model principal axes. Figure 9 shows the computer version of this model with the set 1, 2 and 3 fractures collected laterally into columns.

While successful steady state flow and marker particle dispersion runs were made, the analysis was not completed.

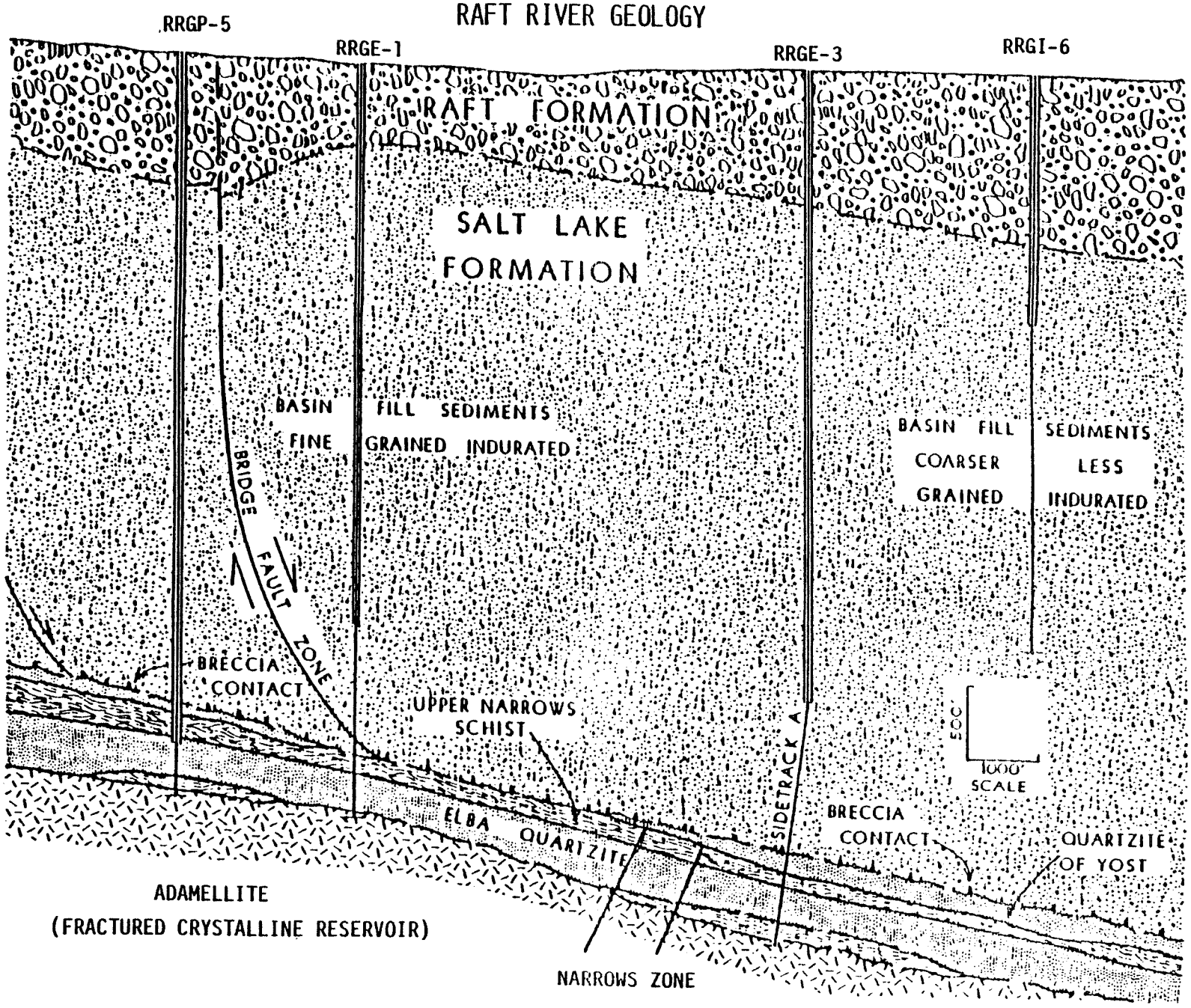
RAFT RIVER GEOLOGY
RRGP-5
RRGE-1
RRGE-3
RRGI-6
RAFT FORMATION
SALT LAKE FORMATION
BASIN FILL SEDIMENTS
FINE GRAINED INDURATED
BASIN FILL
COARSER GRAINED
SEDIMENTS
LESS INDURATED
BRIDGE FAULT ZONE
BRECCIA CONTACT
UPPER NARROWS SCHIST
SIDETRACK A
500'
1000'
SCALE
BRECCIA CONTACT
QUARTZITE OF YOST
ELBA QUARTZITE
ADAMELLITE
(FRACTURED CRYSTALLINE RESERVOIR)
NARROWS ZONE

FIGURE 1

RRGP-5BF Well Construction

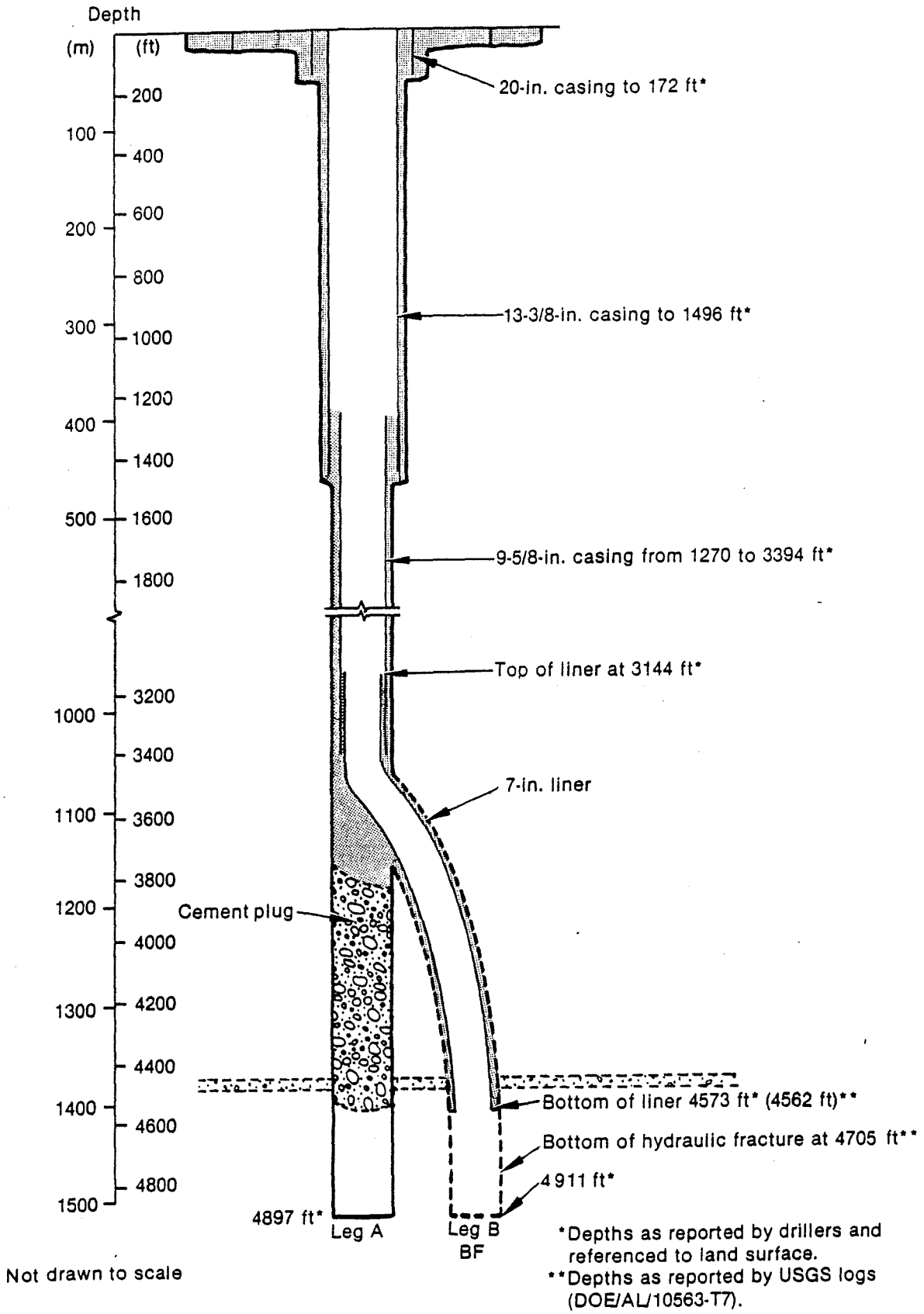

FIGURE 2

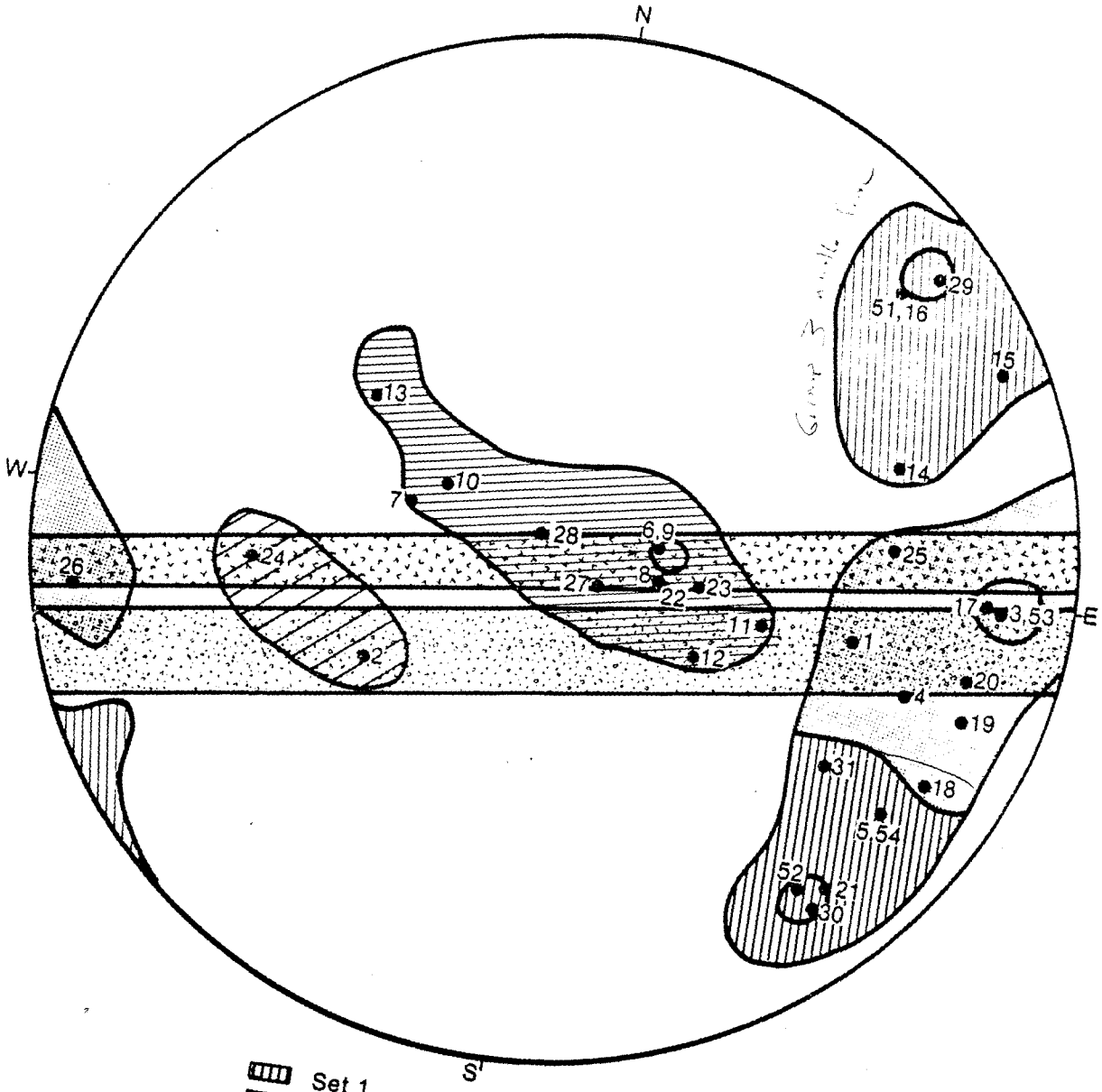

FIGURE 3. Equal area stereonet for 35 acoustic televiewer discontinuities in RRGP-5B between depths of 1341.1 and 1491.1m. (4400 amd 4895 ft.)

FIGURE 4. Vertical profile of discontinuity orientations and density for RRGP-5B.

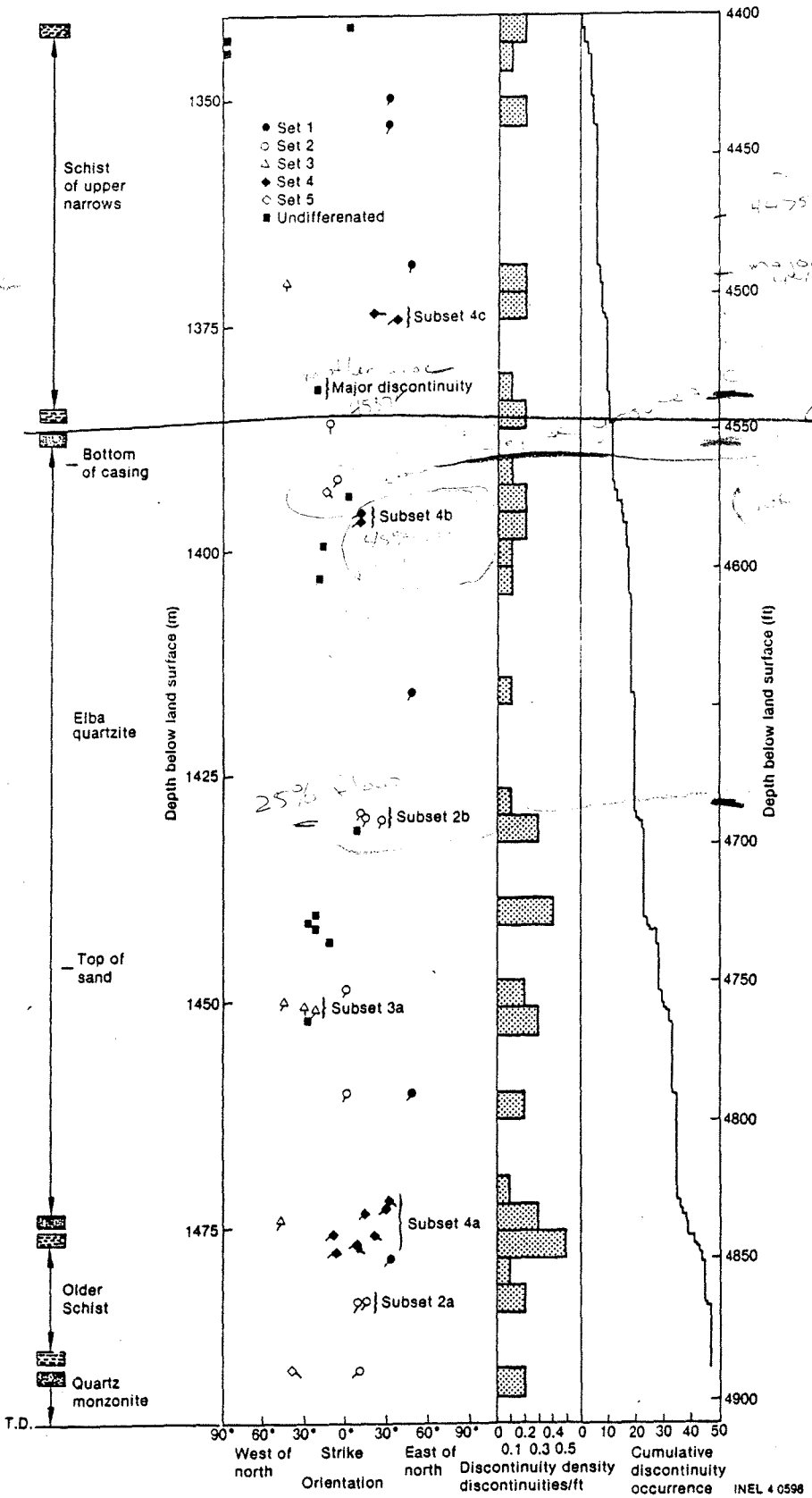

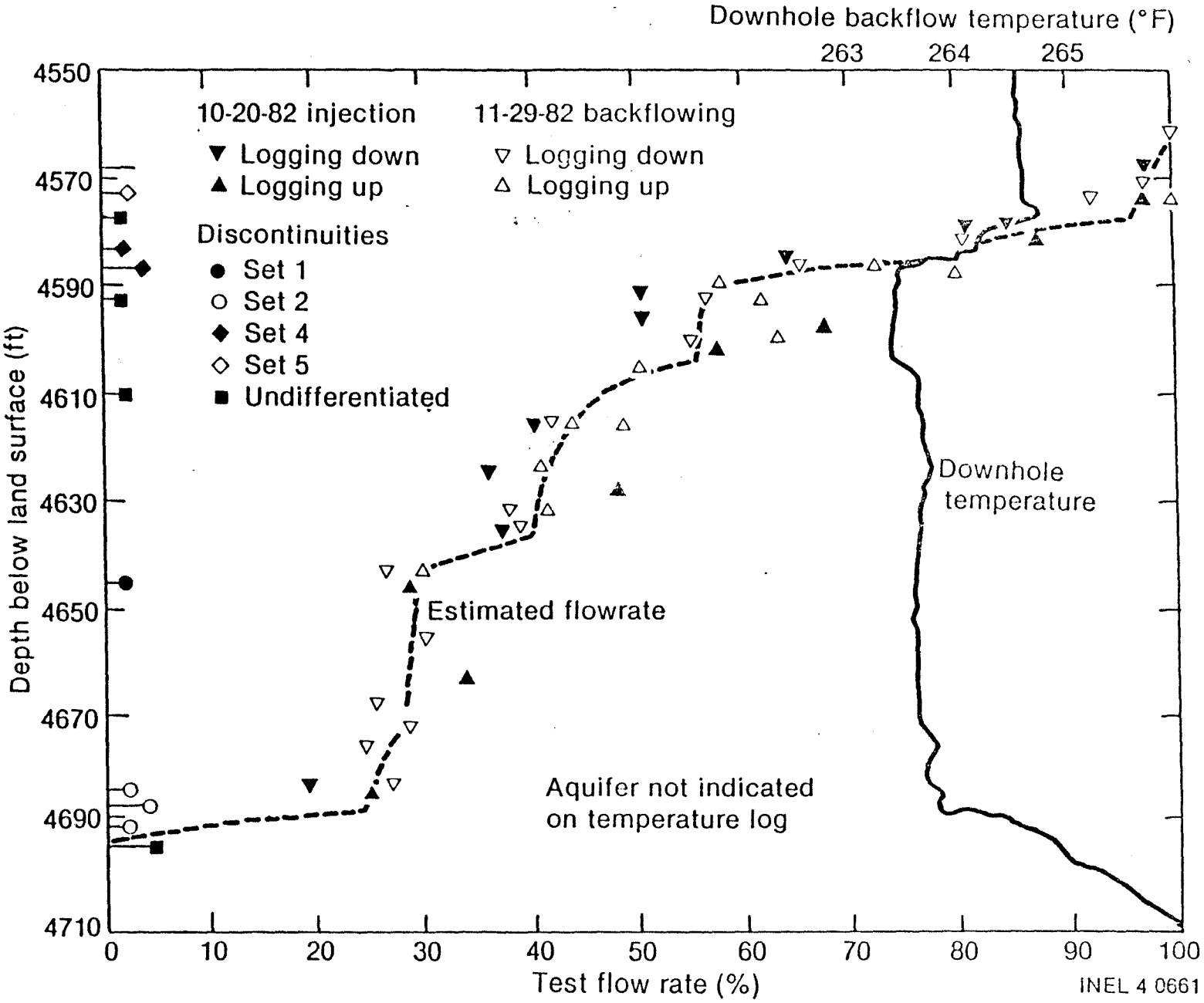

FIGURE 5. Production/receiving zones discharge/uptake as a percentage of flow rate and discontinuity locations for RRGP-5BF. A temperature log during backflow of test 2D is also plotted.

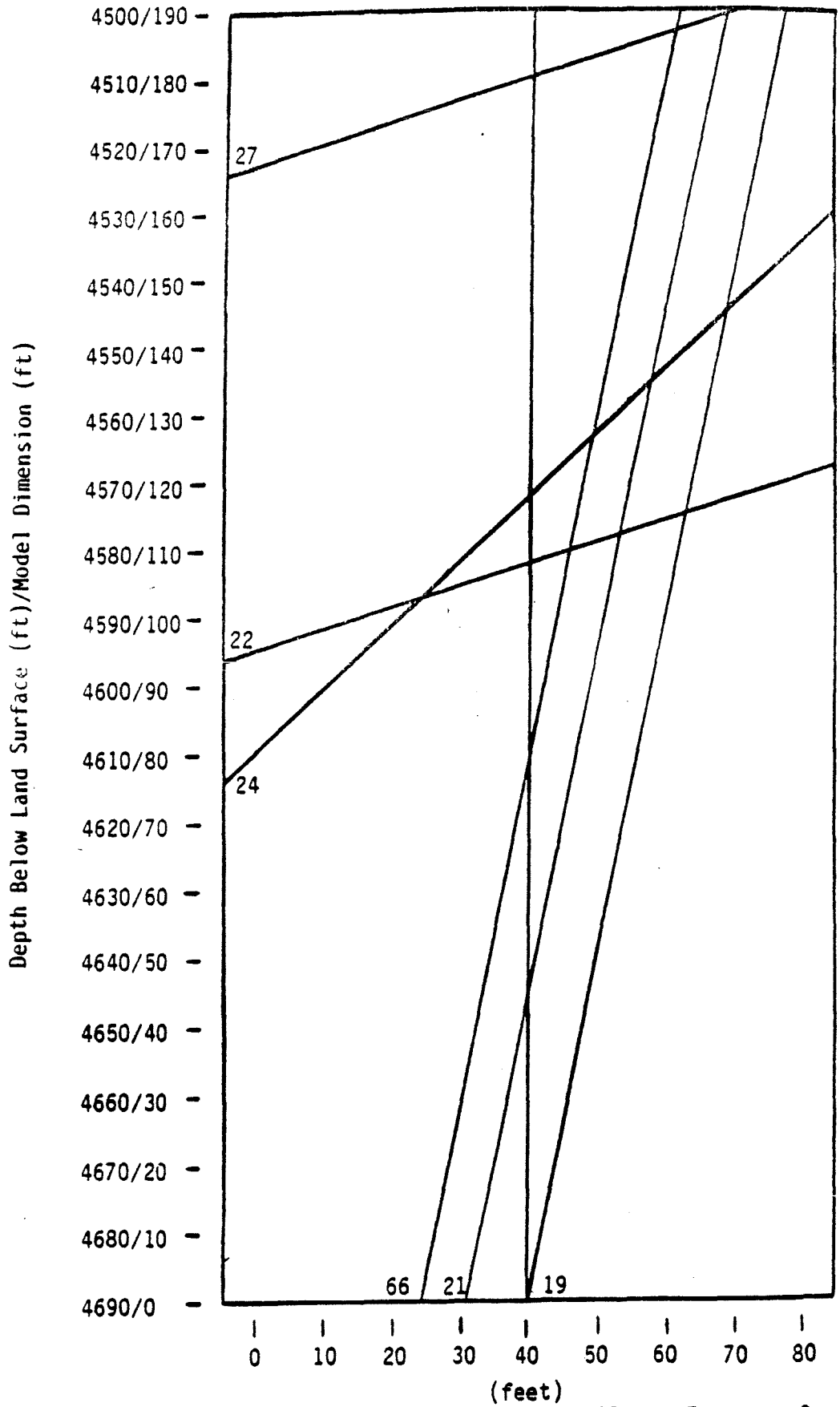

Figure 6 . Raft River Well RRGP-5BF Near Wellbore Fracture System

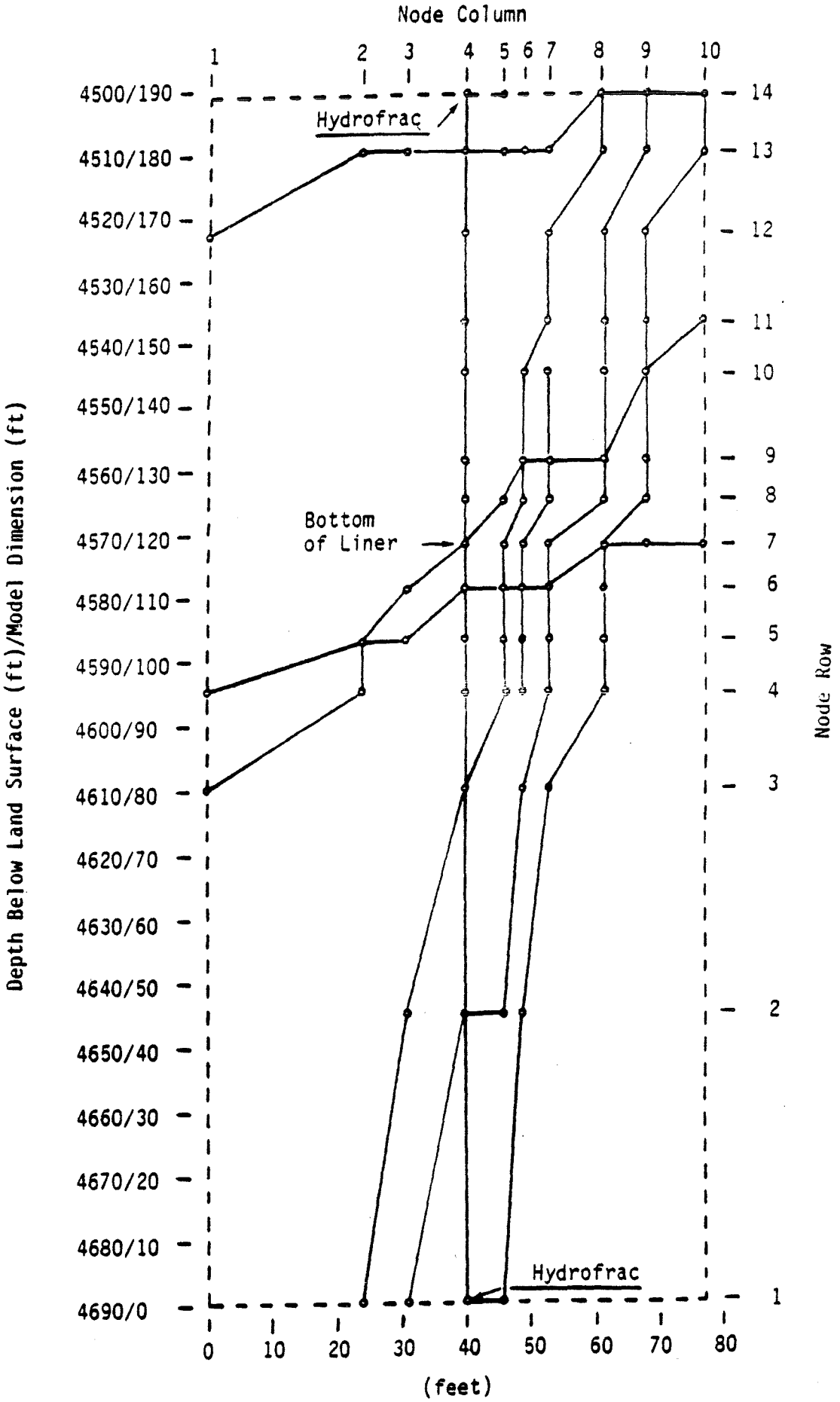

Figure 7 . Raft River Well RRGP-5BF Near Wellbore Computer Model

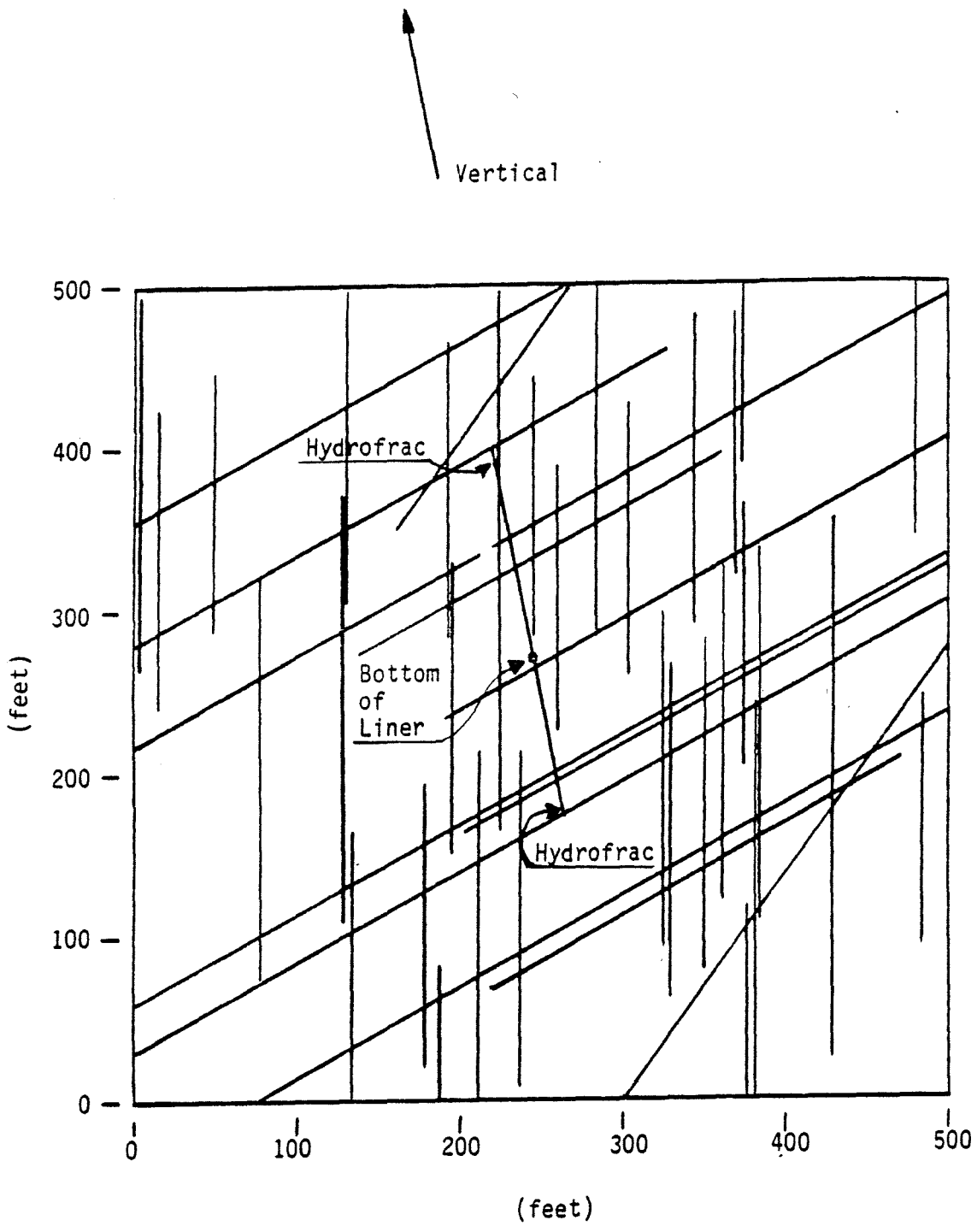

Figure 8. Raft River Well RRGP-5BF Large Reservoir Fracture System

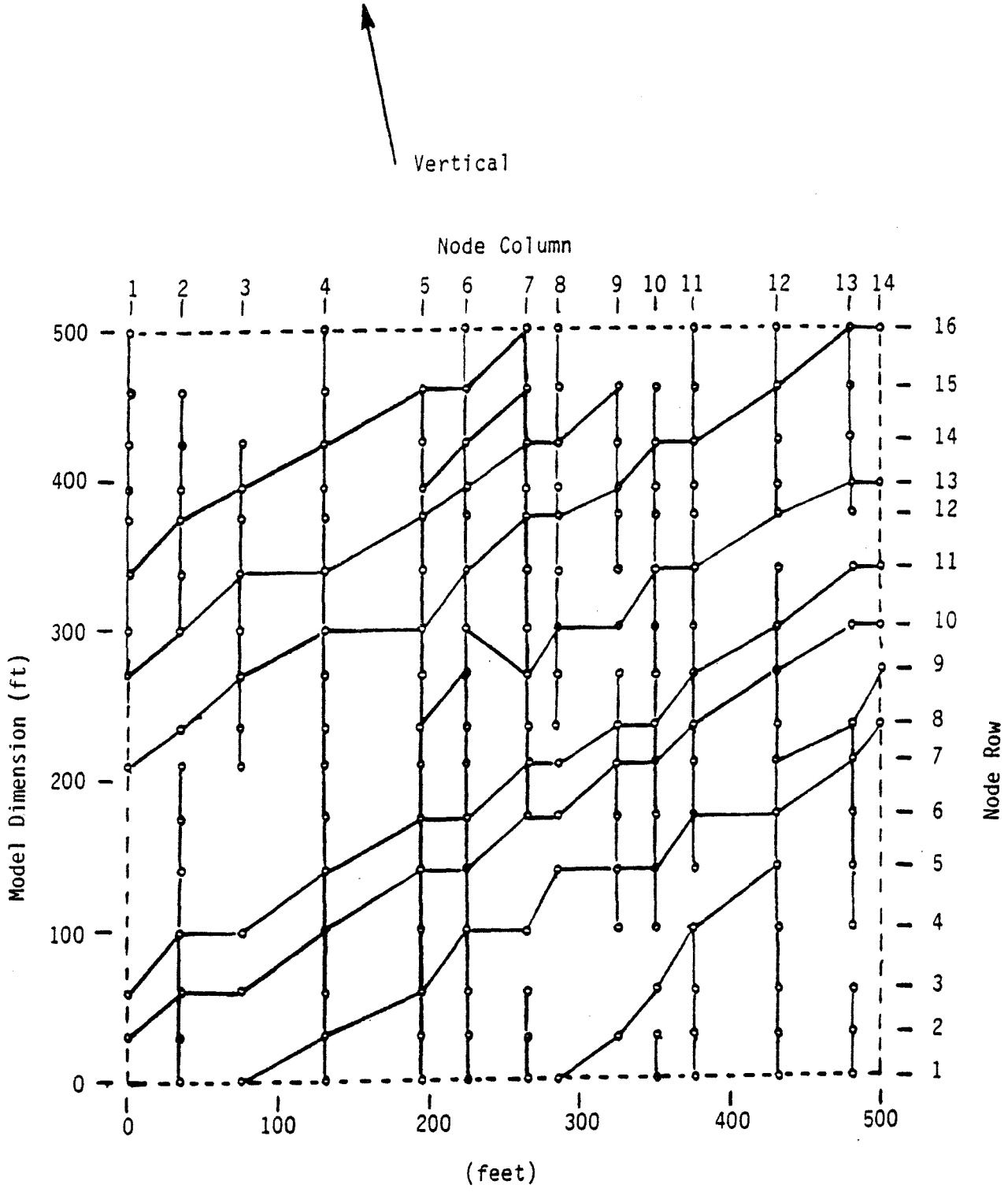

Figure 9 . Raft River Well RRGP-5BF Large Reservoir Computer Model

RAFT RIVER FRACTURE CHARACTERIZATION AND RESERVOIR SIMULATION

INTRODUCTION

Raft River Well RRGP-5BF was tested in September through November 1982 as part of an effort to develop and refine new techniques for reservoir analysis when simultaneous injection and production are planned. The use of tracers in single well injection and recovery tests is an integral part of the technique under study. The Raft River Geothermal Field was selected as the site for the initial field testing in this program beacuse the field was immediately available with excellent facilities and because the moderate formation temperatures provided an ideal testing environment. The Raft River Reservoir is highly fractured and it is a program objective to develop techniques for fractured reservoir analysis.

During the interim since the tests were completed, a significant effort has been expended in developing analytic, physical and numerical methods for analyzing flow and dispersion in fractured media. The inital objective of this effort is to correlate the data collected in the Raft River tests. The FY-84 physical model development work is presented in a separate report. This document presents the numerical modeling work and the fracture characterization research conducted to provide the required description of fractured media characteristics. The characterization work consisted of a survey of generic fracture literature, an analysis of borehole data leading to a partial description of the local fracture system and the synthesis of a stochastic fracture system in the vicinity of the borehole. The numerical modeling effort involved the development of a fractured media simulation code, the evolution of two numerical models and a scoping analysis using one of the models.

FRACTURE SYSTEM CHARACTERIZATION

An extensive review of the literature and the specific characteristics of the Raft River geology and fracture system has been made as the basis for the detailed computer models. Since the models address the discrete fracture nature of the aquifer, the emphasis in these studies is on the generic and the specific Raft River characteristics of fractured media.

The literature search was limited to crystalline rock since the schist and quartzite comprising the Raft River production zones are crystalline material. The most extensive source of fracture characterization data for crystalline rocks is the high level radioactive waste repository studies in Sweden, Canada and the United States. Hydrologic data has additionally been obtained from groundwater and geothermal well productivity studies.

Raft River fracture system characteristics were derived from acoustic televiewer, lithology, spinner and temperature logs.

The geologic history of the rock mass must be known to understand the nature of the fracture system. For many crystalline rock systems, the structural history begins with the emplacement and crystallization of a pluton. Norton (1981), in studying fossil magma-hydrothermal systems, describes an intimate relationship between the heat flow, state of stress and extent of mass transfer among minerals and fluids. This structural history should be studied to develop a systematic description of fracture systems. Each tectonic cycle results in folding, fracturing and faulting (Seeburger and Zoback, 1982) with each cycle adding its own fracture set and modifying previous systems. These fractures, once formed, are then modified by mineral and chemical alteration (Dugal and Stone, 1981).

The initial group of studies reported are concerned with the measurable geometric properties of discrete fractures. Since flow is dependent on a more detailed geometric description than can be readily obtained, many studies directly address this process. These studies are reported in a concluding section.

GENERIC FRACTURE CHARACTERIZATION

The discontinuities encountered in a fractured formation range from major faults caused by large scale displacements, through stress induced macrofractures to the microfractures which describe the finest detail of the rock matrix. The discussion which follows addresses this complete range.

The void space in a fractured formation can be divided into three categories (Knapp, 1975). The first, flow porosity, is the void space in which the predominant transport mechanism is fluid flow, the second, diffusion porosity, is the void space where the predominant transport mechanism is molecular diffusion. The third, residual porosity, consists of isolated voids that are not connected to the flow or diffusion porosity. This data given for several grantic rocks indicates a flow porosity of about 1% of the total, diffusion porosity of about 5% and residual porosity of about 94%. It should be noted that the water in the residual portion does not affect the dispersion phenomena but rather modifies the mechanical and thermal properties of the rock mass.

The characteristics which describe the geometry of a fracture system include orientation, persistence (length), spacing and aperture. These characteristics are based on the commonly made approximation that fractures are planar. The shape of this planar surface is poorly defined in the literature but is most frequently assumed to be circular. The variation in the third dimension, typically referred to as asperity, has not been defined by geometric characterization. A frequently observed characteristic is the echelon behavior in which a fracture steps laterally by a small distance before continuing in the same direction. Connection between these segments is sometimes visible (Segall and Pollard, 1983) but is assumed to exist at depth. The discontinuous fracture is treated as a single feature. The final sections address fracture filling mineralogy and permeability.

Orientation

Fracture orientation data for a crystalline rock mass may be obtained from surface mapping with the highest quality data for the characteristics at depth generally being obtained from borehole data. Fracture orientation is defined by strike and dip. The dip is the maximum angle which any planar feature makes with the horizontal. The strike is perpendicular to the dip. A scanline mapping method which consists of stretching a measuring tape along an exposed rock surface and recording pertinent features is commonly used for mapping exposed surfaces (ERTEC, 1983). There are problems in defining a single joint, as Segall and Pollard (1983) observed in granodiorite. It was rarely possible to locate the end of a joint to within 10 to 20 cm on the surface outcrops studied in the Sierra Nevada in California (Figure 1). Besides the errors due to exposure and individual mapping skills, the data must be corrected for the effects of nonrandom orientation of the rock surface mapped and for nonrandom borehole orientation(s) (Terzaghi, 1965).

For statistical quantification, a sufficient number of fractures must be sampled. Hudson and Priest, (1979) found at least 200 measurement values were needed for statistical purposes with a scanline length at least 50 times the mean discontinuity spacing.

Statistical quantification of fracture orientation characteristics is difficult. A bivariate normal distribution has been used by Zanback (1977) to provide confidence limits for joint set orientations for stereographic plots, however, the method is statistically invalid (Evans, 1983). A sterographic projection is a projection of a perpendicular line to the planar feature from the origin to its point of intersection on the southern hemisphere. Stereonet contoured diagrams are statistically invalid since individual poles may be counted more than once, thereby violating probability theory (Int'l Soc. of Rock Mech. 1978). Spherical normal distributions have been applied to describe joint sets (Mahtab et al., 1972), but they frequently do not accurately describe the actual variation that may be present (Evans, 1983). Because of these statistical limitations, "only limited efforts have been made to statistically

characterize the variability or orientation within individual joint sets." (Evans, 1983).

There are usually three or four (Gale, 1982) and occasionally six (Hsieh et al., 1983) sets of fracture planes present in most rock masses. The orientations vary both within and between the sets of fractures (Gale, 1982). For example, numerous studies have been conducted at the Stripa Mine in Sweden. A typical fracture system is indicated in Figure 2 (Olkiewicz et al., 1979).

Persistence

Persistence is the size or linear extent of a planar discontinuity (ERTEC, 1983). Scanline surveys have several limitations (Cruden, 1977): the scanline will preferentially intersect larger trace length discontinuities; large discontinuities may extend beyond mappable exposure; and small discontinuities are difficult to measure. Statistical methods are available to correct the biased field data (Priest and Hudson, 1981; Baecher et al., 1977; Baecher and Lanney, 1978; Segall and Pollard, 1983). Based on several assumptions, the distribution of trace lengths can be estimated. By assuming: (a) the fractures have constant geometry (usually circular); (b) the distribution of the centroids of the fracture surfaces is known (usually random); and (c) the distribution of the fracture lengths is known (usually log-normal or exponential), a censored and truncated field sample of measurements can be corrected to estimate the true size distribution (Evans, 1983). Log-normal distributions have been found to provide the best fits for Baecher et al., (1977), McMahon (1974), Bridges (1975), and Barton (1977) among others. Stone (1980) found a log-normal distribution with a mean length of 4.05 m in the Eye Dashwa pluton at Atikokan, Ontario. An exponential distribution provided the best results for Robertson (1970), Stetten et al., (1975), and Call et al., (1976) among others. It appears that there is no single statistical distribution that can be used to describe all fracture length distributions.

Lengths of joints in the plane of the outcrop were determined by Segall and Pollard, (1983) at two sites in the Sierra Nevada of California, Figure 3. A power-law distribution of the form l^{-n} was found to fit the observed data reasonably well, with l being the joint length and n ranging from 1.3 to 1.8. This power law apparently overestimates the number of joints having lengths less than 2 m. However, mapping resolution was on the order of 1 to 2 m. Additional mapping of joints having lengths on the order of 1 cm suggested there were 10^4 small cracks from 0.01 m to 1.0 m for the Ward Lake outcrop. The power law predicts 4×10^3 cracks whereas an exponential law predicts only 10^2. Thus, a power law provided the best estimate of joint lengths.

Results at the time-scale heater experiment at the Stripa Mine in Sweden (Thorpe, 1980), were best defined by a log-normal probability equation, Figure 4. The data in Figure 4 are biased since the minimum length of the fractures mapped was 0.3 m and the limited dimensions resulted in censored data when one or both ends of the fracture are not visible. Thus, extreme values outside the range of the raw data cannot be predicted.

Rouleau and Gale (1984) determined trace length characteristics for the four censored and truncated joint sets encountered in the HG and R boreholes in the ventilation drift at the Stripa Mine in Sweden. Figure 5 contains histograms for the four joint sets and also indicates the effects of censoring: (a) when both ends of the fracture trace are mappable; (b) when only one end is mappable; and (c) when neither end is mappable. The trace length statistics in Table 1 list the basic statistics for two levels of censoring as well as truncation and censoring parameters fitting an exponential and log-normal model to the data. Correcting for sampling bias clarifies the differences between the fracture sets.

Spacing

Spacing is defined as the perpendicular distance between adjacent discontinuities of the same orientation set. The inverse of the spacing value, joint frequency, is often used (Priest and Hudson, 1981). Average joint spacing in a rock mass depends on the spacing for each joint set as well as the number of joint sets (Cameron-Clark and Baddvari, 1981). Priest and Hudson (1976, 1981) suggest that any arrangement of randomly positioned discontinuities (an absence of a predominance of evenly spaced discontinuities) will result in a negative exponential relationship between spacing values and frequency of occurrence.

Canadian investigations for an Underground Research Laboratory (Atomic Energy of Canada Ltd. 1982[a], 1982[b], Gale et al., 1981, Leech and Cooper, 1982) as reported in ERTEC (1983) found spacings for orientation sets that varied from less than 0.5 m to more than 10 m within a single outcrop. At the Lac du Bonnet pluton where the Underground Research Laboratory is being constructed, Soonawala et al., (1982) found that the fracture density decreased downward with no fractures recognized over a distance of 1000 m below a depth of 350 m (ERTEC 1983).

The Reynard Lake Pluton in Canada was found by Wallis and King (1980) to have a negative exponential discontinuity frequency distribution. Apparent fractures as determined from geophysical logs, Figure 6, appear to be more frequent between depths of 2000 and 2750 m (Davis and Tammemagi, 1982). Microfracture frequencies were determined by Davis and Tammemagi (1982) from thin sections Figure 7.

Segall and Pollard (1983) mapped granitic rock outcrops at two sites in the Sierra Nevada. They found nonuniform spacing, with spacings of the single joint set varying from ~20cm to ~25m. The spacing of joints is not controlled by variations in joint geometry or rock type with depth.

For the time-scale heater experiment at the Stripa Mine in Sweden, the joint spacing is best defined by a log-normal probability function, Thorpe, (1980), Figure 8. According to Thorpe et al., (1980) "It would be

difficult to draw a line greater than a few millimeters long anywhere in the rock which does not cross a fracture of some sort, and in many places the original matrix minerals are thoroughly riddled with fractures down to the finest scale." These conclusions of Thorpe et al., (1980) are based on time-scale and full-scale drifts. For the ventilation drift at Stripa, the fracture density was computed assuming the fracture density is equal to the fracture frequency. The average fracture densities are 1.03, 2.64, 0.91, and 1.83 m^{-1} for the four fracture sets in the HG and R boreholes (Rouleau and Gale, 1984).

Norton (1981) when studying fossil magma chambers in the western U.S. and Canada found fracture spacings on the order of 1 m common in all of the 30 chambers studied. Surrounding this heavily fractured zone is a region of fracture spacings from 1 to 10 m. At the Mayflower pluton in Utah, the fracture abundance ranged from 0.06/cm to 0.21/cm with higher abundances within 100 m of the Mayflower vein system. Norton found fracture frequencies rarely less than 0.005/cm with frequencies of 0.1 cm over areas of 10^4 m^2. The central region of the Dells granite pluton in Arizona has fracture spacing ranging from 0.5 to 2 m.

Fracture spacing information is available for productive geothermal zones in New Zealand (Grant et al., 1982). Usefully productive fractures are typically spaced 100 m or more apart (Fradkin, et al., 1981) in New Zealand geothermal fields. Finer fractures often occur within the large blocks and may be the dominant flow mechanisms within the large blocks.

Aperture

The aperture is the perpendicular distance between the walls of a fracture in which the intervening space is air or water filled (Evans, 1983).

The majority of aperture measurements have been made in terms of effective hydraulic properties which are discussed in the subsequent section on measured responses. One of the few studies of physical aperture was made by Bianchi and Snow (1969). They compared surface and underground fracture apertures in the Pikes Peak granite near Manitoic Springs, Colorado and found that the average fracture aperture along surface outcrops is three times the average apertures in tunnels. They also noted that due to stress release, fracture apertures measured in underground openings will not be representative of in situ apertures. They found the surface outcrop apertures to be log-normally distributed.

Some data are available on fracture apertures measured in the laboratory (Evans, 1983). Sharp and Maini (1972) have made direct measurements on large laboratory samples containing rough natural fractures. Iwai (1976) measured fracture contact areas as a function of stress by using pressure sensitive plastic on laboratory samples containing rough induced fractures.

Microfracture studies using a scanning electron microscope have also been conducted. Chernis (1981) obtained data on fracture apertures for different crack types in granite at Pinawa, Manitoba. An example of these data, Table 2, and Figures 9, 10, have been used to determine porosity distributions. Batzle et al., (1980) have studied microfracture closure under stress, Figure 11. Microfracture aperture deformation under stress depends on orientation, shape, proximity of other fractures, propping by small grains or other debris, and fracture roughness. These factors affecting behavior of microfractures also affect the behavior of larger fractures.

"Effective hydraulic" apertures have been calculated from flow rates and pressure data during packer tests (Gale, 1982). However, these calculated apertures will be less than the real apertures because of the degree of fracture interconnection and the variations in fracture aperture.

Fracture aperture width has been calculated by Gustafsson and Klockars (1981) for the study at the Finnsjö research area. One method based on the hydraulic conductivity data result in a calculated aperture of approximately 7×10^{-5} m. Another based on flow and travel times in the fracture plane result in a calculated fracture aperture of approximately 1.7×10^{-3} m. In the later case the assumption of no water being introduced into the fracture zone in a vertical direction is probably invalid, thereby affecting the calculated aperture.

Filling Mineralogy

Filling mineralogy or filling material is the term for the material other than air or water contained between the adjacent rock walls of a partially filled or sealed discontinuity. Filling material mineralogy can provide valuable information on emplacement and tectonic history.

Detailed studies at the Atikokan Research Area in Ontario, Canada provide information on the history of the area (Dugal and Stone, 1981, Stone 1980). Initially the area was intruded by aplite dykes. This was followed by high-temperature (200-500°C) deposition of epidote and chlorite, which was followed by epidote and chlorite in a more extensional environment. Clinozoisite, hematite, sphene, fluorite and quartz were deposited during this early period. Next hematite, adularia, calcite, gypsum, and clay were deposited at less than 300°C. The fracture fillings can be used for fracture correlation as can the alteration haloes around the discontinuities. The ability to correlate fractures based on infilling minerals and to determine the tectonic history is of significant importance in understanding the discontinuity system.

Davis and Tammemagi, (1982) determined fracture infillings using 11 cores in a 3066 m deep borehole at the Reynard Lake pluton in Saskatchewan, Canada. Muscovite occurs as fibrous crystal aggregate infillings. Epidote occurs as crystals dimensionally oriented parallel to the fracture and also in a direction almost perpendicular to the fracture. The former was presumably formed during deformation whereas the latter probably formed after the cessation of shearing or straining. Other infilling minerals include chlorite, dimensionally oriented gains of quartz and calcite, as well as opaque minerals such as pyrite and magnetite or ilmenite. The authors concluded that there was no significant change in fracture filling materials with depth. All of the infilling minerals are high temperature and were probably emplaced by hydrothermal solutions. The lack of gypsum indicates no recent deposition of minerals in the fractures by saline ground water (Kamineni et al., 1979).

At the Stripa Mine in Sweden, fractures are often infilled primarily with chlorite and occasionally with calcite. Open fractures are often lined with clay (Olkiewicz et al., 1979). Thorpe et al., (1980) were able to distinguish several types of fractures based on the predominant mineralogy of the ultra-large core and of cores from the time-scale and full-scale drifts. Chlorite was the most common filling mineral in veinlets <0.1 mm in width to fractures up to several centimeters in width. These fracture fillings appeared to be black microscopically even though quartz is almost as abundant as the chlorite. A second type of fracture was <0.3 mm wide, and was filled with sericite having a fine sheath-like aggregate growth habit. The third type of fracture was filled with epidote. Because of problems in identifying epidote, the extent to which this mineral occurs in fractures is not known. This is evidence that fracture formation and filling mineralogy are related to matrix alteration. Fracture mineralogy can be used to distinguish fractures.

Permeability

Flow through individual fractures has been shown to be a function of normal stress, shear stress and fracture surface characteristics.

Witherspoon etl at., (1979a) has demonstrated that flow through natural fractures in granite, basalt and marble, assuming parallel planar fracture sides, varies with the cube of the aperture. Tsang and Witherspoon (1981) demonstrate that the effective aperture must be replaced by an appropriately weighted average to include the effect of fracture roughness.

Maini (1970) considered the variation of aperture in the transverse direction. Lucite copies of a fractured rock block and a dye were used to show that flow in fractures occurs over paths which are irregular, not straight. The experiments demonstrated that flow tends to deflect around narrow portions of the fracture. Neuzil and Tracy (1981) included an aperture frequency distribution in deriving a modified Poiseuille equation.

Evans (1983) described a system for laboratory measurement of air flow through a single fracture. In addition to determining the equivalent parallel plate aperture, the volume of the fracture was measured using an air pycnometer which measures the pressure after expanding a known mass of air into the fracture.

Wilson and Witherspoon (1976) have conducted laboratory experiments to show that flow resistance at fracture intersections is trivial compared to the resistance of the fracture itself.

Permeability measurements are known to depend on sample size. Tsang (1983a) has suggested that the size of the rock sample should be larger than the typical wave length of roughness. As shown by the Stripa Ultra-Large core test (Thorpe et al, 1983) even very large samples may not give satisfactory data. In-situ tests, while avoiding the removal problem, would be preferable provided that the fractures were not disturbed and could be adequately characterized.

Gale also describes the effect of stress in modifying the effective aperture. Tsang (1983b) shows that the fracture contact area and tortuosity and the connectivity of flow paths increases with increasing stress.

In several investigations of the effect of normal stress on conductivity it has been observed that as maximum stress was applied to cores of varying cross-sectional area, measured conductivities were not repeatable (Witherspoon et al., 1979a).

Permeability tests in a heated block flatjack test in granitic gneiss at the Colorado School of Mines Experimental Mine (ONWI-1981) demonstrate a strong dependence of fracture permeability on temperature (Ubbes, in press). The block being monitored in the flatjack test consists of four sub-blocks which behave primarily as rigid bodies with deformation of the main block, with applied stress, a result of rotation and displacement of the sub-blocks along joints (Ubbes, in press).

RAFT RIVER RRGP-5B FRACTURE SYSTEM

The Raft River KGRA, located in southern Idaho near the Utah border, has been extensively developed and tested by the U.S. Department of Energy. The geology of this reservoir is shown in Figure 12, a completion drawing is shown in Figure 13 and a summary of the completion history is given in Table 3. The final completion steps consisted of hydrofracturing and cleanout of the sand used as proppant.

The well characterization prior to the fall 1982 test series consisted of drillers logs, borehole geophysical logs including acoustic televiewer surveys and limited coring. This data, together with some of the borehole logging during the test series, was analyzed to determine fracture orientation, spacing, correlation with producing/receiving zones and apertures.

The acoustic televiewer surveys were performed by W. Scott Keys of the United States Geological Survey. The earlier log was run prior to well completion and covers depths below land surface between 1341.1 and 1491.9 m (4400 and 4895 ft). The later log was taken after setting this liner and hydrofracturing and was limited to the open interval between depths of 1390.4 and 1491.9 m (4562 and 4895 ft). Examination of this common section shows no discernible differences in prehydrofracturing discontinuities attributable to the hydrofracture. In the open interval therefore, the log providing the highest quality data was used. The pre-completion log was used to provide additional data for the upper interval.

Only discontinuities having an apparent width greater than 1.3 cm (0.5 in.) were observable. These discontinuities therefore formed a truncated sample. Only 35 discontinuities, table 4, in the 151 m (495 ft) vertical interval exhibited the well-defined sine waveform necessary to determine the orientation. The discontinuities are numbered beginning from the bottom of the borehole.

Orientation

Thirty-one discontinuities exhibited the full sine wave form and were numbered 1 through 31. Four discontinuities, numbered 51 through 54, were identified whose partial trace matched a discontinuity in the previous series. Eleven remaining traces could not be matched to any well-defined sin forms and were numbered 61 - 72. A strike could be determined, but dip could not be estimated. The fractures were then corrected for magnetic declination and borehole inclination (N 54° W, dip of 85° NW). The true oriented fractures were then corrected using Terzaghi (1965) for occurrence frequency.

The distance between the upper and lower points of intersection between the discontinuity and the borehole wall was measured along with mean borehole diameter in order to determine dip. An X-Y Caliper log was used to measure gross borehole diameter neglecting any compensation for borehole ellipticity. The direction of dip was determined using the orientation of the upper and/or lower points of intersection of the discontinuity and the borehole wall. The strike is perpendicular to the direction of dip.

A southern hemisphere stereonet of the orientation of the poles of the well-defined fractures is contained in figure 14. The fields for 5 presumed discontinuity sets are delineated by the outer contours while the inner contour indicates the maximum apparent density using data corrected by the Terzaghi (1965) method. All the contours are not indicated on the figure since the sample sizes are small relative to Terzaghi correction factors. Therefore, the validity of the contours is questionable. The divisions between the discontinuity sets are somewhat arbitrary, but generally are defined by estimated discontinuity densities.

Table 5 contains the positions of the estimated maximum density for each set, as well as the number of discontinuities in each set, and the number of discontinuities corrected by Terzaghi's method for fracture-borehole intersecting angle. The acoustic televiewer recorded the

hydrofracture in RRGP-5B from a depth of 1390.0 to 1429.4 meters (4462 to 4690 ft). The strike of the hydrofracture has been reported as N 29° E. (Republic et al., 1980), but using the mean orientation of the midpoint between the intersection of the two limbs of the hydrofracture and the borehole, the strike is approximately N-S, but varied over an angle of more than 90 degrees.

Discontinuity Distribution in Borehole

The discontinuities for the various sets are not necessarily uniformly distributed in the vertical section of the borehole, but rather occur in subsets or clusters, Table 6 Figure 15 is a vertical profile of RRGP-5B indicating the lithologic log (Covington, 1979), the fracture orientation according to sets and subsets, discontinuity density, and the cumulative discontinuity occurrence. The strike is indicated by the lateral symbol position and the dip by the inclination from the horizontal of the tail.

The 12 discontinuities in set 4 can be subdivided into 3 subsets with separations in the borehole between subsets 4a and 4b of approximately 78.0 m (265 ft.) and between subsets 4b and 4c of approximately 19.5 m (64 ft.) for an average of 48.8 m (160 ft.).

Another discontinuity set affected by vertical clustering is set 3. The separations in the borehole between the midpoint of subset 3a (1450.6 m [4759.5 ft.]), the lowermost (1474.2 m [4837 ft.]) and uppermost (1370.6 m [4497 ft.]) discontinuities, table 6 are approximately 23.8 m (78 ft.) and 80.16 m (263 ft.), respectively, for an average of 51.8 m (170 ft).

Discontinuity set 2 is also affected by vertical clustering. The effects of clustering essentially reduce the 10 discontinuities observed to 7 dispersed discontinuities.

Vertical discontinuity patterns have developed over 2 depth intervals that are conducive to the development of aquifers. The development of a relatively high transmissive, areally extensive, lithologically controlled aquifer in fractured rock with essentially impermeable matrix would be

favored by the occurrence of many intersecting permeable fractures. Discontinuities numbered 1 to 4 inclusive occur between depths of 1490.7 to 1483.1 m (4891 and 4866 ft.) within the Older Schist, Figure 15, Table 4. These discontinuities occur within 3 sets, 2., 4, and 5 Figure 15, in a band (Older Schist) on the stereonet where the strike is approximately N 9° W. The dip of these discontinuities range from 75° W to 36° NE, Table 4. The wide spectrum of dips almost insures that the discontinuities will intersect and thus have the potential for forming an aquifer.

The next set of numerous intersecting discontinuities occurs between depths of 1397.1 and 1374.0 m (4584 and 4508 ft.), Table 4. These 7 discontinuities which are numbered from 22 to 28, Figure 14, occur in a band on the stereonet labeled, "Schist of Upper Narrows," with a strike that is depicted as being the same as that for the Older Schist. The dips of these discontinuities in the Schist of the Upper Narrows range from 84° NE to 55° SW, a wide range of values which almost assures that the discontinuities will intersect, and if permeable, will form an aquifer. An interesting aspect of the dips is that in general the discontinuity "planes" rotate counterclockwise looking to the north as the depth decreases. The significance of this dip variation is not known. Borehole geophysical logs indicate a major aquifer at a depth of 1379.5 m (4526 ft.) in RRGP-5A approximately 3.0 m (10 ft.) from RRGP-5B. A high production rate 63 ℓ/s (1000 gpm) was reported in RRGP-5A at a depth of approximately 1368.8 in. (4491 ft.) in the Schist of the Upper Narrows just above the zone from 1397.1 to 1374.0 m (4584 to 4508 ft). Evidence indicates that major production zones are either in or near the zone in the Schist of the Upper Narrows containing discontinuities with a wide range in dip with a strike approximately N-S.

Production/Receiving Zone Distribution in Borehole

The location of the major production/receiving zone in the open borehole section during injection-backflow testing indicate a correlation between major production/receiving zones and discontinuities. Figure 16 indicates the vertical distribution of production/receiving zones and

discontinuities. The major producing/receiving zones in RRGP-5BF are all located near major discontinuities. The hydrofracture resulted in only the near vertical hydrofracture with no additional discontinuities being created. All of the discontinuities, except for discontinuities numbered 25, 24, and 68 at depths of 1392.6, 1393.5 and 1394.7 m (4569, 4572 and 4576 ft.) respectively are either centered at or within a few feet of the major producing/receiving zones. These nonproductive discontinuities may have been cemented during the cementing of the casing liner which extends to 1390.4 m (4562 ft). Since the discontinuities intersect the borehole over a vertical interval of a few feet, the midpoint of the intersection of the borehole and the discontinuity would not necessarily coincide with the exact location of the production/receiving zone.

The intersection of discontinuities which are presumed structural zones of weakness and the hydrofracture would be expected to result in an enlarged cross-sectional area for the hydrofracture due to additional fracturing and erosion during the injection of approximately 390,000 lb. of sand. The propping of the hydrofracture would probably occur primarily in the narrow sections. The least intergranular stress in the proppant would occur in the conduits at the intersection of the hydrofracture and the natural zones of structural weakness. The estimated 4 to 15+ $yd.^3$ of sand subsequently pumped from the fracture would originate, in part, from these conduits. The productivity of the the well has been increasing as additional sand has been removed from the fracture conduit system. Based on productivity/receiving zone locations, it appears that the majority of these occur at the intersections with the hydrofracture and natural prehydrofracture discontinuities which are, for the most part, presumed to be fractures.

Separation

The discontinuity separation has been determined using the spacing between discontinuities of a set/subset as measured in the borehole. The sets and subsets used are indicated in Table 6. Because the subsets are closely spaced discontinuities, it was decided to treat the subsets as a single discontinuity within the set. The midpoints between the depths of the upper and lower discontinuities of the subset are used to define the presumed subset depths, Table 7. The spacing distributions as measured in the borehole are plotted for sets 1 to 4 in Figure 17. The means and standard deviations are listed in Table 8. The means and standard deviations have also been determined for subsets 2b, 3a, and 4a, Table 7. The data points for these subsets are plotted in Figure 17. The standard deviations in Table 7 range from -0.32839 to -0.03469 m (0.18761 to 0.48132 ft). The small sample sizes of 2 values for sets 3 and 4 and subsets 2b and 3a results in a low confidence level for the standard deviations and means for these sets and subsets. The standard deviation for sets 1 and 2 and subset 4a is approximately 0.13 m (0.38 ft). There does not appear to be a significant difference in the standard deviations between the sets and subsets.

Aperture

"The televiewer log only detects changes in acoustic reflectivity at the face of the borehole," Republic et al., 1980. It is incapable of penetrating rock mass for a three dimensional view and does not distinguish between open and closed fractures. Heavy mineralization, which can partially or totally fill a fracture, appears the same on the televiewer log as an open fracture (Paillet and Keys, 1984). Discontinuities that intersect the borehole at an acute angle are liable to breakage (Davison et al., 1982) which results in an increased apparent aperture. Discontinuity width was measured at the point of inflection in an attempt to mitigate the effect of broken edges. Image width, however, should still be treated as a relative measurement of discontinuity width. Thus all apertures having an apparent width less than 1.3 cm (0.5 in.) are not addressed in this report. Keys (1980) reported the hydrofracture had a apparent maximum width of 1.5 cm (0.6 in.).

Apparent discontinuity widths were separated into categories beginning at a width of 1.3 cm (0.5 in.) and incremented by 1.3 cm (0.5 in.intervals to 6.4 cm (2.5 in.). The majority of fractures range in width from 0.5 to 1.5 in. (Figure 16). Discontinuities varying in width from 2.5 cm to 3.8 cm 1.0 to 1.5 in. are nearly evenly distributed throughout the recorded vertical section (Figure 19). A major discontinuity appears at a depth of 1382.8 m (4537 ft.) which has an apparent aperture of 12.7 cm (5 in.). This discontinuity was a major producing zone in Leg A.

RAFT RIVER RESERVOIR SIMULATION

RAFT RIVER RESERVOIR MODELS

Implementation of the generic and Raft River characterization data in a reservoir model suitable for computer simulation requires a compromise between the complexity of the real world and the capabilities of the simulation. It also requires reasonable assumptions for the missing elements of the characterization, specifically fracture length and aperture. The discussion of these areas includes a summary of the capabilities of the FRACSL flow and transport code, the approximations made in creating the computer models and the evolution of the two models used in the analysis. The first of these models is used to study the hydrology of the "known" system including the wellbore, the hydrofracture and the significant fractures intersecting the wellbore. The second model is substantially larger, incorporates a stochastic description of the entire fracture system in the area, but has not been sufficiently exercised to yield reportable results.

FRACSL Simulation Code

The FRACSL (FRactured media - Advanced Continuous Simulation Language) code was developed at EG&G to specifically address flow and dispersion in fractured media.

The EG&G-developed code is implemented within the ACSL problem-solver software. The dynamic problem of interest is described by the user in terms of algebraic equations and first order non-linear differential equations. The ACSL software then applies a large repertoire of utilities which are useful for any problem of interest: input, integration, interpolation, special functions and output including line-printer plotting. The integration algorithm used in these studies is Gear's stiff system algorithm, which is extremely efficient for those systems having a wide range of eigenvalues or characteristic frequencies. Another capability used extensively is the direct steady state by Newton-Raphson iteration rather than integration. ACSL is a commercial code which is widely distributed and is supported by telephone consultation. The advantage of this approach is that a much wider

set of mathematical capabilities is available than the user would himself provide, and at no effort on his part.

FRACSL is a two-dimensional simulation of isothermal flow and solute transport in a fractured porous media. The fractures are superimposed on the edges or diagonals of rectangular matrix blocks. Nodes are defined at the intersection of vertical and horizontal grid lines which define grid cells.

In the FRACSL flow calculation, the conservation of mass relationship is applied to the cumulation of quarter grid cells adjacent to the node. This summation of fracture and matrix flow into the cumulated area yields the head derivative and the set of differential equations is solved for the head at each of the nodes. Matrix flow is calculated between vertically and horizontally adjacent nodes. Fracture flow, according to the cubic law, is computed between fracture end-points which must lie on the same cell. A long fracture is represented as a series of segments, each complete in a cell.

A flux may be applied at any node and the head may be fixed at any node. A very useful, continuous boundary condition may be applied by specifying the distance from a boundary node to a remote boundary which is at zero head. Flow over this distance occurs in a media, fracture or matrix, with the same conductivity as that media had inside the boundary. This effectively "continues" the flow approaching the boundary from inside the model. The distribution of head and leaving flow at the boundary may be specified by varying the distance to the remote boundary. The limitation of this approach is in the dynamic case. Only the matrix fluid within the system supplies or receives storage fluid. The system boundary must, therefore, be sufficiently large to permit dynamic response over the period of interest.

After the matrix and fracture velocity distribution is found the transport of a solute is calculated by moving imaginary marker particles, each tagged with a mass of tracer. This approach was chosen because 1) it avoids the numerical dispersion inherent in conventional solutions of the advection-dispersion equation, 2) it is well matched to the discrete fracture approach, 3) it

accepts junction dispersion effects simulated by an elementary fluid dynamics code and 4) it is more easily visualized.

The marker particle calculations are accomplished by a set of component models describing particle movement in fractures and in the matrix and the transfers between them. As detailed in Table 9, these calculations move the particles under the influence of local fracture or matrix velocities. Additional random displacements are computed due to molecular diffusion and, in the matrix, due to dispersion. There are no forces involved since these particles are imaginary and move with the fluid. Particles are introduced at a point corresponding to the bottom of the well liner, moved through the system in the injection flow field and returned to the well in the backflow velocity field. Motion of a large number of particles, on the order of 1000, provides a population of adequate statistical significance.

The limitations of this code are firstly, its 2D character as addressed in the next section. Secondly, computer core requirements and the current lack of a fracture geometry preprocessor limit the maximum number of nodes which can be used. The synthesized fracture system presented subsequently required 327,000 octal words when used with 1000 marker particles.

Model Orientation and Effective Thickness

Each of the models represents a vertical plane one foot thick, oriented with its top face in an approximate E-W direction. Since the model is one foot thick, it is necessary to 1) determine the effective thickness of the aquifer which carries the entire test flow rate and 2) scale the total flow through the effective thickness down linearly to the model flow through the one-foot thickness. The effective thickness of the small model is 160 feet and the effective thickness of the larger model is 263 feet. The rationale for these decisions is given in the following discussion.

The principal plane was selected so as to include the dominant flow paths and their intersections. As shown in the stereonet in Figure 14, the fractures observed at the borehole have been clustered into five orientation sets. Sets 2, 4 and 5 form a band with a strike of N9°W and dips varying from 41°E for set 5 to 18°W for set 4 to 77°W for set 2. A model plane

normal to the N9°W strike, i.e., N81°W, therefore shows the intersections of these three fracture sets. Sets 1 and 3 are at the same dip as set 2 and bracket it in strike. They are therefore represented in this model plane as if they were part of set 2.

In addition to a component in the plane of the model, the flow moves in the fractures in a direction normal to the plane of the model. The simplest case is a system of sets of common strike, varying dip and equal extent into and out of the model plane. Flow would leave the wellbore, move in the inital fractures in a direction into and out of the model plane until it reached the extent of these fractures and then move parallel to the model plane. The effective depth in this case is the extent of the fractures in the direction normal to the model plane.

The next higher level of complexity includes variation in extent normal to the model plane within an orientation set and between orientation sets. In addition to spreading to some depth normal to the model plane before turning to flow parallel to the model plane, there is a true three dimensional flow condition established. Flow continues in a direction normal to the model plane and, in addition, the effective thickness of a 2D section increases as the flow moves away from the well in the plane of the simulation. This condition is further enhanced by the variation in strike provided by sets 1 and 3. The desirability of a 3D simulation is obvious as is the necessity to proceed with a reasonable 2D approximation. The approximation used in this analysis begins with the weighted mean fracture length of 138 feet on the assumption that fractures have as great an extent normal to the model plane as in it.

The effective thickness is assumed to grow by an amount equal to the extent of the model in the E-W direction. The average effective thickness over the E-W extent of the model is then

$$\bar{T} = \frac{138 + (138 + W/2)}{2} = 138 + W/4$$

A strategy for a 3D fracture synthesis to refine the estimated effective thickness and to address the significance of flow in the third dimension is presented subsequently.

Near Wellbore Model

Figure 20 shows the model developed to try to scope effective apertures from acoustic televiewer data on fracture location and orientation and spinner data on flow distribution in the various producing/receiving zones. The model includes fractures 19, 21, 22, 24 and 66 (Table 4) which correspond to major deflections in the spinner record. Fracture 66 was not assigned an orientation since it was reentrant, i.e., it entered the borehole at a near vertical orientation and curved back out. For purposes of this analysis, it is assumed to have a 79° effective dip. Fracture 27 at the top of the figure is above the production zone but is believed to be the 1000 gpm aquifer observed in leg A of this well. Each of the fractures is assumed to extend to the boundaries of the model.

The height of the model section is defined by the complete production zone plus fracture 27. The width is that required to include all of these fractures. The effective thickness of the model, using the approximation developed in the previous section, is 160 feet. Figure 21 shows the computer version of this model, incorporating a 10 column by 14 row grid and a total of 82 fracture segments. Aperture selection and simulation results are given subsequently.

Large Reservoir Model

The acoustic televiewer data on fracture orientation and frequency have been used as a partial basis for the synthesis of a stochastic fracture system.

Table 10 summarizes three of the most interesting fracture system synthesis models from the literature. The Andersson (1984) approach is highly detailed although lacking in specific input data. The assumption that fractures are independent permits the determination of the variance of the estimate to determine, for example, whether additional sampling is warranted. Rouleau (1984) presents a synthesis based on Stripa data including an adjustment of mean aperture to match a measured macropermeability. Long (1982) used data from Baecher and Lanney (1977) and determines the valid regimes for porous and discrete fracture approaches. Sledz and Huff (1981) used

extensive data on the variation in shale and siltstone fracture characteristics over an area to synthesize porous media properties. Huang (1984) has synthesized 3D fracture networks from inputs of shape and distribution of location, orientation, size and aperture.

The synthesis procedure used in this study is that given by Andersson. The model again lies in a vertical plane with E-W strike. The length and width were arbitrarily chosen as 500 feet. A stochastic realization of each of the five orientation sets is created by:

1) drawing a convenient scan-line through the center of the model
2) selecting a location on the scan-line equally probable over its length
3) determining the model chord cut by an infinite line at the selected location and with the set orientation
4) selecting a length from a distribution assumed, on the basis of the literature, to be log normal. The mean length of each set was selected as 3.5 times the mean perpendicular spacing of that set, based on the 3-4 range given by Gale (1982). The standard deviation of the log of the length was taken as corresponding to a doubling of the mean length.
5) selecting a distance from the scan-line along the fracture to its center which is equally probable over the interval

$$-\frac{C+1}{2}, \frac{C+1}{2} \quad \text{where}$$

C is the chord length and 1 is the fracture length. The fracture is now completely determined and may be added to the sketch.
6) the procedure is continued until the total number of fractures intersecting the scan-line equals the number required by the mean separation and the length of the scan-line.

Table 11 summarizes the synthesized fracture system. Figure 22 shows all of the synthesized fractures for sets 4 and 5, which have relatively great mean separation. A total of 778 fractures were synthesized for sets 1, 2 and 3. The longest of these are shown on the figure. It should be

noted that the figure has been rotated 11°CW to align the steeply dipping fracture set with the vertical axis.

Figure 23 shows the computer model of the same system, again rotated 11°CW. The longest of the steeply dipping fractures have been collected laterally along the 14 columns. The effective aperture of a combination of fractures is computed as the cube root of the sum of the cubes of the individual apertures. The model has a 14 column by 16 row grid and a total of 230 net fracture segments.

An extension of the synthesis procedure to refine the effective thickness estimate is given as follows: The fracture set orientation is taken, for simplicity, normal to the scanline. The planar model is enclosed by a right cylinder with the scanline as its centerline. The model chord found in step 3 is now the diameter of the cylinder. A new step (5.5) is added to select an angle, equally probable over the interval from 0 to 360°, for the line from the scanline to the center of the fracture. Circular fractures are now synthesized in three-dimensional space. The development of flow area in these and fractures of the other orientation sets, from the well injection point at the center of the cylinder and in the direction normal to the enclosed 2D model plane, can now be evaluated.

RESERVOIR SIMULATION

The near wellbore model described in the preceding section has been used to simulate some of the tests conducted at the Raft River test site in late 1982. The following sections summarize the test program and the preliminary hydrologic studies performed with the smaller model of the known fractures in the wellbore region.

Raft River Test Program

The geology of the Raft River KGRA and a drawing and verbal description of the well construction have been presented in an earlier section. The intent of the test program was to help develop and ultimately to verify new techniques for reservoir analysis for operation with simultaneous injection and production. The basic test procedure was to inject a fluid into a well with tracers and to then backflow the well and monitor the return of the tracers. Chemical analyses were performed on the injected and returned fluid and system pressure, temperature and flows were monitored during the test. From these data information on flow, dispersion, chemical reactions and heat transfer in the formation was deduced.

Table 12 presents a brief summary of the test program. A typical test involved injecting a tracer at a specified rate and duration, allowing a period of quiescence and then backflowing a sufficient volume of fluid to recover all of the injected fluid. Tracers were incorporated both continuously and as short duration slugs. The initial test was limited to injecting and recovering tracer from the wellbore itself. The remaining tracer tests involved injection into and recovery from the formation. The effect of increasing injection volume was studied in test series 2. Studies of natural drift in the reservoir were made in the test 4 series by varying the quiescent time between injection and backflow. Test 5 was a long duration test to accomplish breakthrough to well RRGE-1, approximately .5 miles away (breakthrough was not achieved). The final portion of test 5 incorporated a series of short term backflow (pulse) tests at flows ranging from 75-325 gpm.

Figures 24 through 27 show the test results most indicative of the flow and dispersion phenomena being correlated in this simulation study.

The wellhead pressure decrease at the initiation of backflow and the pressure recovery at the termination of backflow are shown in Figure 24. The data is presented as curves of net pressure change at fixed times vs. flow rate. Each of the test data points were obtained by regression through a pressure oscillation caused by the rapid starting or stopping of the backflow. The test data shown is for 50 seconds with the build-up on recovery consistently higher than the drawdown on flow initiation. A curve has been drawn as the mean of the two. It is apparent that the variation with flow rate is non-linear, probably reflecting some turbulent losses in the wellbore and the initial fractures. The estimated wellbore pressure loss at 150 gpm, assuming commercial steel, is approximately 0.8 psi. As much as half of the total pressure loss may be due to turbulent losses, based on an extrapolation of the inital slope of the curve.

A similar curve is shown for the pressure changes at 30 seconds. These two curves, in conjunction with the repeated observation of pressure leveling at 20 psi (150 gpm tests) at approximately 1.5 minutes, show a rapid exponential rise or fall to the equilibrium level.

Figure 25 shows the reduced concentration curves for the three tests in the variable volume series. The ordinate of this curve is the reduced concentration or the ratio of the return concentration to the injected concentration. The abscissa is the reduced volume or the ratio of return volume to injected volume. The injection phase, volumes from -1.0 to 0.0, is at a nominal reduced concentration of 1.0. If this injection and a subsequent backflow were made into a pipe, the backflow portion of the curve would be the mirror image of the injection portion and would drop back to 0. at a reduced volume of 1.0. This process is purely advective movement.

The measured curves show a delay in the return of a large part of the tracer. This delay is due to dispersion in the formation. This return curve shape, particularly the extended tail, is typical of fractured media.

Figure 26 shows reduced concentration curves for pipe flow and for a one-dimensional solution of the advection-dispersion equation. The curve for the smaller Peclet number (see definition on figure) is closer to that observed at Raft River. This comparison is qualitative only because of the

1D approximation and because of the application of porous media theory to a fractured media.

The two figures together indicate the significance of dispersion in the Raft River formation and indicate that the relative proportion of advection and dispersion processes is unchanged as the injection volume is increased.

Figure 27 shows the raw concentration vs. recovery time data for the slug tracers in the 96 hour injection test, no 2D. The Iodide slug was injected at the beginning of the injection period and the Boron slug was injected 24 hours later.

Near Wellbore Model Simulation

Simulation of the hydrology near the wellbore was performed with two different sets of apertures in order to study the possible range of values.

In the initial study, the hydrofracture aperture was set at .025 feet. This is one half of the maximum apparent aperture given by the USGS in their review of the acoustic televiewer log. The fracture segment immediately above the injection point, which corresponds to the bottom of the liner, was closed for simulation purposes. This causes all of the injected flow to move downwards to the five intersecting fractures whose locations on the acoustic televiewer log correspond to major spinner deflections as shown in Figure 16. Fracture 29, the 18° dip fracture at the top of the model, is thought to be the major aquifer which yielded 1000 gpm in leg A of this well. Its effective aperture was set equal to that of the hydrofracture at .025 feet.

The distance from each of the boundary modes to the zero head location discussed in the FRACSL code section was arbitrarily selected as 1000 feet. The apertures of each of the five fractures intersecting the hydrofracture below the wall liner was initially set at .025 feet. Starting from the one closest to the wellbore, the upper four were adjusted until the distribution of flow leaving the hydrofracture matched that measured by the spinner tool. The resulting apertures moving down from the well liner were .0095, .0095, .018, .018 and .025 feet. The resulting head at the injection node was .036 feet. A total of 49% of the injected flow left the model in the two ends of the uppermost (major aquifer in leg A) fracture. The largest flow was

from the right end of this fracture, at 33% of the total. The head at this point was .024 feet. The remainder of the heads at the model nodes ranged from .023 to .035 feet.

Approximately two thirds of the head rise in the system, corresponding to a 150 gpm injection rate, occurred outside of the model due to the choice of the 1000 feet length to the zero head location. The choice of a minimum value of this dimension would have reduced the head rise by a factor of 3. A much more sensitive parameter in this simulation is the effective aperture since the head, for the same flow, varies inversely as the cube of the aperture.

A second case was therefore run with all of the apertures reduced by a factor of 10. The flow distribution was only slightly changed, but the head at the injection node was increased to 34.6 feet. As discussed in the review of the test program, the steady state pressure rise was measured as 20 psi (49 feet of head). Since some of the head rise can be attributed to wellbore and turbulent flow losses not included in the model, the simulation value is within reason. While not conclusive the implication is clear that the apertures may be relatively small.

The final simulation performed with this model was an attempt to match the transient character of the drawdown or recovery pressures. Figure 28 shows the transient head rise at the injection point for a number of values of specific storage. While matrix flow velocities are very low, the fluid storage in the model is within the matrix. Specific storage coefficients are given by Domenico (1972) for fissured and jointed rock as 1.E-6 to 2.1 E-5 per foot with lower values for sound rock. Figure 28 shows the transient head rise for values of 1.E-7, 1.E-6 and 1.E-5 per foot. Reasonable agreement with test data is shown for the smallest value of specific storage. Since the volume of the model and the flow boundary condition influence the result this answer is again of a scoping nature.

Dispersion calculations were deferred to the larger model and the synthesized fracture system.

Large Reservoir Model

While steady state flow and marker particle calculations have been performed, the results have not been sufficiently developed to be reported.

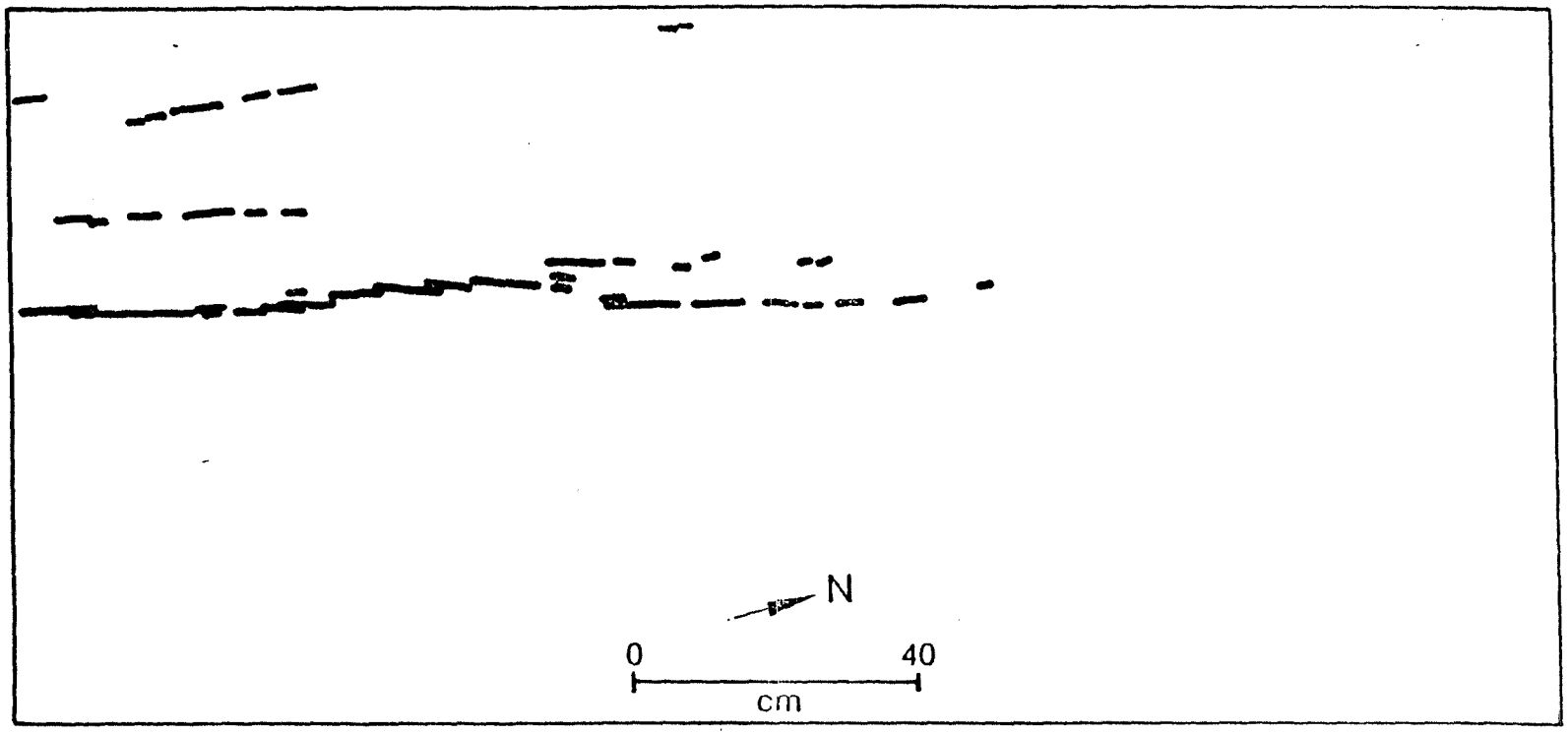

INEL 4 0658

FIGURE 1. Detailed map of joint termination at the Ward Lake outcrop in the Sierra Nevada, California. (Segall & Pollard, 1983)

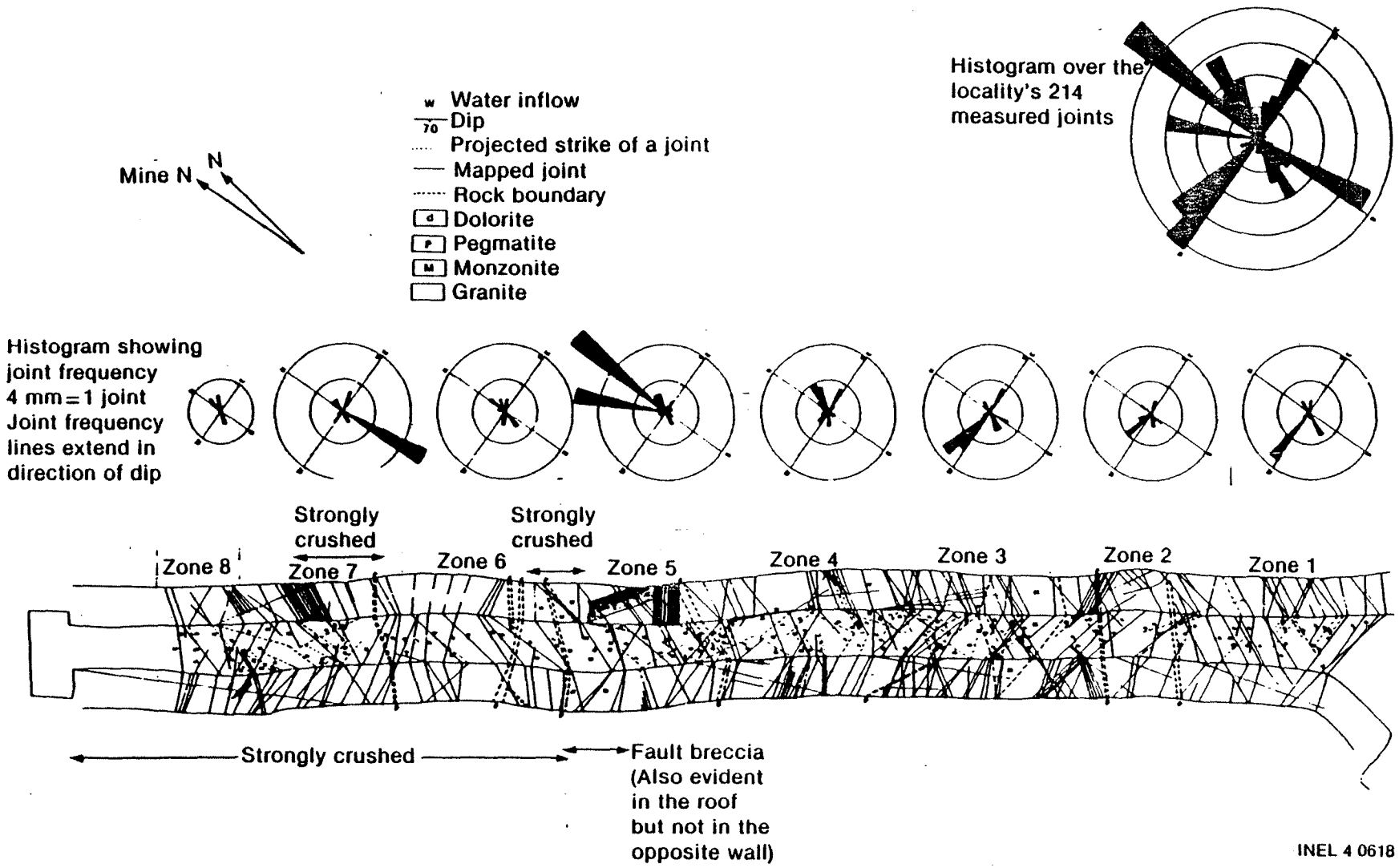

FIGURE 2. Rock-types and fracturing within the ventilation tunnel at the 360-m level, Stripa Mine, Sweden. Original scale 1:100. (Olkiewicz et. al., 1979)

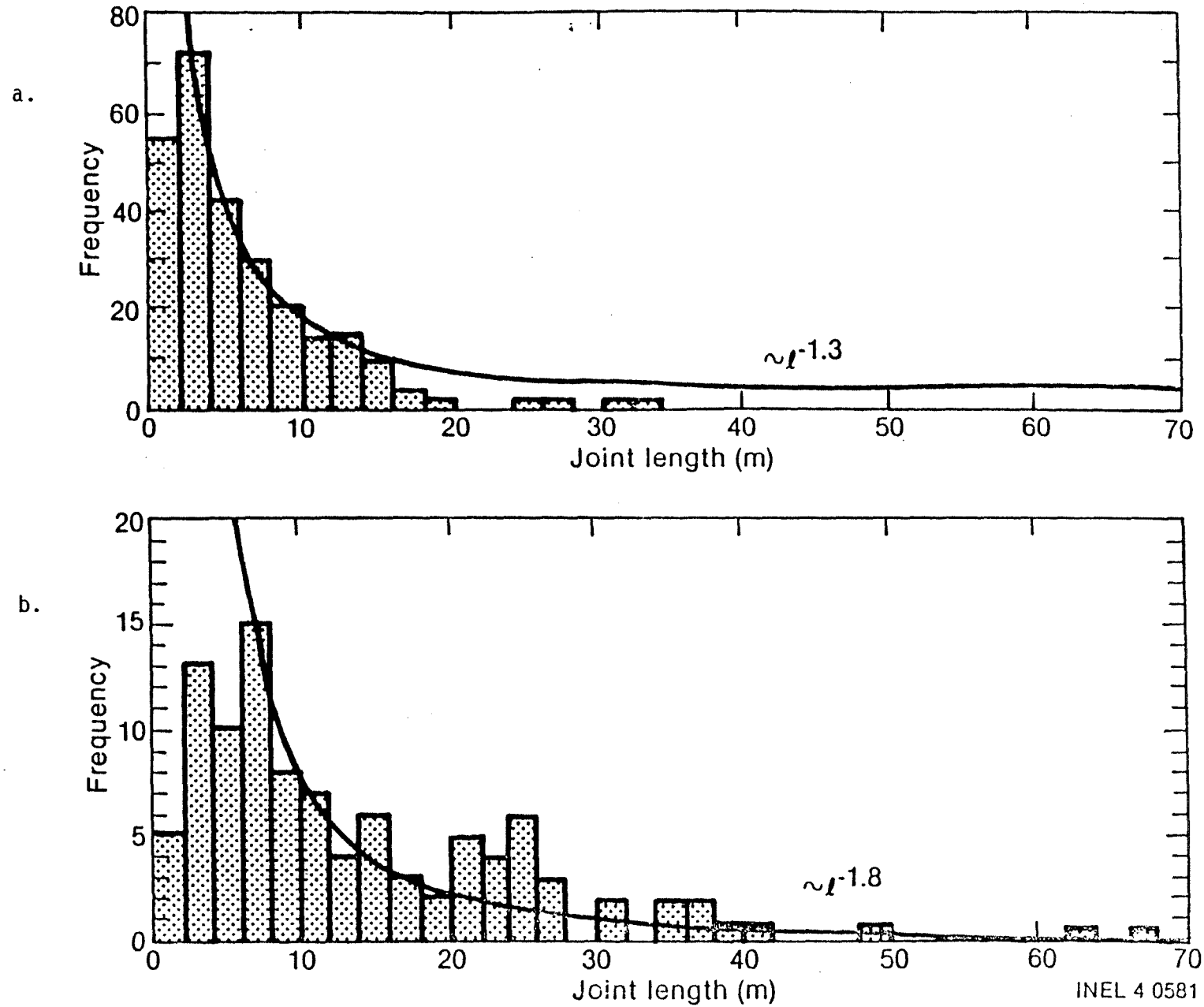

FIGURE 3. Distribution of joint lengths a. Florence Lake outcrop. b. Ward Lake outcrop, Sierra Nevada, Cal nia. Histograms show obse data, and curves show possible power-law ibutions. (Segall and ,1983)

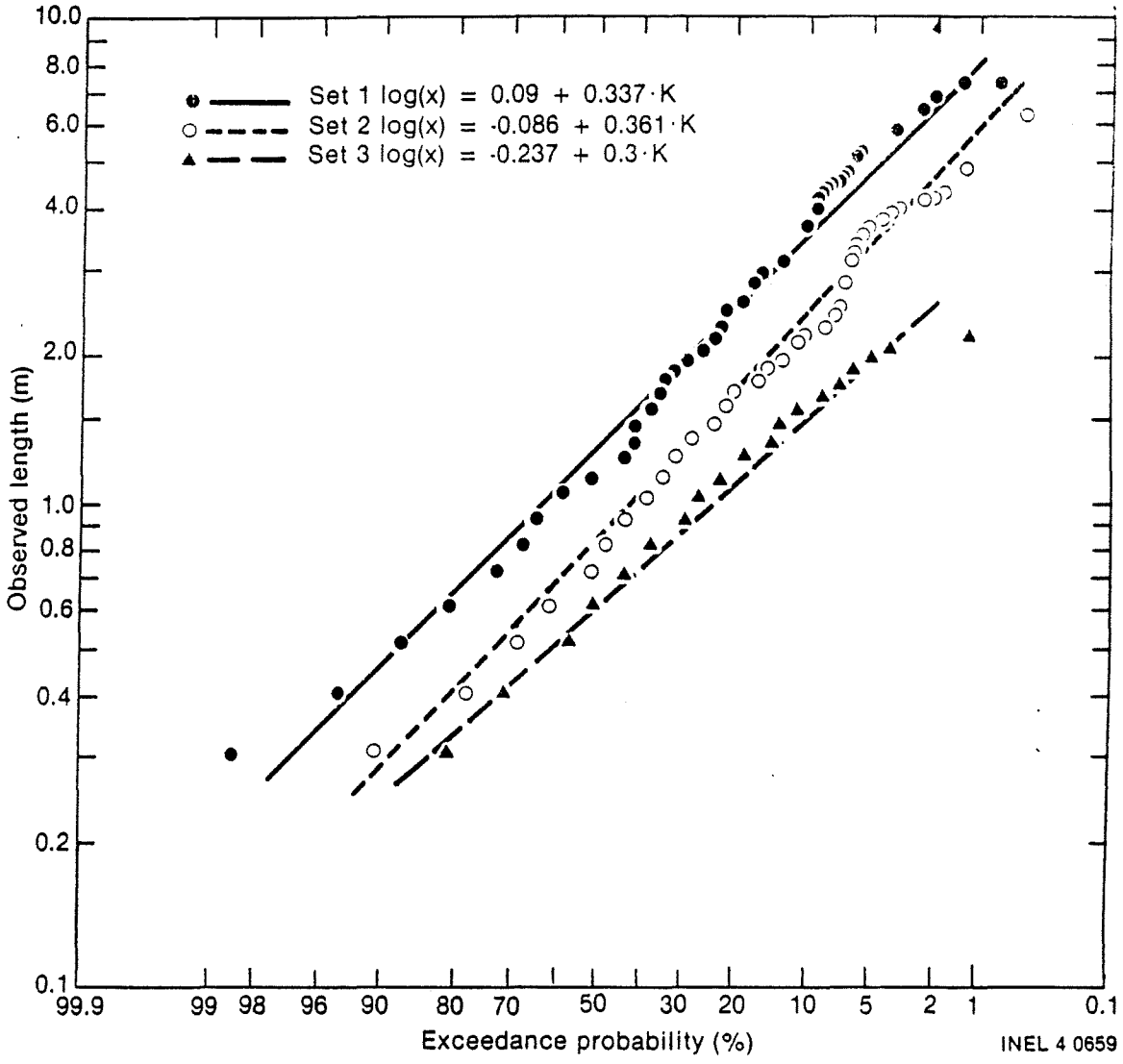

FIGURE 4. Lognormal joint length distribution at the time-scale heater experiment, Stripa Mine, Sweden (Thorpe, 1980).

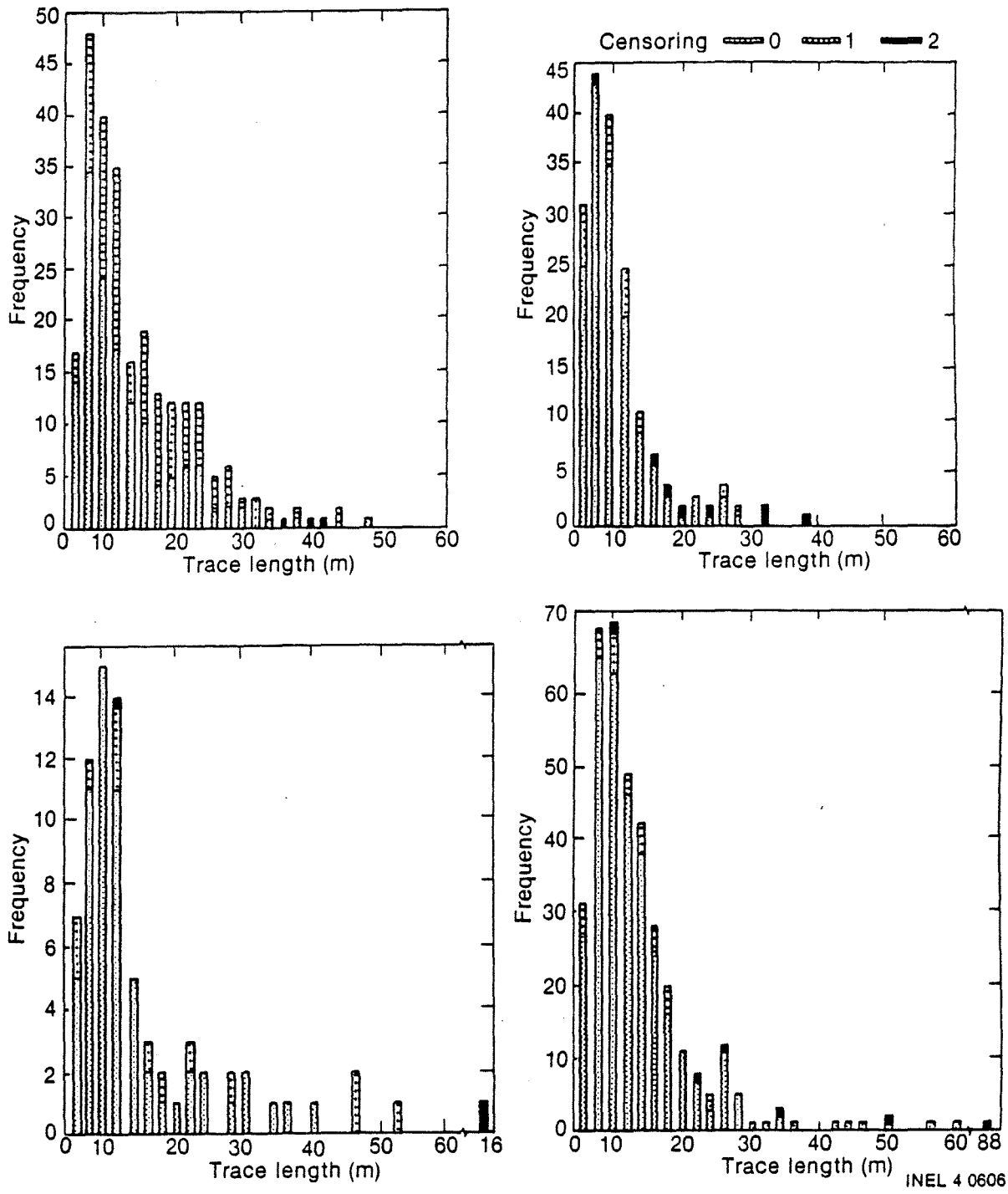

FIGURE 5. Histograms of fracture trace lengths on the faces of the ventilation drift, Stripa Mine, Sweden. (Rouleau and Gale, 1984)

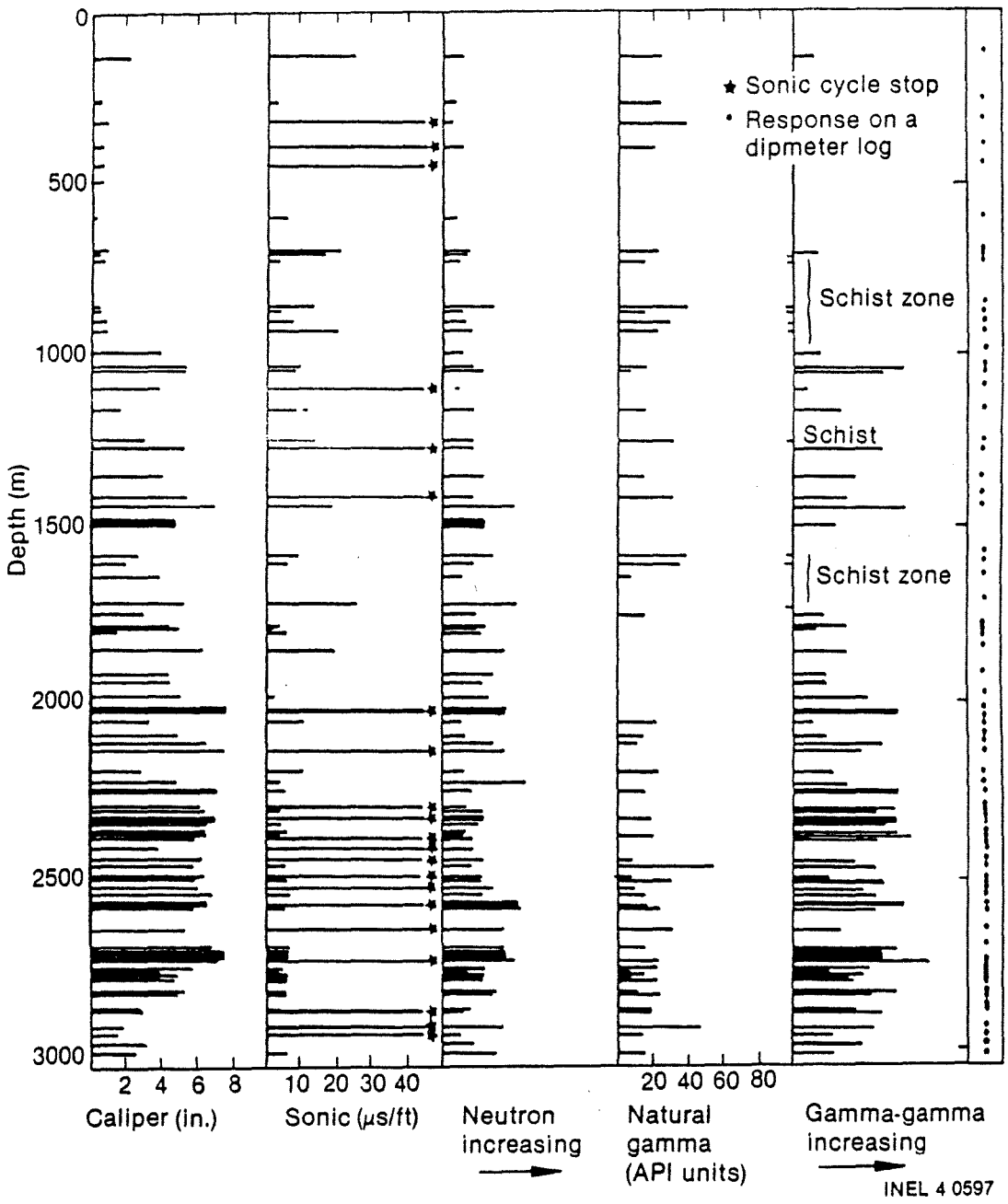

FIGURE 6. Net positive or negative amplitudes of typical fracture responses on various logs at Reynard Lake pluton, Saskatchewan, Canada. (Davis and Tammemagi, 1982)

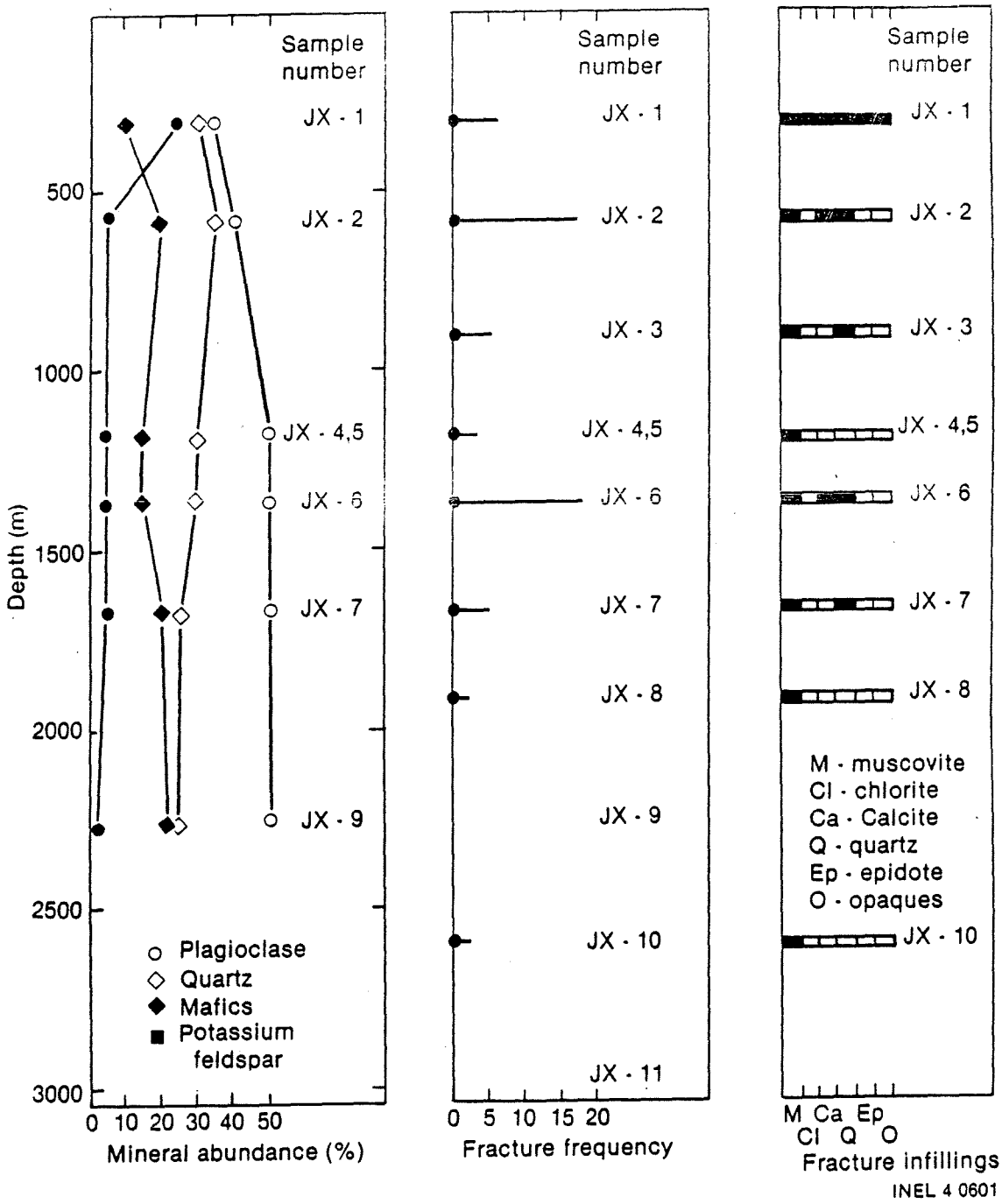

FIGURE 7. Data obtained from Petrographic Analysis at Reynard Lake pluton, Saskatchewan, Canada. (Davis and Tammemagi, 1982)

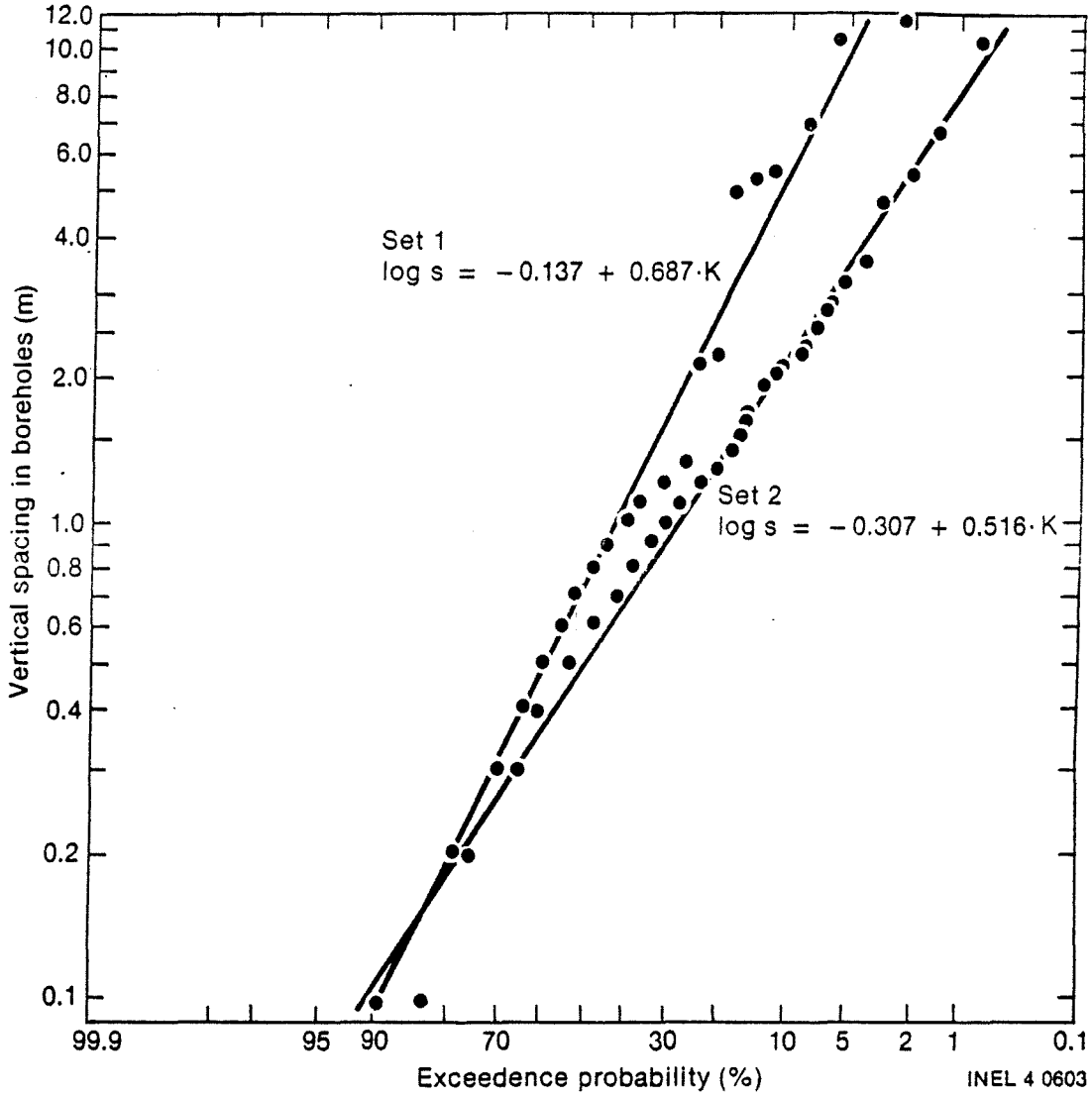

FIGURE 8 (a)Lognormal plots of joint spacings for (a) sets 1 & 2 and (b) sets 3 & 4 at the time-scale heater experiment, Stripa Mine, Sweden. (Thorpe, 1980)

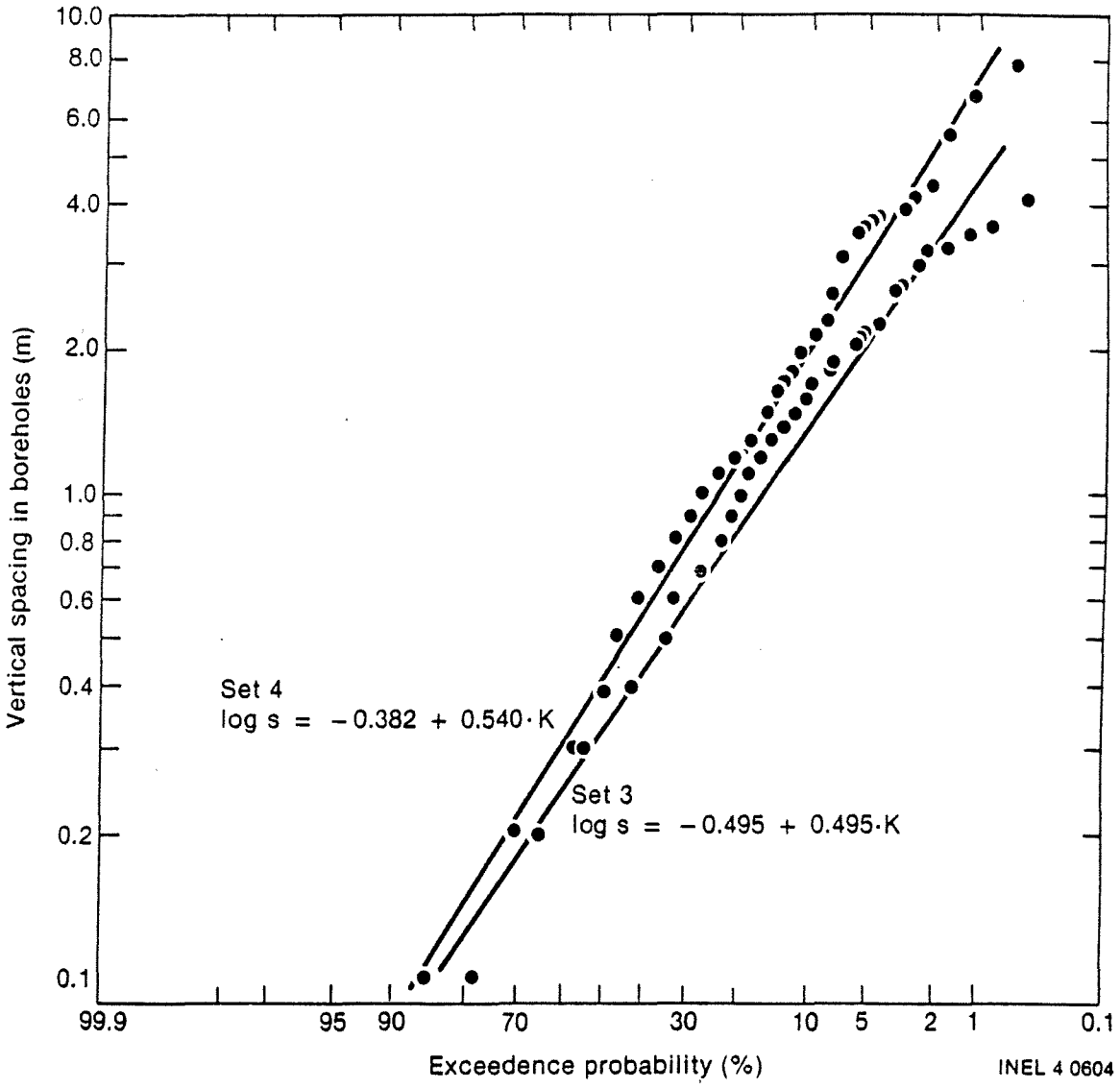

FIGURE 8 (b)Lognormal plots of joint spacings for (a) sets 1 & 2 and (b) sets 3 & 4 at the time-scale heater experiment, Stripa Mine, Sweden. (Thorpe, 1980)

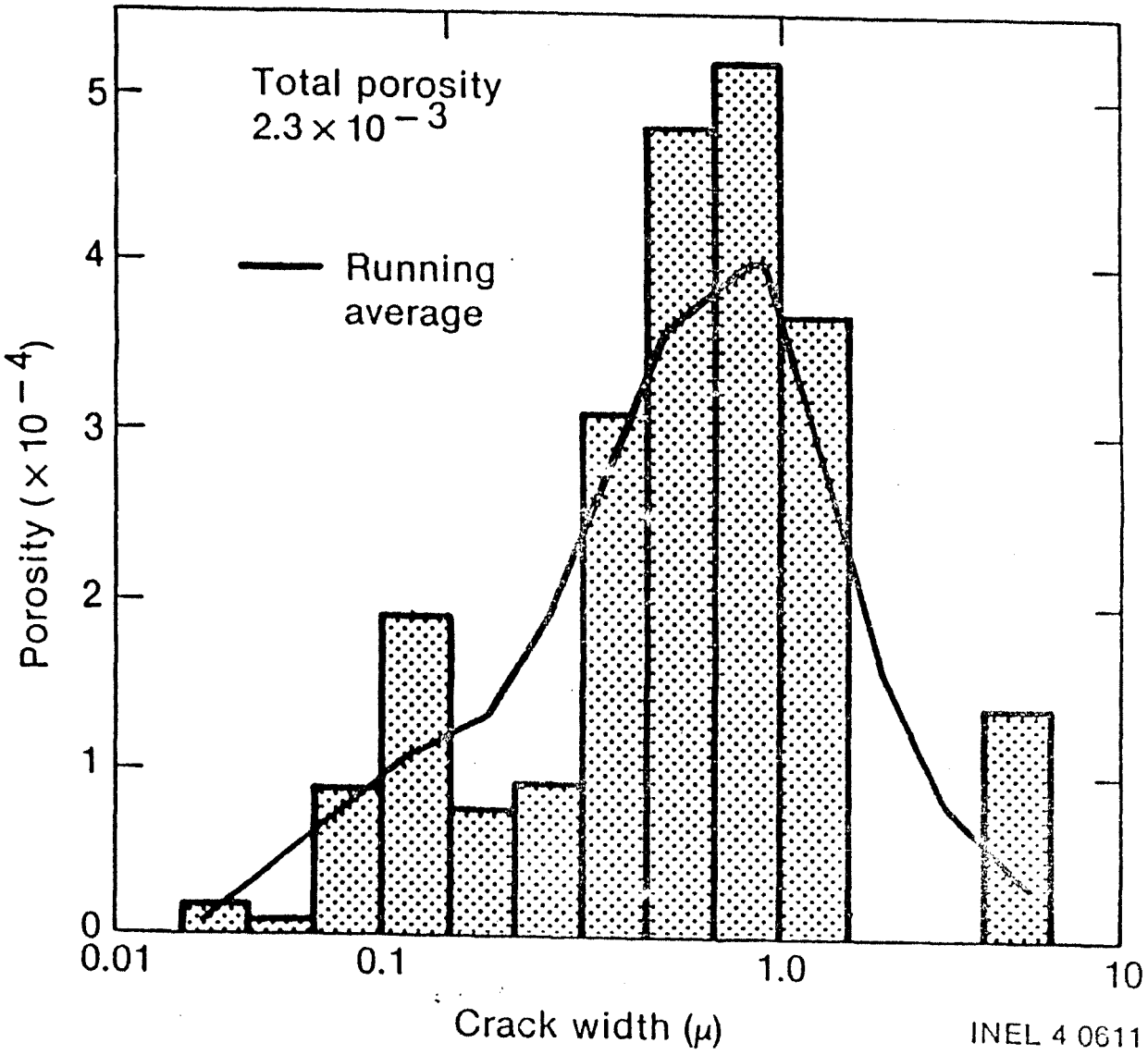

FIGURE 9. Pore size distribution for WN1-160.7, Pinawa, Manitoba, Canada, scanning electron microscope analyses. (Chernis, 1981)

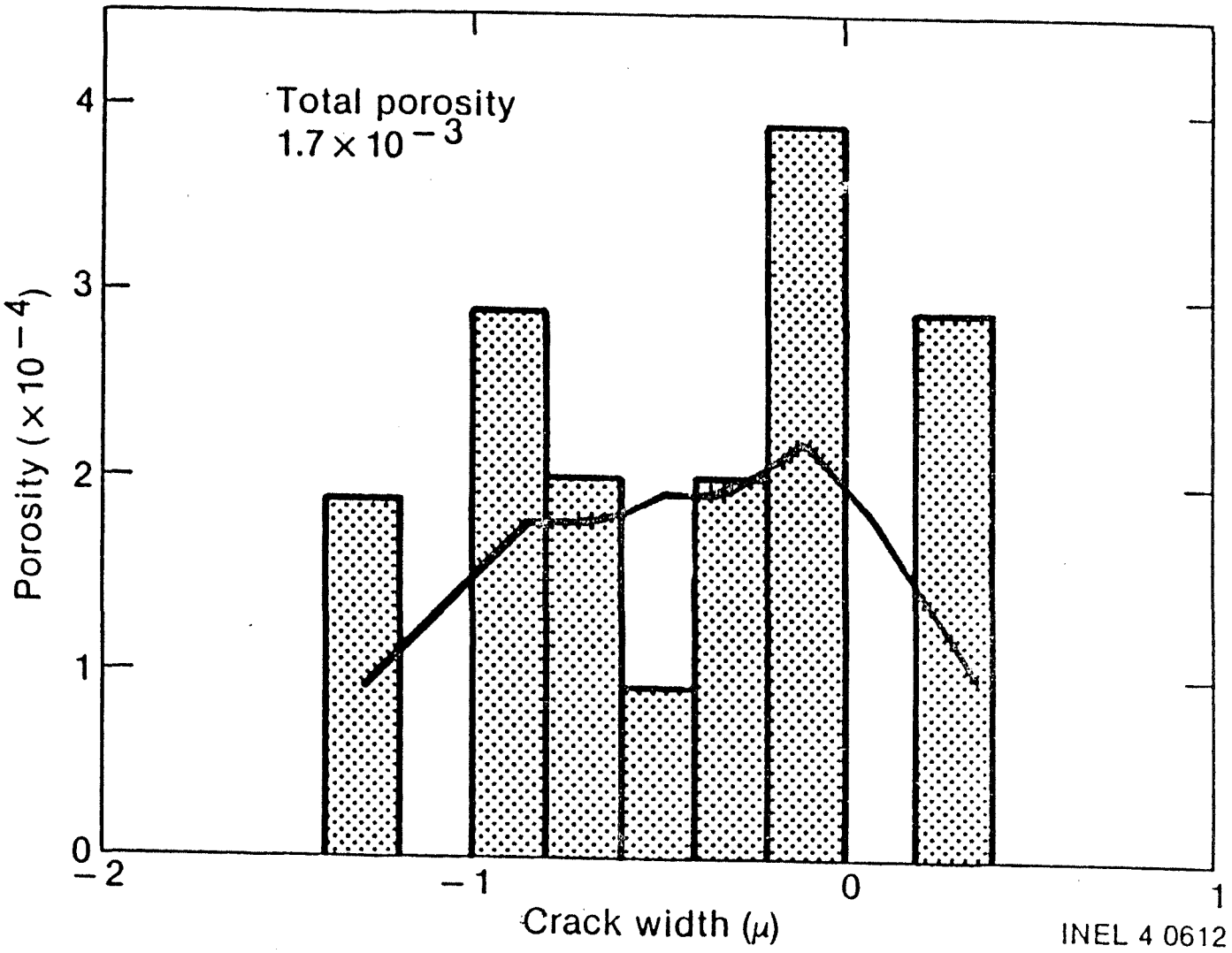

FIGURE 10. Pore size distribution for another sample , Pinawa, Manitoba, Canada. Produced by Mercury Porosimeter. (Chernis, 1981)

FIGURE 11a. Thermally cycled Westerly granite. (a) 1 bar. The fracture has formed around a quartz grain Q, through a K-feldspar K, and into a plagioclase P grain. (b) 50 bars. Closure is almost complete along portions of the fracture oriented normal to the applied stress. (Batzle, et. al., 1980)

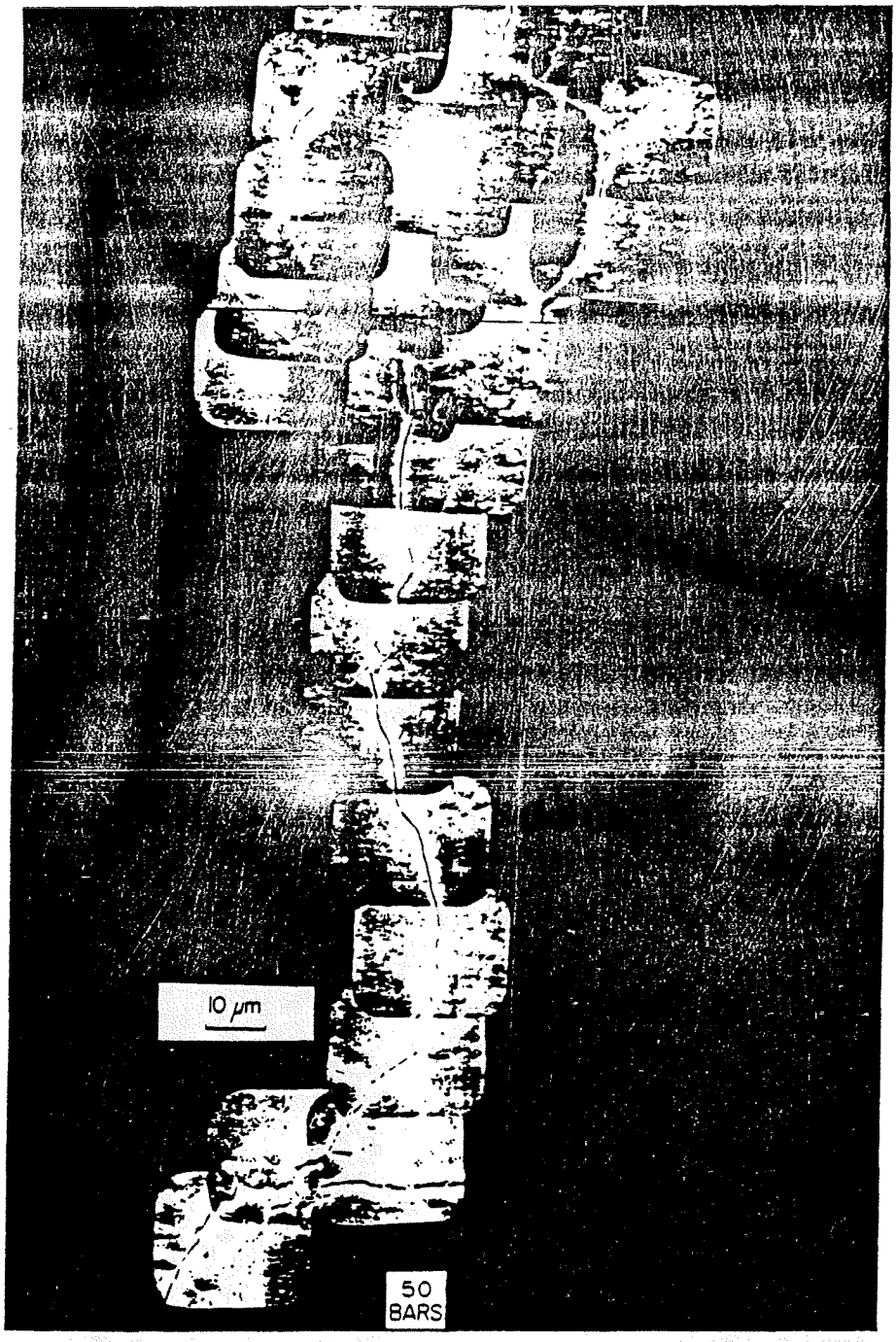

FIGURE 11B

RRGP-5BF Well Construction

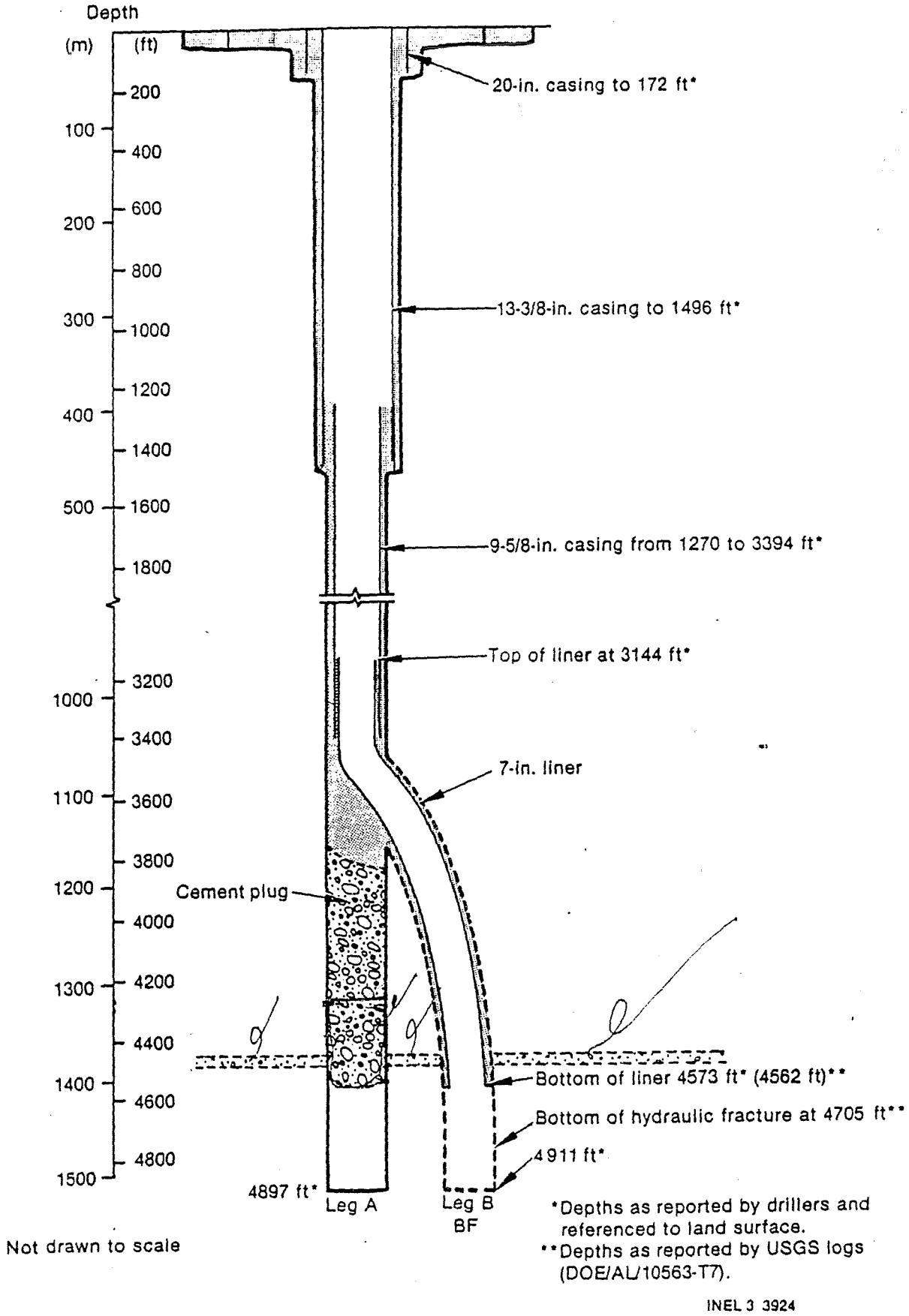

FIGURE 13

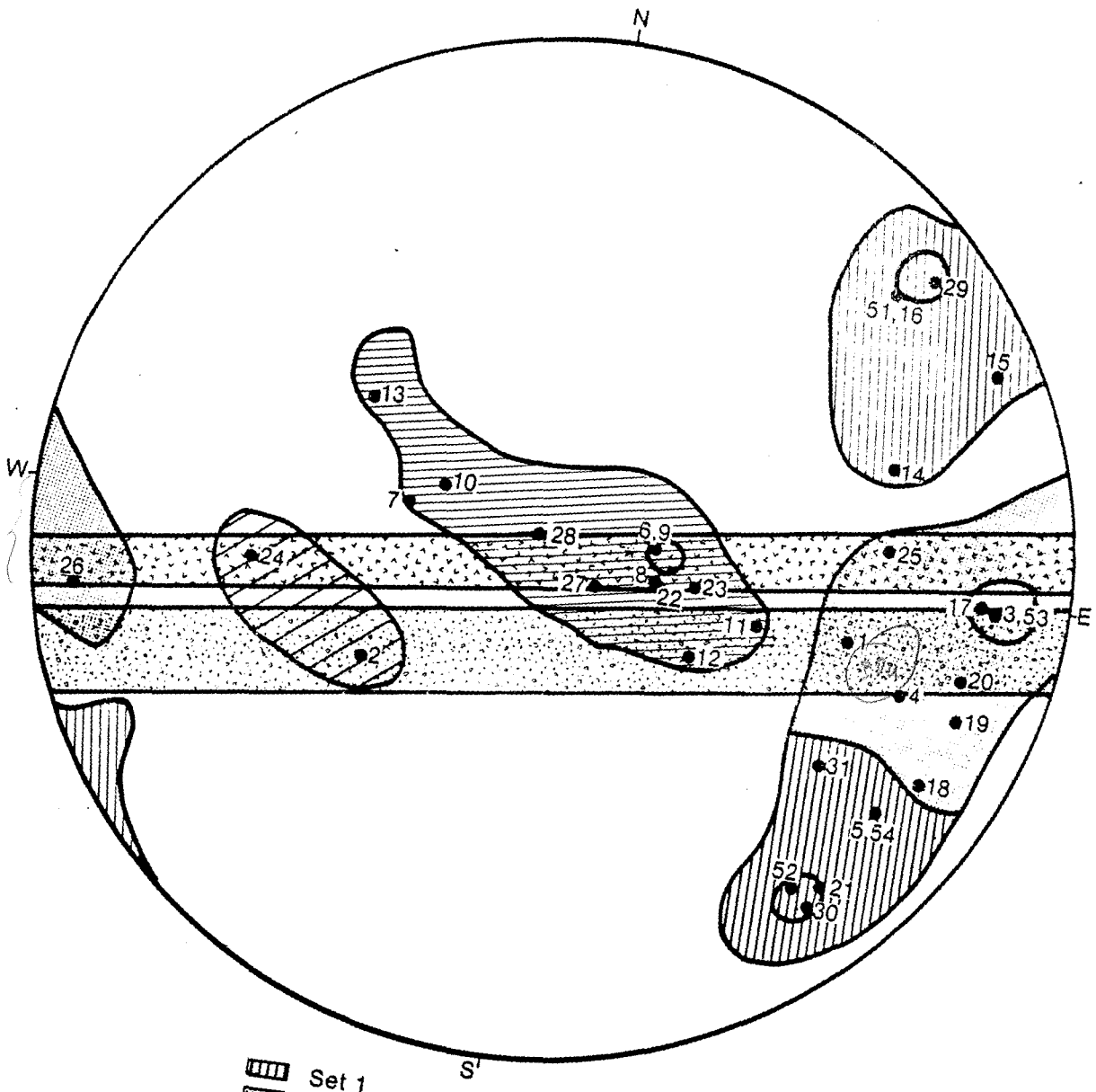

FIGURE 14. Equal area stereonet for 35 acoustic televiewer discontinuities in RRGP-5B between depths of 1341.1 and 1491.9m (4400 and 4895 ft.)

FIGURE 15. Vertical profile of discontinuity orientations and density for RRGP-5B.

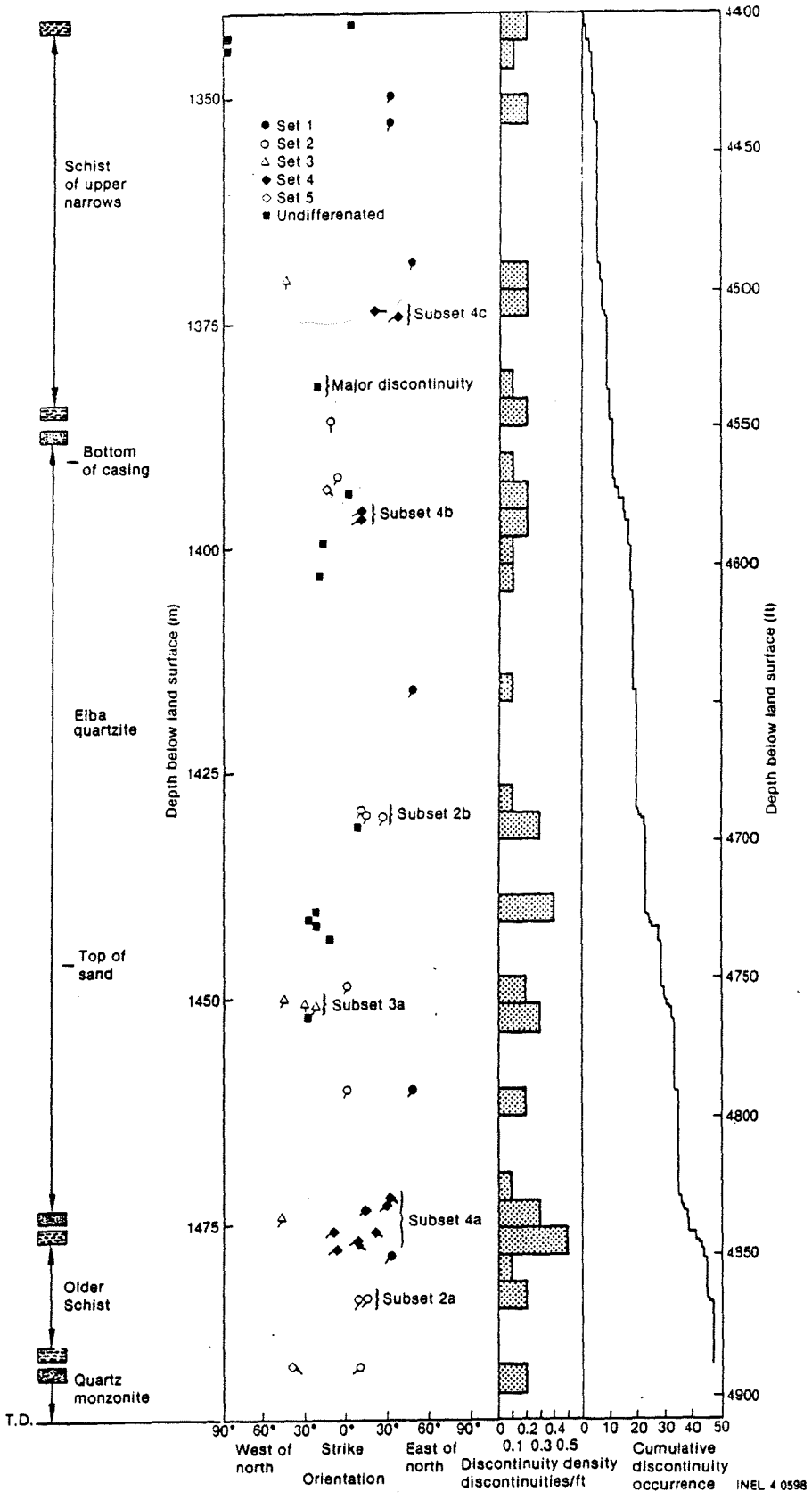

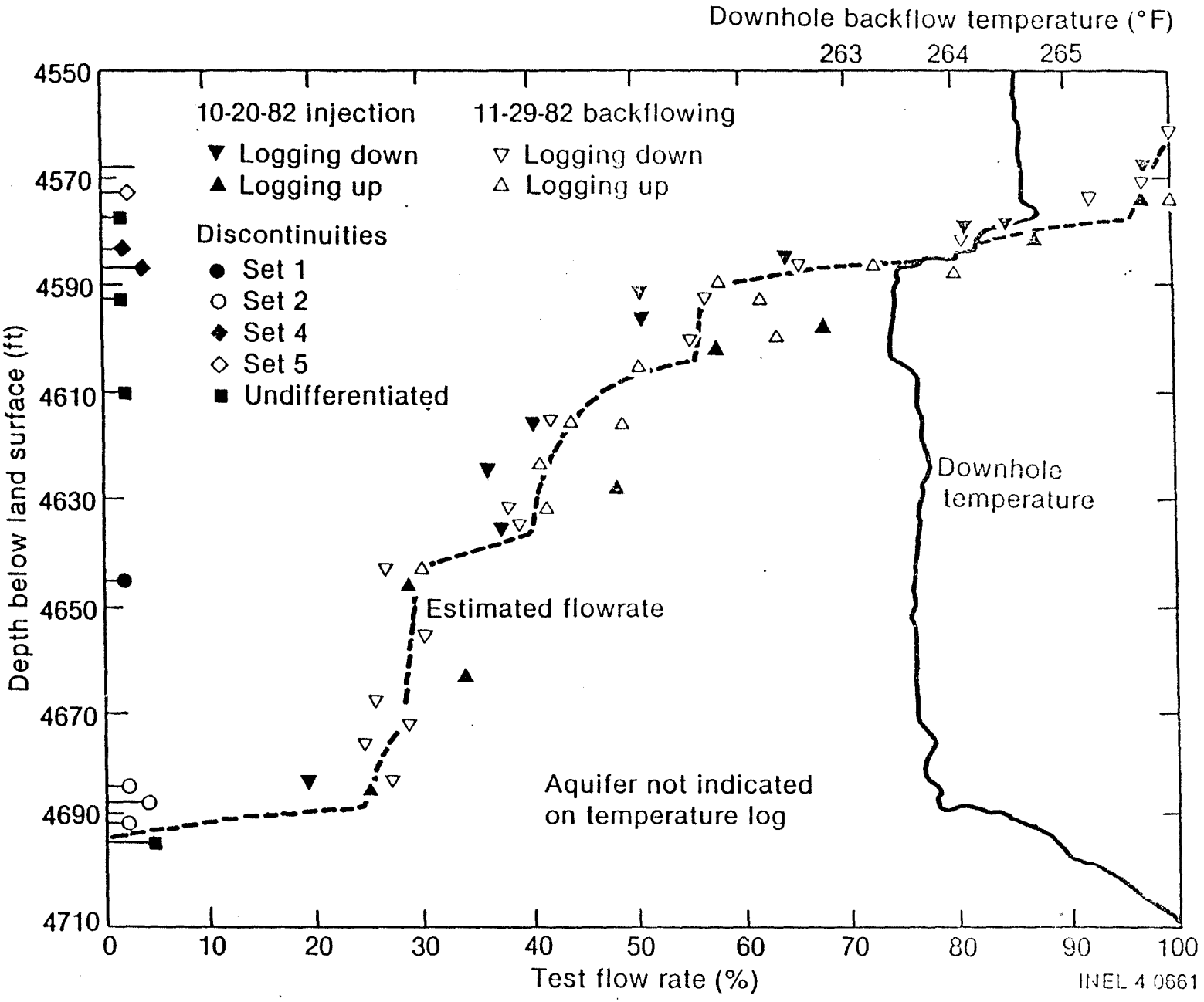

FIGURE 16. Production/receiving zones discharge/uptake as a percentage of flow rate and discontinuity locations for RRGP-5BF. A temperature log during backflow of test 2D is also plotted.

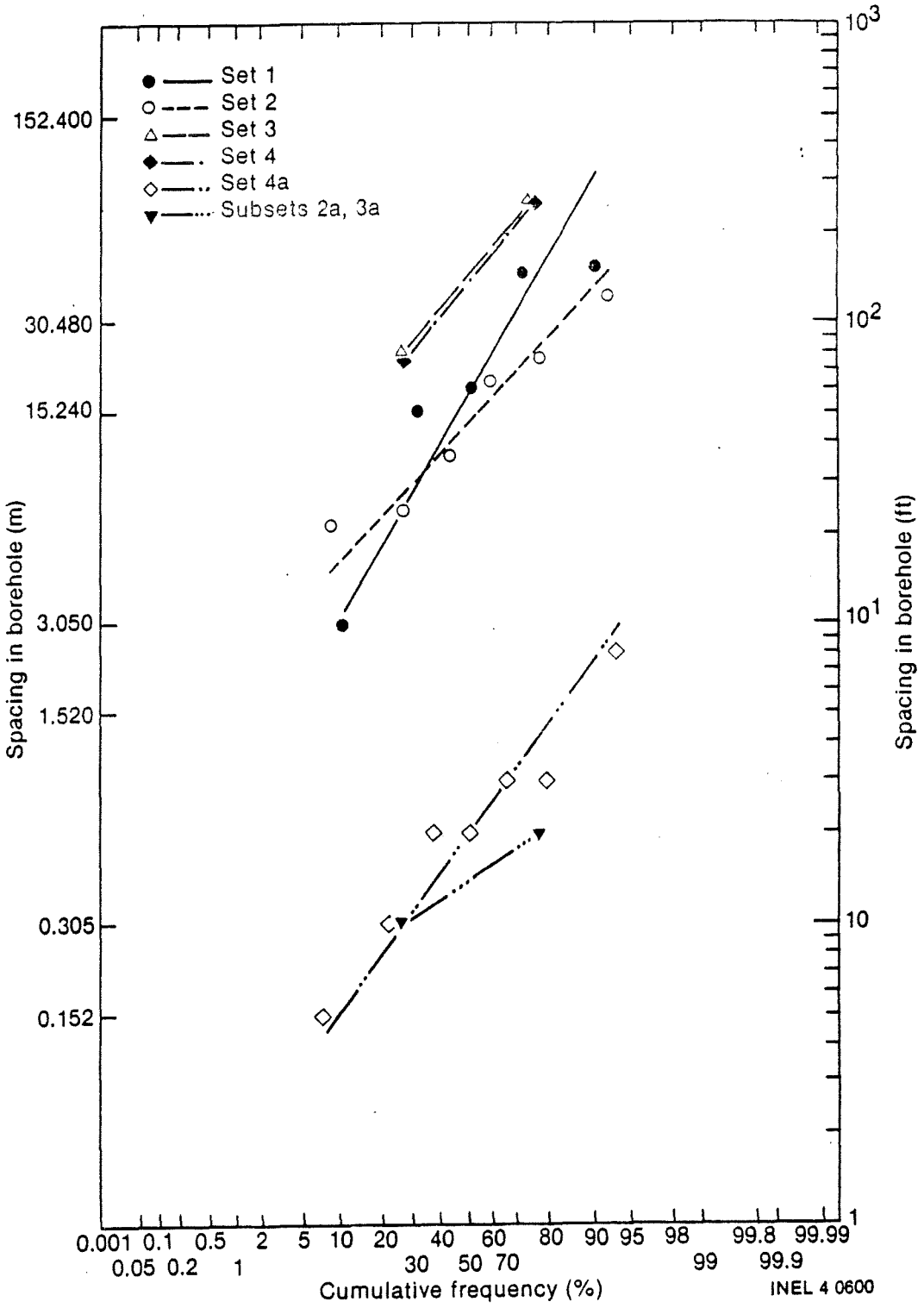

FIGURE 17. Probability distribution for wellbore spacing of discontinuity sets and subsets in RRGP-5 B.

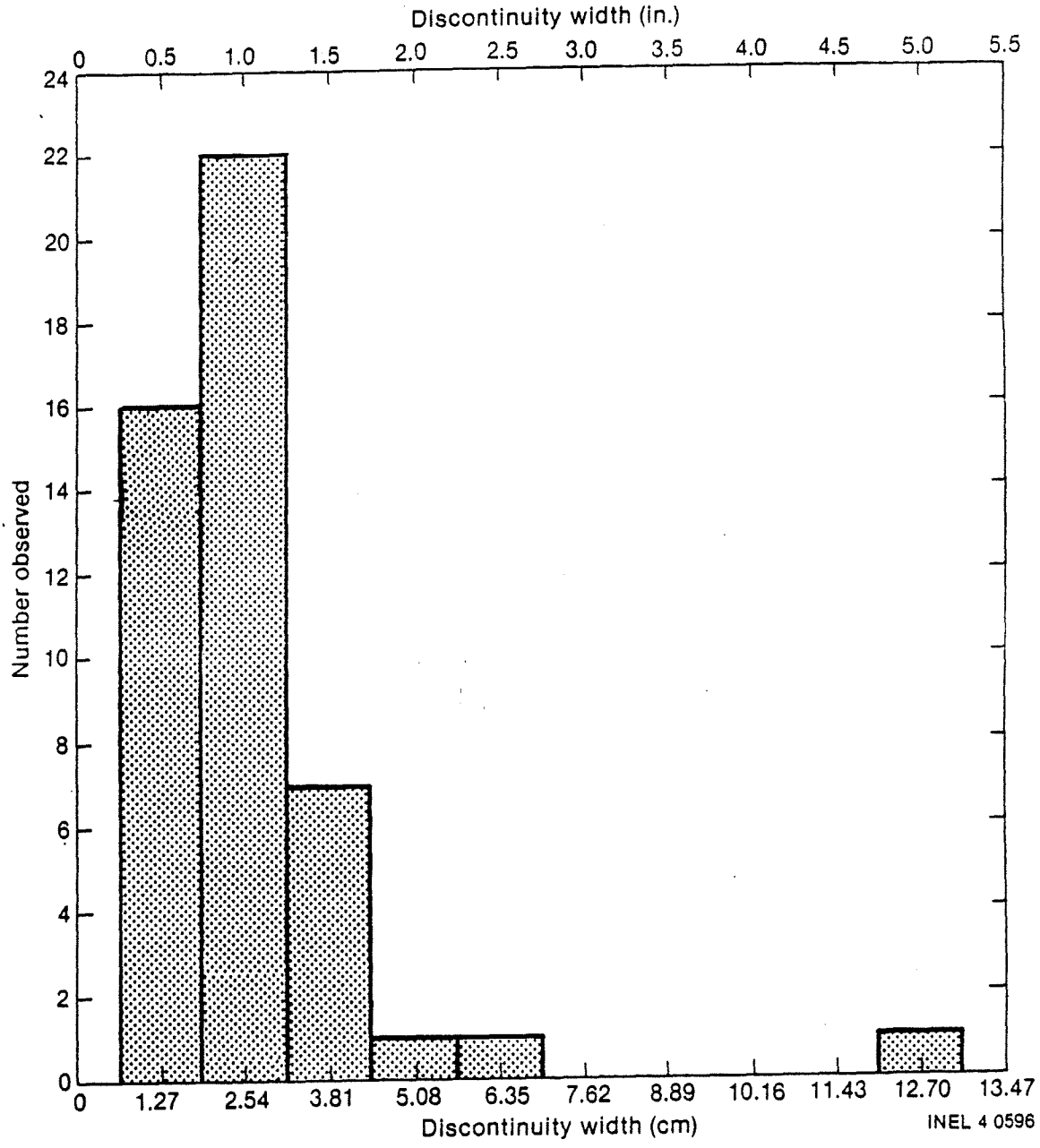

FIGURE 18. Discontinuity widths for all discontinuities.

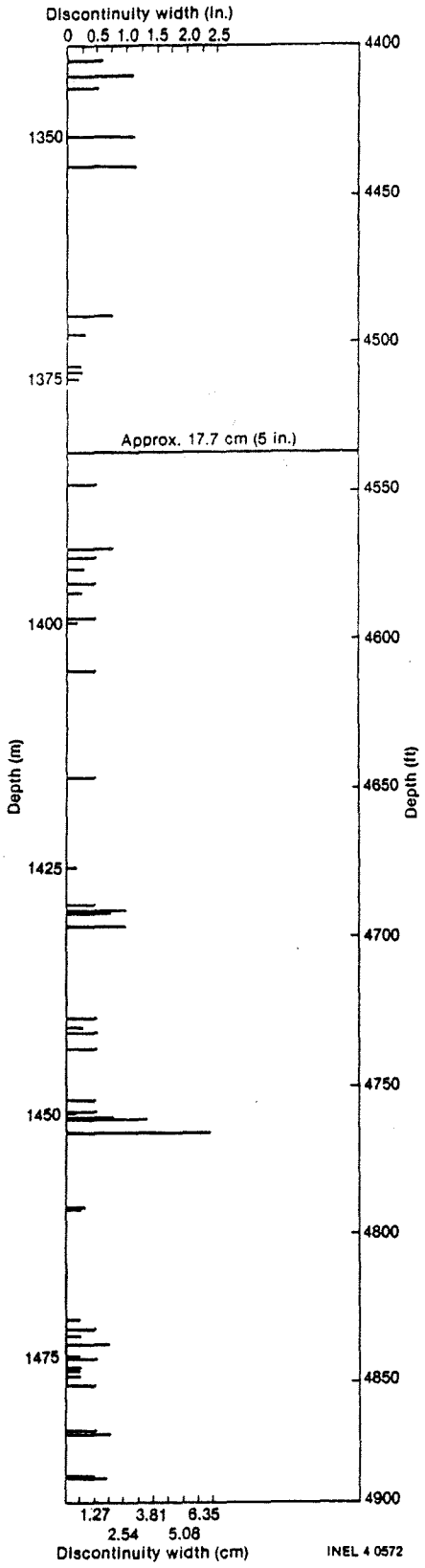

FIGURE 19. Vertical distribution of discontinuity apertures for RRGP-5 B.

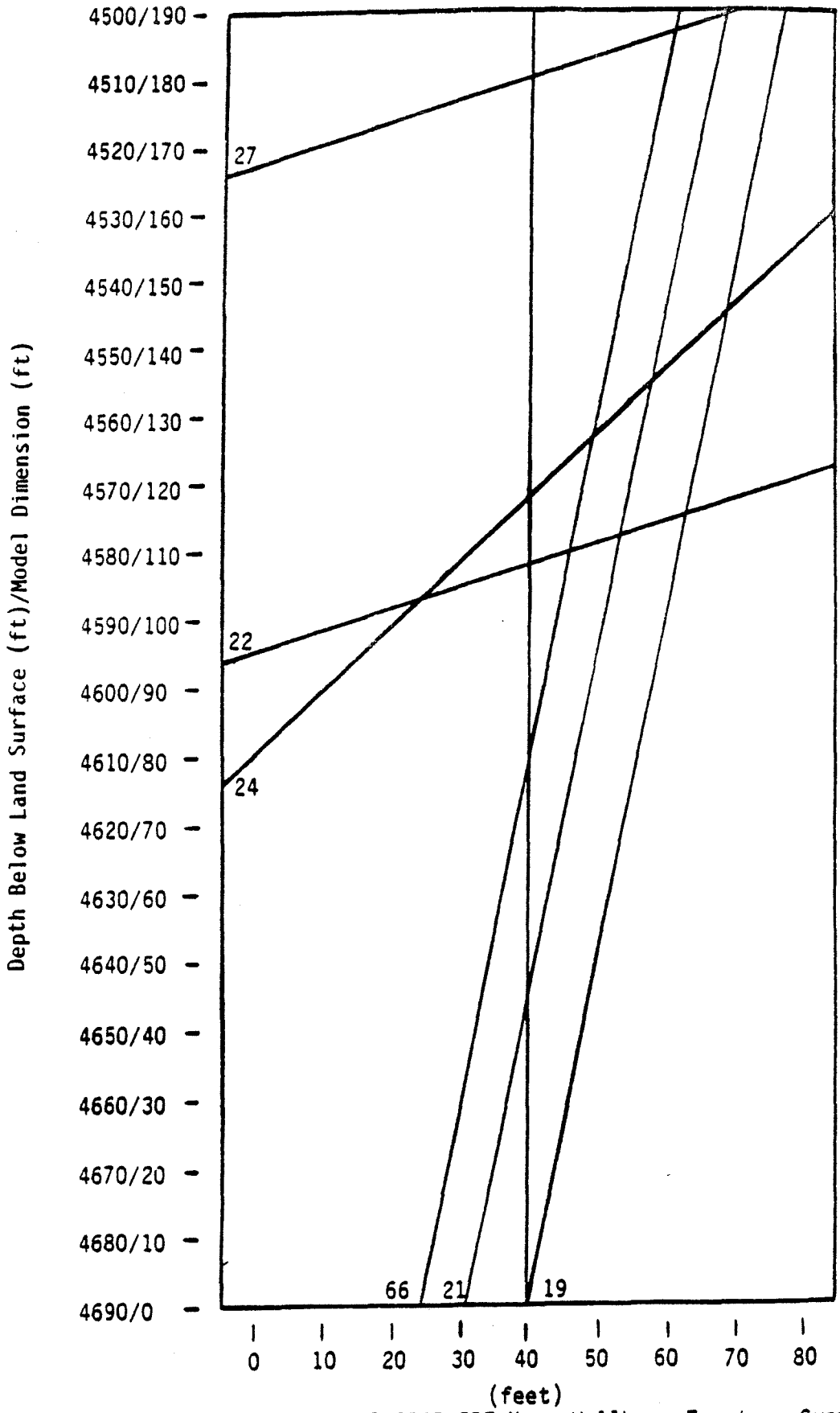

Figure 20. Raft River Well RRGP-5BF Near Wellbore Fracture System

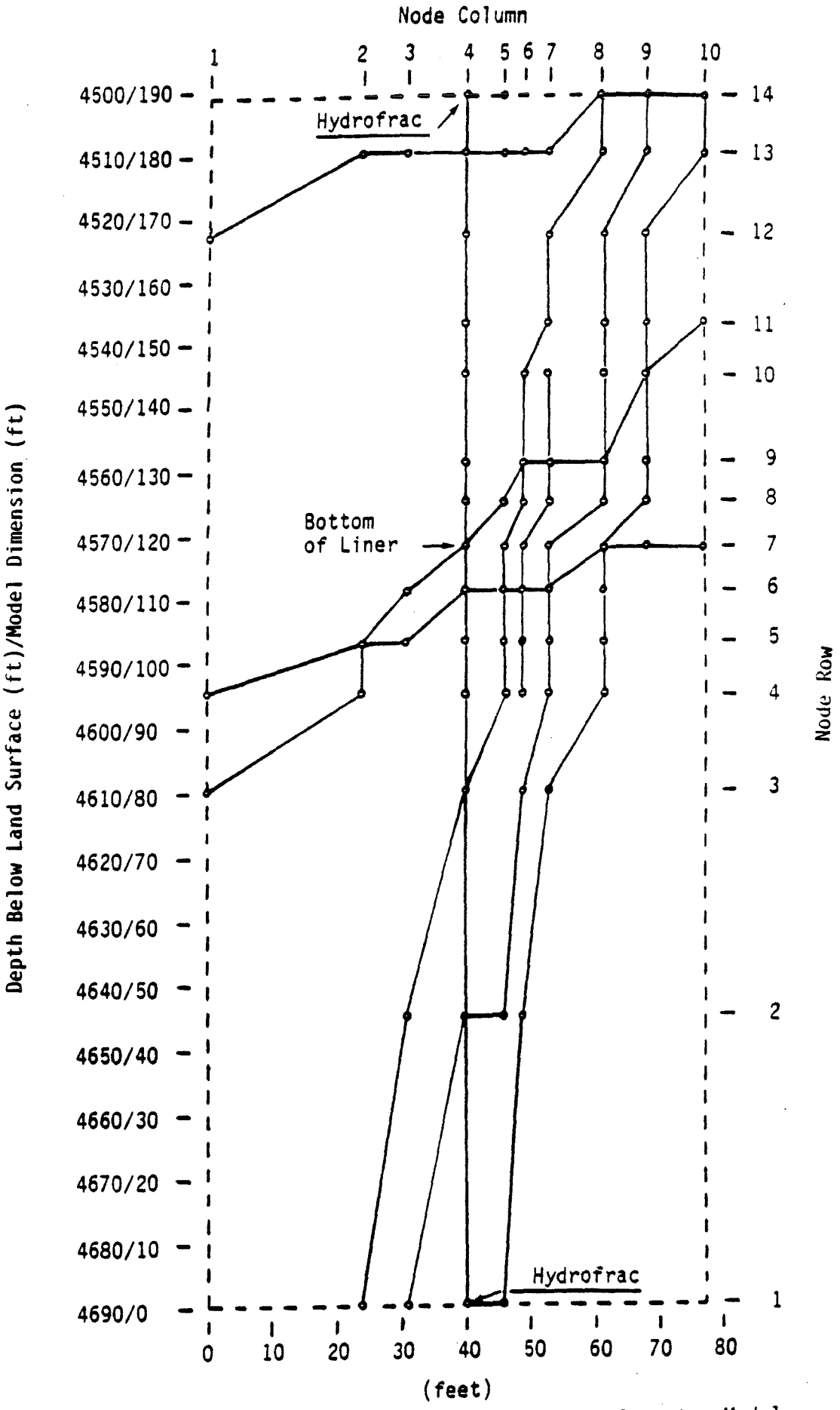

Figure 21. Raft River Well RRGP-5BF Near Wellbore Computer Model

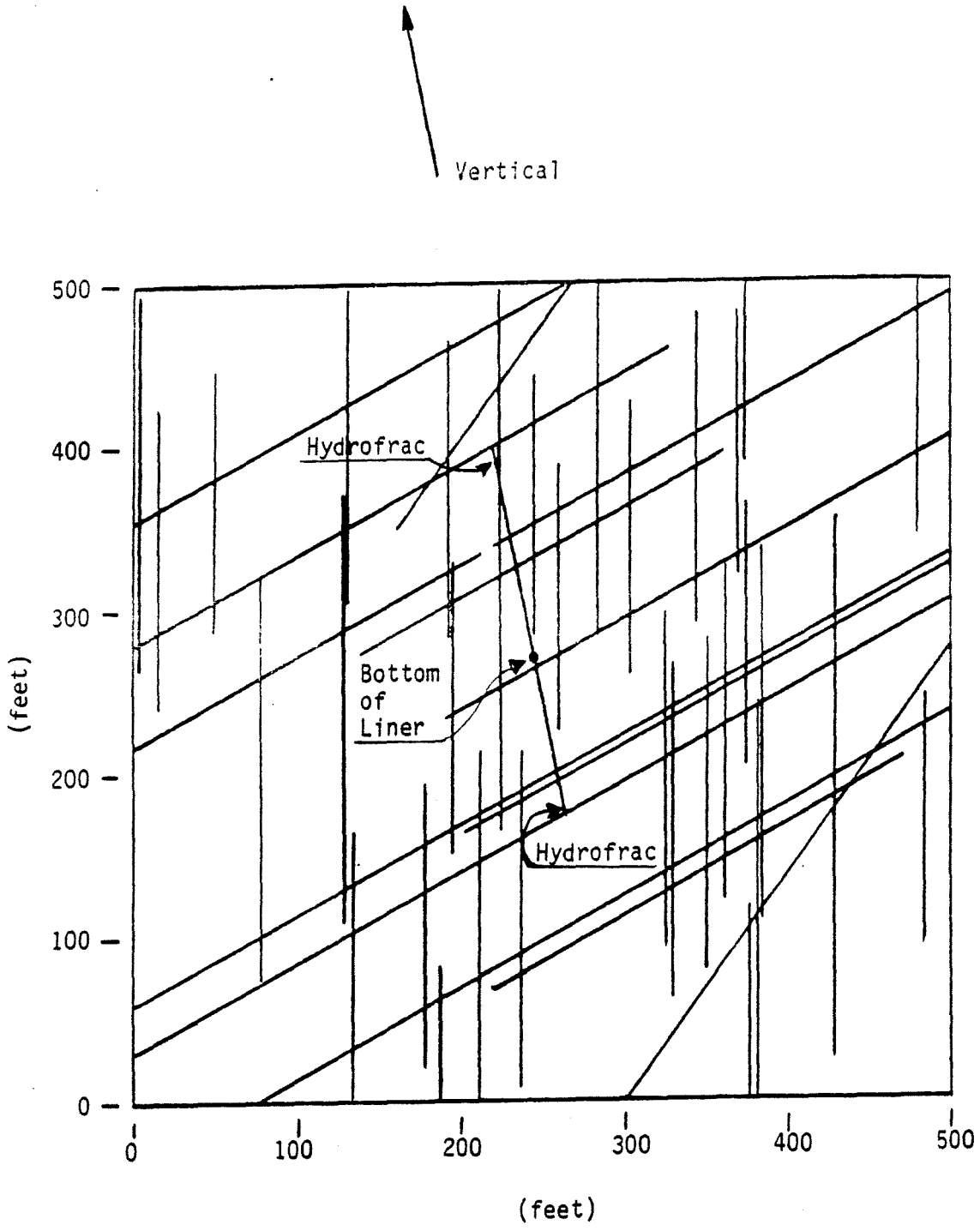

Figure 22. Raft River Well RRGP-5BF Large Reservoir Fracture System

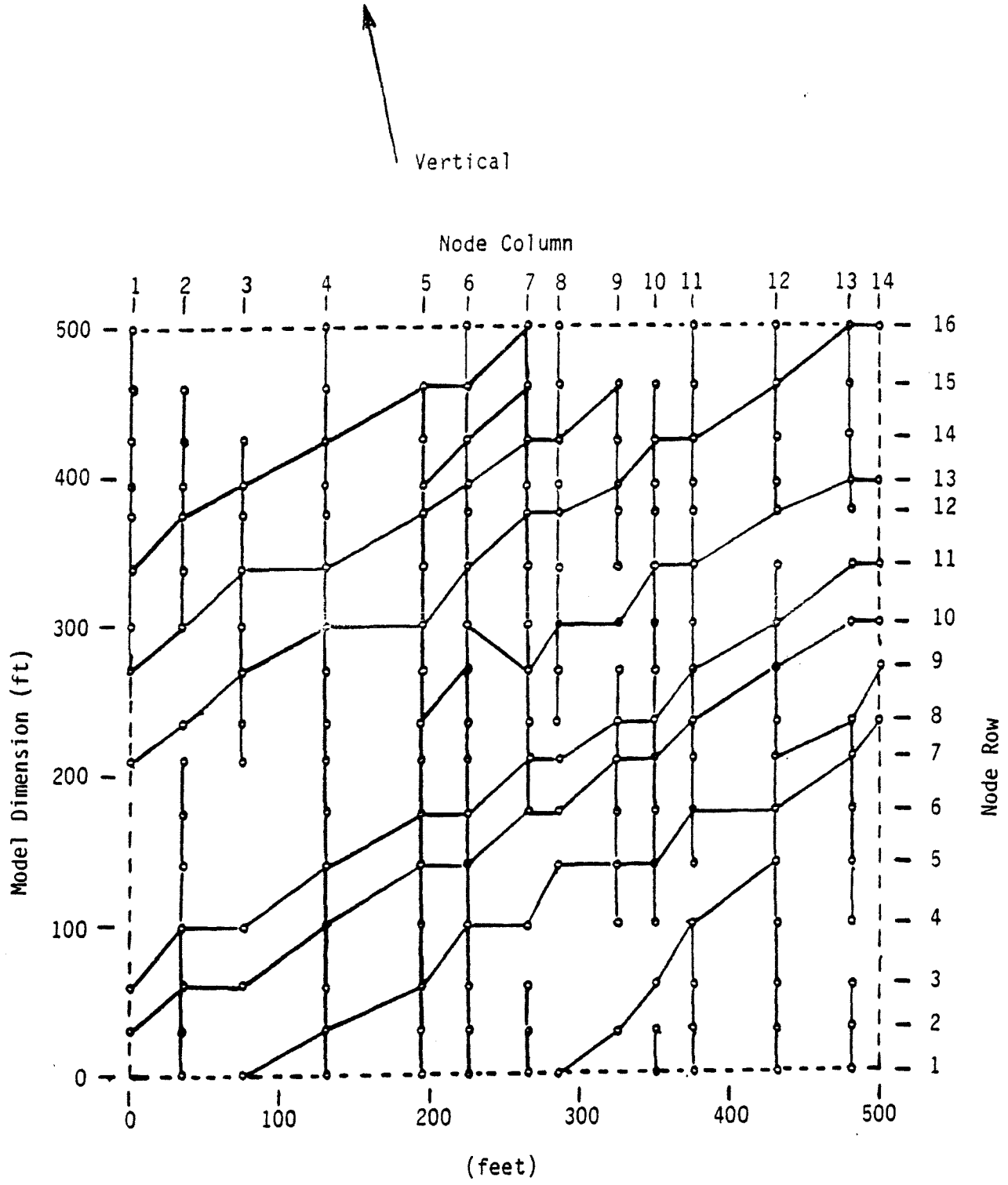

Figure 23. Raft River Well RRGP-5BF Large Reservoir Computer Model

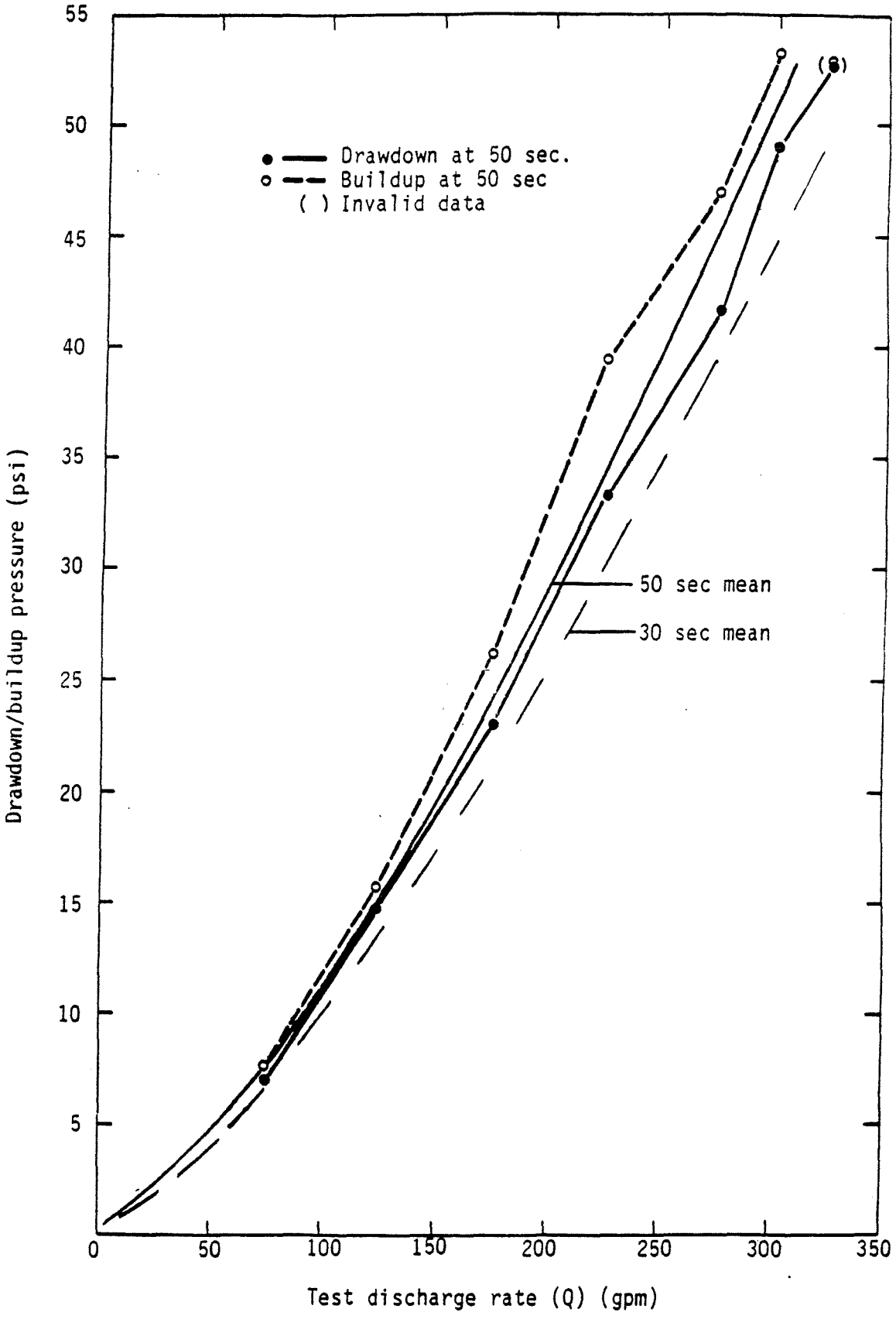

Figure 24. Calculated drawdown and buildup pressures at 30 and 50 seconds after initiating/terminating discharge for RRGP-5BF versus Q.

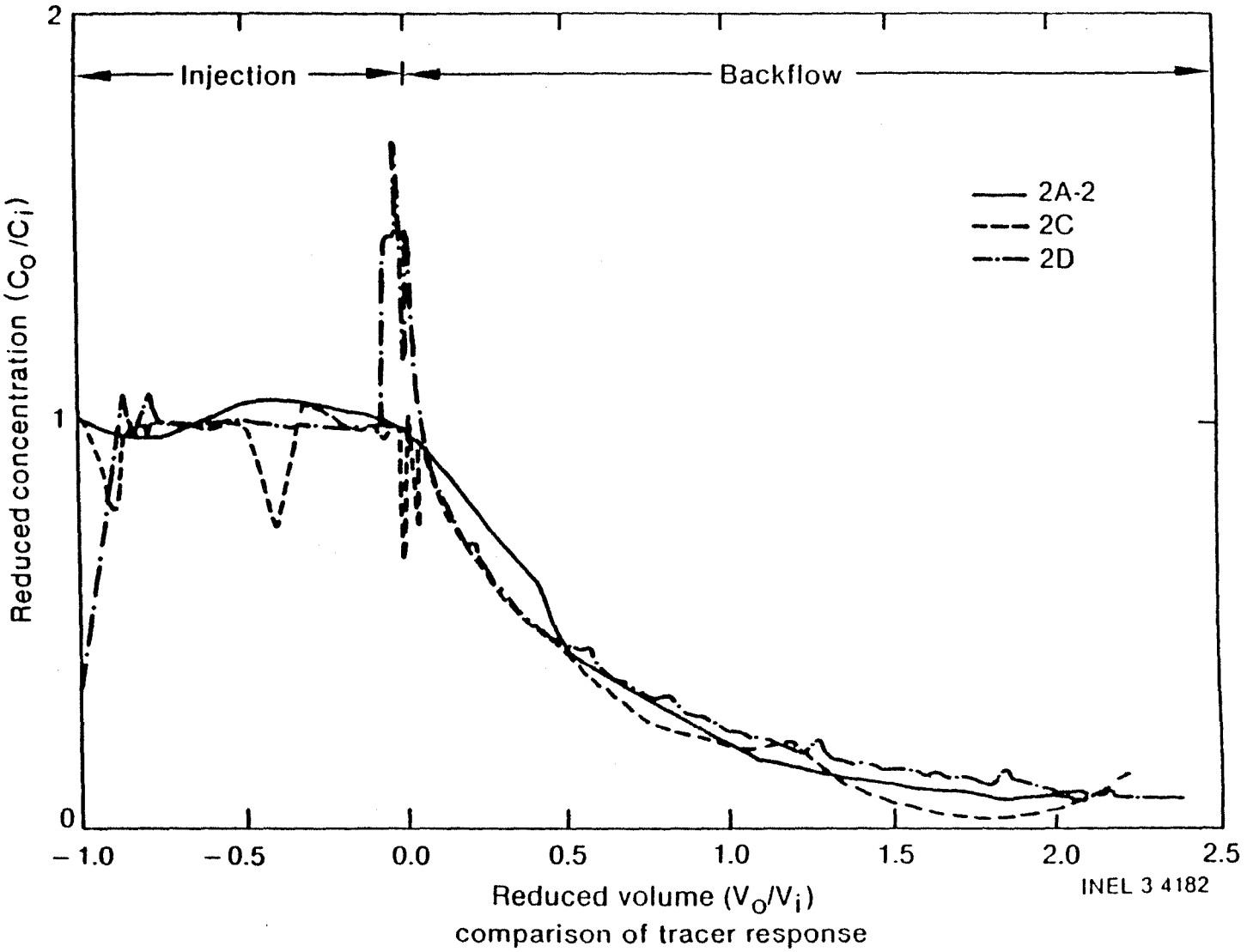

Figure 25. Comparison of normalized conservative tracer responses for Test 2 experiments.

$$\frac{C}{C_o} = \frac{1}{2}\left[\operatorname{erfc}\left(\frac{1-\tau}{2\sqrt{\tau/Pe}}\right) + \exp(Pe)\operatorname{erfc}\left(\frac{1+\tau}{2\sqrt{\tau/Pe}}\right)\right]$$

$\tau = V/V_i$

$Pe = VX/D_L$

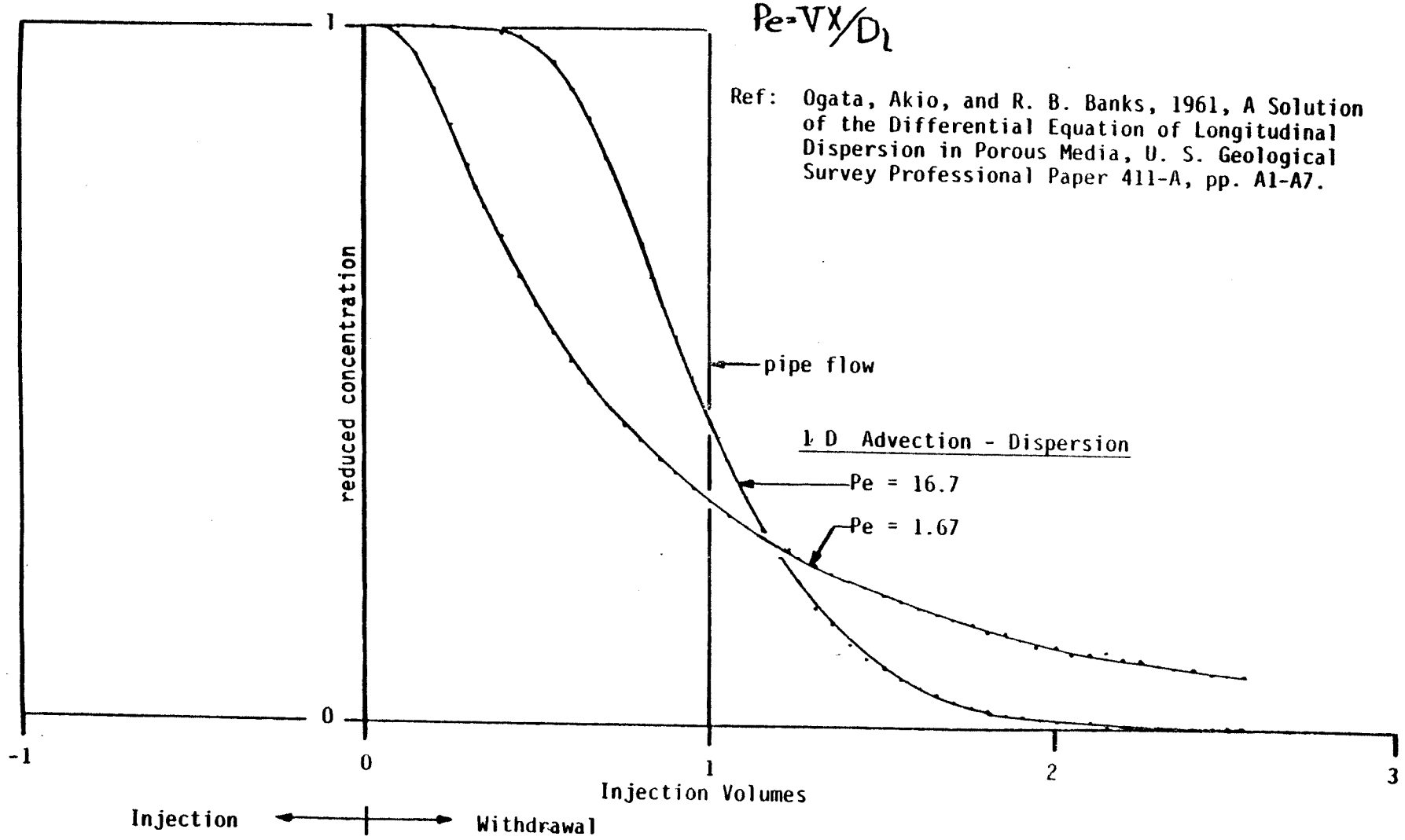

Ref: Ogata, Akio, and R. B. Banks, 1961, A Solution of the Differential Equation of Longitudinal Dispersion in Porous Media, U. S. Geological Survey Professional Paper 411-A, pp. A1-A7.

Figure 26. Reduced Concentration Plot Format

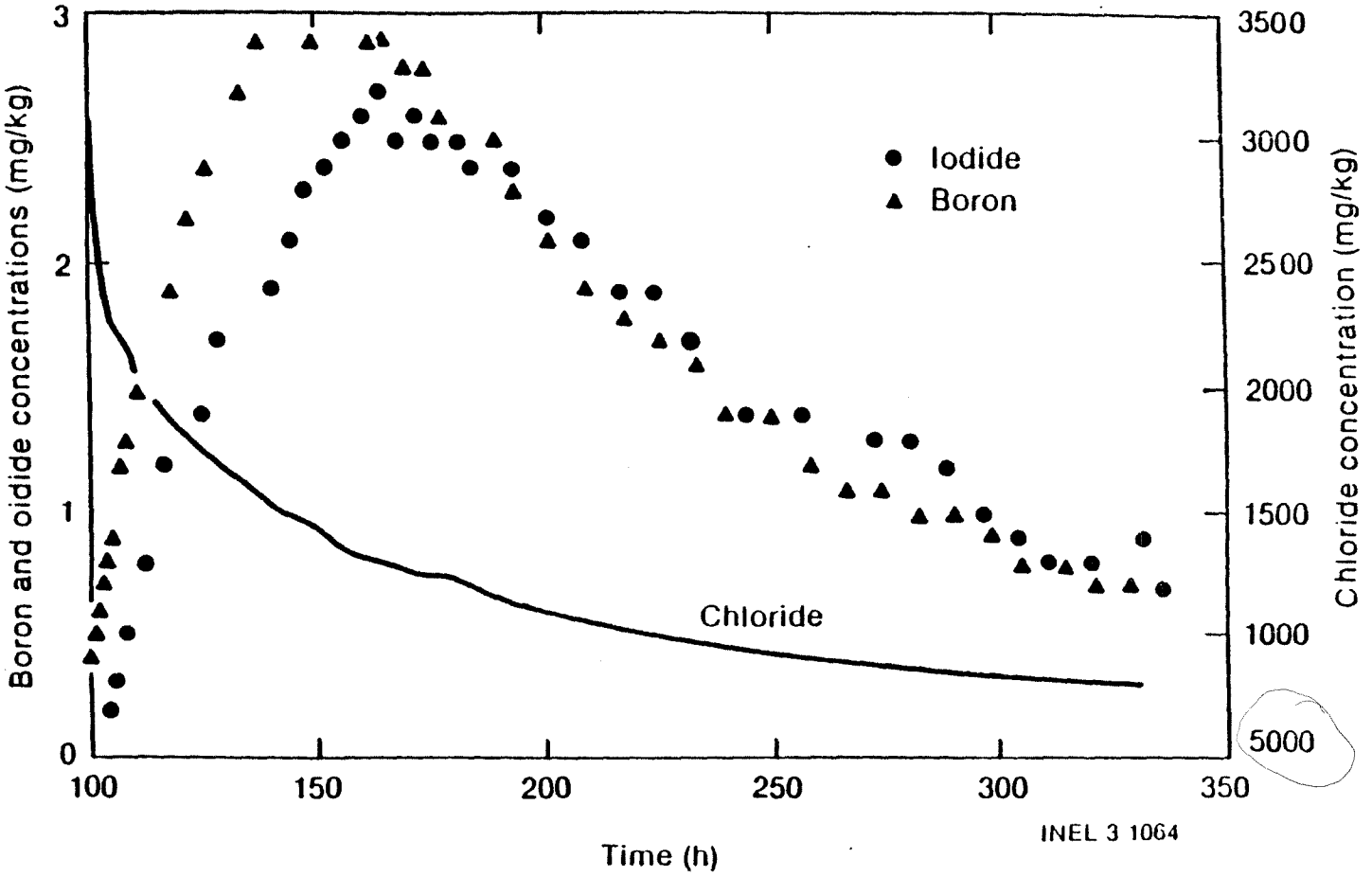

Figure 27. Test 2D tracer concentration as a function of time during backflow.

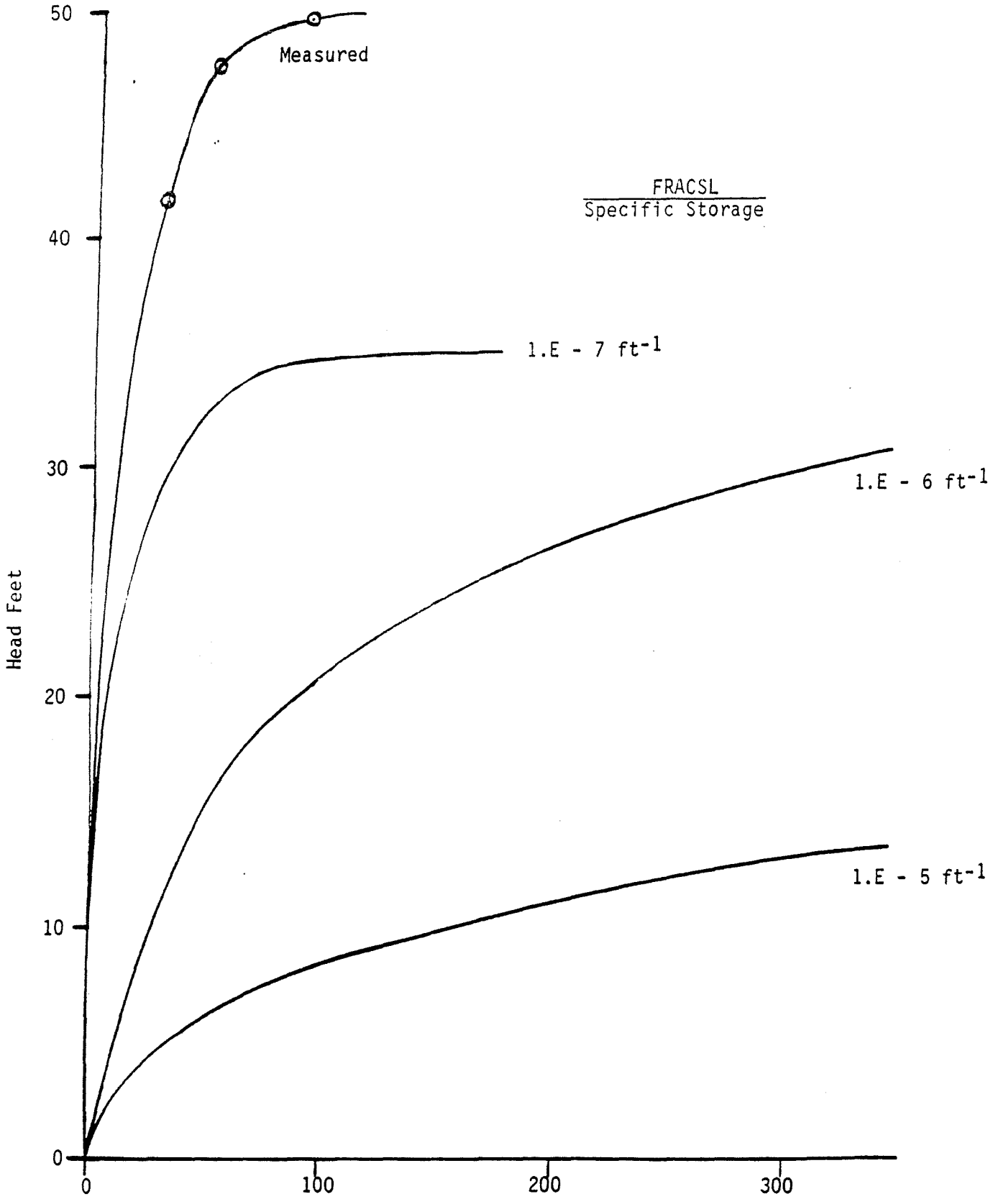

Figure 28. Raft River Pressure Rise at 150 gpm

TABLE 1 TRACE LENGTH STATISTICS FOR THE VENTILATION DRIFT, STRIPA MINE, SWEDEN

	Set 1		Set 2		Set 3		Set 4	
Basic Statistics (by Level of Censoring)								
Censoring	0	1	0	1	0	1	0	1
N	140	109	150	26	61	13	327	35
Total length (m)	181.6	183.3	158.1	36.4	82.4	28.8	435.4	59.1
Mean (m)	1.30	1.68	1.05	1.40	1.35	2.22	1.33	1.69
Standard Deviation (m)	0.68	0.86	0.45	0.88	0.77	1.71	0.73	1.53
Bias - Corrected Parameters (Truncation and Censoring)								
Exponential Model								
$\hat{\mu}_\epsilon$ (m)	2.16		0.83		1.51		1.03	
Log-normal model								
$\hat{\mu}_{LN}$	0.426		-0.047		0.058		0.165	
$\hat{\sigma}_{LN}$	0.846		0.554		0.912		0.558	
$\hat{\mu}$ (m)	2.19		1.11		1.61		1.38	
$\hat{\sigma}$ (m)	2.27		1.04		1.85		1.13	

NOTE: $\hat{\mu}_\epsilon$ is the computed mean assuming an exponential model; $\hat{\mu}_{LN}$ and $\hat{\sigma}_{LN}$ are the mean and the standard deviation computed for the natural logarithm of the data; μ and σ are the mean and the standard deviation of the original data computed from $\hat{\mu}_{LN}$ and $\hat{\sigma}_{LN}$. (Rouleau and Gale, 1984)

TABLE 2. GRAIN BOUNDARY APERTURE SPECTRUM, PINAWA, MANITOBA, CANADA

Aperture Range	Average[a] Aperture	Frequency	Porosity	Permeability
Log μm	μm		(x 10^{-4})	(x 10^{-18} m^2)
-2.0--1.8	0.01	0	0.0	0.0
-1.8--1.6	0.02	3	0.11	0.000
-1.6--1.4	0.03	1	0.01	0.000
-1.4--1.2	0.05	17	0.67	0.014
-1.2--1.0	0.08	10	1.78	0.103
-1.0-- .8	0.13	5	0.67	0.090
- .8-- .6	0.19	6	0.45	0.140
- .6-- .4	0.32	4	0.78	0.805
- .4-- .2	0.50	2	0.49	1.286
- .2- .0	0.79	2	0.68	3.653
.0- .2	1.25	0	0.0	0.0
.2- .4	1.99	0	0.0	0.0
.4 .6	3.16	0	0.0	0.0
.6 .8	5.01	1	1.58	0.0
TOTALS		51	7.22	6.09

(Chernis, 1981)

a. Authors numbers replaced as apparent typos.

TABLE 3.

RAFT RIVER WELL RRGP-5 COMPLETION

- LEG RRGP-5A FLOWED 1000 GPM AT 275°F
- DRILLING CONTINUED IN EFFORT TO LOCATE HIGHER TEMPERATURE FLUID
- DRILL STEM TWISTED OFF
- INITIAL LEG COMPLETED WITH 198 TONS OF SALT AND 1030 BAGS OF CEMENT
- DRILLED LEG RRGP-5B AT AN OFFSET
- CASED NEW LEG TO DEPTH BELOW MAJOR AQUIFER
- HIGH FLOWS WERE NOT REESTABLISHED
- HYDROFRACTURED LEG RRGP-5BF AND INJECTED 215 TONS OF SAND
- HYDROFRAC IS ABOUT 140 FT. LONG WITH MAXIMUM WIDTH OF 0.6 INCHES
- WELL NOW CAPABLE OF SHORT TERM ARTESIAN FLOW AT 300 GPM

TABLE 4. DISCONTINUITY DATA FOR RRGP-5B BETWEEN DEPTHS OF 1341.1 AND 1491.9 m (4400 and 4895 ft)

Discontinuity No.	Depth		Uncorrected		Corrected[a]		Terzaghi Weighting Factor
	ft	m	Strike	Dip	Strike	Dip	
1	4891	1490.7	N5°W	54°E	N10°E	50°W	2.0
2	4891	1490.7	N49°W	36°E	N39°W	36°E	1.2
3	4867	1483.4	N15°W	79°W	N-S	75°W	3.8
4	4866	1483.1	N-S	68°W	N15°E	62°W	2.1
5	4851	1478.5	N15°E	72°W	N31°E	70°W	2.9
6	4848	1477.6	N15°W	20°W	N8°W	16°W	1.0
7	4846	1477.0	N15°W	20°E	N8°E	24°E	1.1
8	4845	1476.7	N-S	20°W	N8°E	16°W	1.0
9	4842	1475.8	N15°W	20°W	N8°W	16°W	1.0
10	4842	1475.8	N-S	15°E	N21°W	20°E	1.1
51	4837	1474.2	N60°W	73°W	N46°W	72°W	3.2
11	4834	1473.3	N-S	39°W	N13°E	35°W	1.2
12	4832	1472.7	N15°E	33°W	N30°E	28°W	1.1
13	4829	1471.8	N15°E	33°E	N31°E	38°E	1.2
52	4791	1460.2	N30°E	75°W	N46°E	70°W	2.9
53	4791	1460.2	N15°W	79°W	N-S	75°W	3.8
14	4761	1451.1	N35°W	60°W	N22°W	57°W	1.8
15	4760	1450.8	N45°W	84°W	N30°W	82°W	7.1
16	4758	1450.2	N60°W	73°W	N46°W	72°W	3.2
17	4754	1448.9	N15°W	75°W	N-S	71°W	3.0
61	4737	1443.8	N14°W	--	--	--	--
62	4732	1442.2	N21°W	--	--	--	--
63	4730	1441.6	N45°W	48°W	--	--	--
64	4727	1440.7	N21°W	--	--	--	--
65	4695	1431.0	N9°E	--	N2°E	--	--
18	4692	1430.1	N10°E	78°W	N25°E	74°W	3.6
19	4691	1429.7	N-S	79°W	N15°E	74°W	3.6
20	4689	1429.1	N5°W	77°W	N20°E	73°W	3.4
21	4646	1416.0	N30°E	75°W	N46°E	70°W	2.9
66	4610	1405.1	N21°W	--	--	--	--
67	4593	1399.9	N14°W	--	--	--	--
22	4584	1397.1	N-S	21°W	N10°E	17°W	1.0
23	4581	1396.2	N-S	21°W	N10°E	21°W	1.1
68	4576	1394.7	N10°E	--	--	--	--
24	4572	1393.5	N30°W	55°E	N12°W	59°E	1.9

TABLE 4. (continued)

Discontinuity No.	Depth ft	Depth m	Uncorrected Strike	Uncorrected Dip	Corrected[a] Strike	Corrected[a] Dip	Terzaghi Weighting Factor
25	4569	1392.6	N22°W	59°W	N8°W	55°W	1.7
26	4548	1386.2	N30°W	80°E	N13°W	84°E	9.5
69	4537	1382.8	N30°W E	--	N48 E	--	--
27	4510	1374.6	N30°E	14°W	N37°E	9°W	1.0
28	4508	1374.0	N-S	2°W	N20°E	3°E	1.0
29	4497	1370.6	N60°W	80°W	N45°W	79°E	5.2
30a	4491	1368.8	N30°E	80°W	N46°E	76°W	4.1
31	4440	1353.2	N15°E	62°W	N31°E	57°W	1.8
54	4430	1350.2	N15°E	72°W	N31°E	70°W	2.9
70	4414	1345.3	--	--	--	--	--
71	4410	1344.1	--	--	--	--	--
72	4405	1342.6	N1°E	--	--	--	--

a. Corrected for magnetic declination and borehole orientation

TABLE 5. LOCATIONS OF ESTIMATED MAXIMUM DISCONTINUITY DENSITIES FOR FIVE ORIENTATON SETS

Set Number	Locations Estimated of Maximum Density		Discontinuities	
	Strike	Dip	Number Observed	Number Terzaghi Corrected
1	N46°E	74°NW	6	17.5
2	N-S	77°W	10	36.5
3	N46°W	78°SW	5	20.5
4	N5°W	18°W	12	12.7
5	N23°W	41°E	2	3.1
Total			35	90

TABLE 6. DISCONTINUITY SEPARATION AND APERTURE DATA

Discontinuity Sets and Subsets	Discontinuity Number	Depth		Separation in Borehole		Apparent Aperture	
		ft	m	ft	m	in.	cm
Set 1	5	4851	1478.5	60	18.3	1.0	2.54
	52	4791	1460.2	145	44.2	0.5	1.27
	21	4646	1416.0	155	47.2	1.0	2.54
	30	4491	1368.8	51	15.5	1.5	3.81
	31	4440	1353.2	10	3.0	1.0	2.54
	54	4430	1350.2	--	--	1.0	2.54
Set 2	1	4891	1490.7	24	7.3	1.0	2.54
1 Subset 2a	3	4867	1483.4	1	0.30	1.5	3.81
	4	4866	1483.1	75	22.9	1.0	2.54
	53	4791	1460.2	37	11.3	0.5	1.27
	17	4754	1448.9	62	18.9	1.0	2.54
Subset 2b	18	4692	1430.1	1	0.30	1.5	3.81
	19	4691	1429.7	2	0.61	2.0	5.08
	20	5689	1429.1	120	36.6	1.0	2.54
	25	4569	1392.6	21	6.4	1.5	3.81
	26	4548	1386.2	--	--	1.0	2.54
Set 3	51	4837	1474.2	76	23.2	1.5	3.81
Subset 3a	14	4761	1451.1	1	0.30	1.5	3.81
	15	4760	1450.8	2	0.61	1.0	2.54
	16	4758	1450.2	261	79.5	1.0	2.54
	29	4497	1370.6	--	--	0.5	1.27
Set 4							
Subset 4a	6	4848	1477.6	2	0.61	0.5	1.27
	7	4846	1477.0	1	0.30	0.5	1.27
	8	4845	1476.7	3	0.30	0.5	1.27
	9	4842	1476.8	0	0.0	0.5	1.27
	10	4842	1475.8	8	2.4	1.5	3.81
	11	4834	1473.3	2	0.61	0.5	1.27
	12	4832	1472.7	3	0.91	1.0	2.54
	13	4829	1471.8	245	74.7	0.5	1.27
Subset 4b	22	4584	1397.1	3	0.91	1.0	2.54
	23	4581	1395.2	71	21.6	1.0	2.54

TABLE 6. (continued)

Discontinuity Sets and Subsets	Discontinuity Number	Depth		Separation in Borehole		Apparent Aperture	
		ft	m	ft	m	in.	cm
Subset 4c	27	4510	1374.6	2	0.61	0.5	1.27
	28	4508	1374.0	--	--	0.5	1.27
Set 5	2	4891	1490.7	319	97.2	1.5	3.81
	24	4572	1393.5	--	--	1.0	2.54

TABLE 7. DISCONTINUITY BOREHOLE SEPARATION DATA IN RRGP-5B

Discontinuity Sets and Subsets	Number	Depth ft.	Depth m	Separation in Borehole ft	Separation in Borehole m
Set 1	5	4851	1478.5	60	18.3
	52	4791	1460.2	145	44.2
	21	4646	1416.0	155	47.2
	30	4491	1368.8	51	15.5
	31	4440	1353.2	10	3.0
	54	4430	1350.2	--	--
Set 2	1	4891	1490.7	24.5	17.5
Subset 2a[1]	3	4866.5	1483.2	75.5	23.0
	4	--	--	--	--
	53	4791	1460.2	37.0	11.3
	17	4754	1448.9	63.5	19.4
Subset 2b	18	--	--	--	--
	19	4690.5	1429.6	121.5	37.0
	20	--	--	--	--
	25	4569	1392.6	21	6.4
	26	4548	1386.2	--	--
Set 3	51	4837	1474.2	77.5	13.6
Subset 3a	14	--	--	--	--
	15	4789.5	1450.0	262.5	80.0
	16	--	--	--	--
	29	4497	1370.6	--	--
Set 4	6	--	--	--	--
Subset 4a	7	--	--	--	--
	8	--	--	--	--
	9	4838.5	1474.7	256.0	78.0
	10	--	--	--	--
	11	--	--	--	--
	12	--	--	--	--
	13	--	--	--	--

TABLE 7. (continued)

Discontinuity Sets and Subsets	Number	Depth ft.	Depth m	Separation in Borehole ft	Separation in Borehole m
Subset 4b	22	4582.5	1396.7	73.5	22.4
	23	--	--	--	--
Subset 4c	27	4509.0	1374.3	--	--
	28	--	--	--	--

a. Midpoint of upper and lower values for subsets.

TABLE 8. SEPARATION BETWEEN DISCONTINUITIES WITHIN SETS/SUBSETS IN RRGP-5B

Set/Subset	Mean		Standard Deviation		Number of Observations
	ft.	m	ft	m	
1	1.7675	1.2515	0.48132	-0.03469	5
2	1.6742	1.1582	0.29760	-0.21841	6
2b	0.1505	-0.3655	0.18761	-0.32839	2
3	2.1542	1.6382	0.33190	-0.18411	2
3a	0.1505	-0.3655	0.18761	-0.32839	2
4	2.1373	1.6213	0.33954	-0.17647	2
4a	0.3083	-0.2077	0.38236	-0.13365	7

Values are expressed in logarithums

TABLE 9. FRACSL MARKER PARTICLE CALCULATIONS

Injection - Particles released singly at intervals

- Injected at a node; fracture or matrix and position within that element selected randomly based on flow distribution
- Mass weighted according to local velocity

Longitudinal movement in fracture

- Mean velocity across fracture from flow calculation
- Local velocity varies with transverse position according to Poiseuille distribution

Approach to a fracture dead-end

- Velocity decreases linearly with the distance remaining to the end of the fracture

Transfer across a joint

- Exit fracture selected at random according to flow distribution
- Lateral position same as in inlet fracture

Transfer, in fracture, across sytem boundaries

- Particle leaves system

Transfer from fracture to matrix

- A Darcy velocity is computed at each edge of the fracture due to the head distribution at the nodes and in the diagonal fractures. An outwards Darcy velocity, common to the two edges of a fracture, is computed to account for local matrix storage. The sum of these terms yields a velocity at each edge of the fracture at the axial position of interest. A linear interpolation gives the lateral particle velocity at the appropriate lateral position. If the lateral and axial velocities indicate that the wall is intercepted

TABLE 9. (Cont'd)

before the fracture ends, the particle is transferred into the matrix at that point. This lateral velocity is therefore a result of matrix conductivity and storage and is an approximation of the myriad of small fractures successively stripping off the outer layers of water flowing down the main fracture.

- Diffusion also included

Movement in matrix

- Advective movement is due to head distribution at nodes and in diagonal fractures plus local storage velocity interpolated from a calculated value at a fracture to zero at the mass boundary of the node, divided by porosity
- Dispersive movement calculated using random walk technique from Prickett and Lonnquist and input values of longitudinal and transverse dispersivity
- Molecular diffusion calculated using random walk technique

Transfer, in matrix, across system boundaries

- Particle leaves system

Transfer from matrix to fracture

- Occurs if particle trajectory physically intercepts fractures
- May occur during injection

Recovery at well

- Particle "mass" accumulated upon return to well
- Differentiation of mass curve yields rate of tracer return. Division by rate of tracer injection yields return-to-injected concentration ratio

TABLE 10.

FRACTURE SYSTEM SYNTHESES

Author	Andersson	Rouleau	Long
Date	1984	1984	1982
Location	Generic	Stripa Ventilation Drift	Generic
Data Source	Generic	Borehole & Scanline	Baecher & Lanney Model
Number of Dimensions	2 (3 discussed)	2	2
Number of Orientation Sets	2	4	2
Planar fractures	X	X	X
Independent fractures	X		
Orientation distribution, each set	Normal (arbitrary)	Normal (mean, var?)	Normal [(30, 5), (60, 10)]
Mean Intensity - fracs/m	Arbitrary	1.03, 2.64, .91, 1.83	49, 100 totals
Fracture Location	Equally probable over scanline	Not given	Poisson distribution
Trace Length Corrections	Not applicable	Truncation (value?) Censoring	Not applicable
Trace Length Distribution	Unspecified	Fitted exponential Fitted & used lognormal	Lognormal Data given
Fracture Center	Equally likely $-\frac{1}{2}(c+1), \frac{1}{2}(c+1)$		
Aperture	Under investigation	Lognormal, sigma unstated 5 μm mean matched measured macro-permeability	Lognormal, data given, apparent apertures measured by Bianchi & Snow are lognormal
Aperture Change Over Length	--	--	--
Connected Fractures Only	X	X	X
Final Outputs	Area flow & flow variance vs. no. of cores (infinite length fractures)	Effective (flow) to total porosity; flow in connected fracs	Permeability ellipse, determines when porous and discrete approaches are valid
Comments		Flow in large structural discontinuities such as faults, shear zones and fracture zones should be specifically analyzed	

TABLE 11.

SYNTHESIZED FRACTURE SYSTEM

Set	Apparent Dip Deg	Mean Borehole Separation ft.	Mean Perpendicular Separation ft.	Mean Length ft.	Mean + 1 σ Length ft.	Length ft.	Lateral[1] Position ft.	Center[2] Location ft.
1	79°W	84.2	16.5	57.8	115.6	total of 778 fractures length 5 - 558 ft		
2	79°W	57.2	12.9	45.2	90.4			
3	79°W	170.	24.8	86.8	173.6			
4	18°W	111.7	106.2	371.7	743.4	1748	519	-426
						411	-59	232
						485	-238	-312
						763	102	-586
						2432	397	-668
						156	-190	228
						289	547	-233
						172	875	-84
						404	359	30
						258	94	174
						475	346	-4
						1040	-189	526
						1791	58	-42
						258	498	212
						827	216	384
5	43.4°W	319.	240.7	842.5	1685.	1132	522	588
						557	87	399
						1575	477	285
						1782	-112	-639
						1251	-127	558

(1) Intersection of infinite line containing fracture with scanline across center of model

(2) Distance along fracture line from scanline to center of fracture

TABLE 12.

RAFT RIVER TEST SUMMARY

Objective	Test Number	Flow Rate	Formation Injection Time	Quiescent Time	Formation Backflow Time	Artificial Tracers						
						NaI	NaBr	NaSCN	$MgCl_2$	Borax	Fluor	Rhod
Baseline	2A-1	150 gpm	wellbore only	0	wellbore only	C(1)	C		C	C		
Vary injection volume	2A-2		2 hr	0	12.4 hr	C						
	2C		46.5	0	110				C		S	
	2D		96.5	0	231	S(2)			S	S	S	S
Vary quiescent time	4A		.3 hr	27.5 hr	8.0 hr	C						
	4B		.3	2.2	10.5			C			C	
	4C		.3	12.0	8.5	C						
	4D		.3	50.0	48.5		C				C	
Breakthru(3) to RRGE-1 & Geophysics	5		376 hr.	80 hr	120 hr	S	S				S	S
Pulse tests	5	75-325 gpm										

(1) Continuous
(2) Slug; time varies
(3) Backflow RRGE-1 at 200 gpm

REFERENCES

1. Andersson, J., et al., "A Stochastic Model of a Fractured Rock Conditioned by Measured Information," Water Resources Research, 20, 1, January 1984, pp. 79-88.

2. Atomic Energy of Canada Limited, 1982a. The Geoscience Program--Proceedings of the Twelfth Information Meeting of the Nuclear Fuel Waste Management Program, Technical Record TR-200, I.

3. Atomic Energy of Canada Limited, 1982b. The Geoscience Program-Proceedings of the Twelfth Information Meeting of the Nuclear Fuel Waste Management Program, Technical Record TR-200, II.

4. Baecher, G. B., N. A. Lanney, 1978. "Trace Length Biases in Joint Surveys," Proceedings 19th U.S. Symposium Rock Mechanics, Nevada, 1, pp. 56-65.

5. Baecher, G. B., N. A. Lanney, and H. H. Einstein, 1977. "Statistical Description of Rock Properties and Sampling," Proceedings 18th U.S. Symposium on Rock Mechanics, Colorado, pp. 5C1-1 - 5C1-8.

6. Barton, C. M., 1977. "A Geotechnical Analysis of Rock Structure and Fabric in the CSA Mine, Cobor, New South Wales," CSIRO Aust. Div. Appl. Geomechanics Tech. Paper 24, p. 30.

7. Batzle, M. L., G. Simmons, R. W. Siegfreid, 1980. "Microcrack Closure in Rocks Under Stress: Direct Observation. M. of Geophys. Res., 85, B12, pp. 7072-7090.

8. Bianchi, L., and D. T. Snow, 1969. "Permeability of Crystalline Rock Interpreted from Measured Orientations and Apertures of Fractures," Annals of Arid Zones, 8, 2, 1969, pp. 231-245.

9. Bridges, M. C. 1975. "Presentation of Fracture Data for Rock Mechanics," 2nd Australian-New Zealand Conference on Geomechanics, Brisbane, pp. 144-148.

10. Call, R. D., J. P. Savely, and D. E. Nicholas, 1976. "Estimation of Joint Set Characteristics From Surface Mapping Data," Site Characterization (17th U.S. Symposium on Rock Mechanics held at Snowbird, Utah, August 25-27), Utah Engineering Experiment Station, Univ. of Utah, Salt Lake City, UT, pp. 2B21-2B29.

11. Cameron-Clark, I. S., S. Budavari, 1981. "Correlation of Rock Mass Classification Parameters Obtained from Borecore and In-Situ Observations." Engineering Geology, 17, pp. 19-53.

12. Chernis, P. J., 1981. Scanning Electron Microscope Study of the Microcrack Structure of a Granite Sample from Pinawa, Manitoba. Atomic Energy of Canada, Limited, Whiteshell Nuclear Research Establishment, Pinawa, Manitoba. Technical Record TR-173.

13. Covington, H. R., 1979. Deep Drilling Data, Raft River Geothermal Area, Idaho - Raft River Geothermal Production Well No. 5, U.S. Geol. Surv., Open-File Rept., pp. 79-382.

14. Cruden, D. M., 1977. "Describing the Size of Discontinuities," International Journal of Rock Mechanics and Mining Sciences and Geomechanics Abstracts, Vol. 14, No. 3, pp. 133-137.

15. Davis, C. E., H. Y. Tammemagi, 1982. A Case History of a Deep Borehole in the Reynard Lake Pluton, Saskatchewan-Manitoba border. Applied Geoscience Branch, Whiteshell Nuclear Research Establishment, Pinawa, Manitoba, Technical Record TR-184.

16. Davison, C. L., W. S. Keys, and F. L. Paillet, 1982. Use of Borehole-Geophysical Logs and Hydrologic Tests to Characterize Crystalline Rock for Nuclear-Waste Storage, Whiteshell Nuclear Research Establishment, Manitoba, and Chalk River Nuclear Laboratory, Ontario, Canada: U.S. Department of Energy, issued by the U.S. Department of Commerce.

17. Domenico, P. A., 1972. Concepts and Models in Groundwater Hydrology, McGraw-Hill, New York.

18. Dugal, J. J. B., and D. Stone, 1981. Hydrogeological Testing and Fracture Analysis of the Eye-Dashwa Granitic Pluton at Atiukokan, Ontario, Atomic Energy of Canada Limited, Whiteshell Nuclear Research Establishment, Pinawa, Manitoba, AECL-7363, pp. 16.

19. Earth Technology Corporation, 1983. Evaluation of geologic and geophysical techniques for surface-to-subsurface projections of geologic characteristics in crystalline rock. Topical report.

20. Evans, D. D., 1983. "Unsaturated Flow and Transport Through Fractured Rock-Related to High-Level Waste Repositories," First Report-Phase 1, NUREG/CR-3206.

21. Fradkin, L. J., M. J. Sorey, A. McNabb, 1981. On Identification and Validation of Some Geothermal Models. Water Resour. Res. 17(4), pp. 929-936.

22. Gale, J. E., 1982. Assessing the Permeability Characteristics of Fractured Rock, Geol. Soc. of America, Special Paper 189, pp. 163-181.

23. Gale, J. E., P. A. Brown, K. G. Raven, J. J. B. Dugal, and J. S. O. Lau, 1981. Progress Report on Geological Studies Related to Underground Disposal of Nuclear Fuel Wastes, Technical Record TR-13, Atomic Energy of Canada, Limited.

24. Grant, M. A., P. F. Bixley, I. G. Donaldson, 1982. Geothermal Reservoir Engineering, Academic Press, New York.

25. Gustafsson, E., Carl-Erik Klockars, 1981. Studies on Groundwater Transport in Fractured Crystalline Rock Under Controlled Conditions Using Nonradioactive Tracers. Geol. Surv. of Sweden, Uppsala, SKBF/KBS-TR-81-07.

26. Hsieh, P. A., S. P. Neuman, E. S. Simpson, 1983. "Pressure Testing of Fractured Rocks--A Methodology Employing Three-Dimensional Cross-Hole Tests, NUREG/CP-3212.

27. Huang, C., D. D. Evans, and S. P. Neuman, 1984. Numerical Experiments on Artifically Generated, 3-Dimensional Fracture Networks, AGU Abstract, (and personal communication).

28. Hudson, J. A., and S. D. Priest 1979. "Discontinuities and Rock Mass Geometry," International Journal of Rock Mechanics and Mining Sciences and Geomechanics Abstracts, 16, 6, pp. 339-462.

29. International Society for Rock Mechanical Commission on Standardization of Laboratory and Field Tests, 1978. "Suggested Methods for the Quantitative Description of Discontinuities in Rock Masses," International Journal of Rock Mechanics and Mining Sciences and Geomechanics Abstracts, 15, pp. 319-368.

30. Iwai, K., 1976. "Fundamental Studies of Fluid Flow Through a Single Fracture," Ph.D. Dissertation, Univ. of California, Berkeley.

31. Kamineni, D. C., P. A. Brown, and D. Stone, 1979: Fracture Filling Material in the Atikokan Area, Northwestern Ontario, Scientific and Technical Notes in Current Research Part A; Geol. Surv. Can., Paper 80-1A, pp. 369-374.

32. Knapp, R. B., 1975. "An Analysis of the Porosities of Fractured Crystalline Rocks," (M.S. Thesis). U. of Arizona, pp. 90.

33. Leech, R. E. J., and A. J. Cooper, 1982. Preliminary Terrain Assessment of Three Potential Research Areas in Northern Ontario, Technical Record TR-27, Atomic Energy of Canada, Limited.

34. Long, J. C. S., et al., Porous Media Equivalents for Networks of Discontinuous Fractures, Water Resources Research, 18(3): 645-658, 1982.

35. Mahtab, M. A., D. D. Bolstad, J. R. Alldredge, and R. J. Shanley, 1972. "Analysis of Fracture Orientations for Input to Structural Models of Discontinuous Rock," USBM Report 7669.

36. Maini, T., 1970. In situ Hydraulic Parameters in Jointed Rock--Their Measurement and Interpretation, PhD. Thesis, Imperial College of Science and Technology, London.

37. McMahon, B. K., 1974. "Design of Rock Slopes Against Sliding on Pre-existing Fractures," Proc. 3rd Congr. Int. Soc. Rock Mechanics, 2, pp. 803-808.

38. Neuzil, C. E. and J. V. Tracy, 1981. Flow Through Fractures, Water Resources Research, 17, 1, pp. 191-199.

39. Norton, D. L., 1981. Rock Deformation in Hydrothermal Systems: The Nature of Fractures in Plutons and Their Host Rocks, Technical Progress Report for Department of Energy, Division of Engineering, Mathematical and Geosciences, Office of Basic Energy Sciences, DOE/DE-AC02-81 ER 10842.

40. Olkiewicz, A., J. E. Gale, R. Thorpe, and B. Paulsson, 1979. Geology and Fracture system Stripa. LBL-8907, SAC-21, UC-70. Berkeley, California.

41. Office of Nuclear Waste Isolation, 1981. A Heated Flatjack Test Series to Measure the Thermomechanical and Transport Properties of In Situ Rock Masses ("Heated Block Tests"), ONWI-260, Columbus, OH.

42. Paillet, F. L., and W. S. Keys, 1984, in press Application of Borehole Geophysics in Characterizing the Hydrology of Fractured Rocks. U.S. Geological Survey. Proc. NWWA, San Antonio.

43. Priest, S. D., and J. A. Hudson, 1976. "Discontinuity Spacings in Rock," International Journal of Rock Mechanics and Mining Science and Geomechanics Abstracts, 13, pp. 135-148.

44. Priest, S. D., and J. A. Hudson, 1981. "Estimation of Discontinuity Spacing and Trace Length Using Scanline Surveys," International Journal of Rock Mechanics and Mining Science and Geomechanics, 18, pp. 183-197.

45. Republic Geothermal Inc. Maurer Engineering Inc. Vetter Research, 1980. Raft River well Stimulations Experiments, Sect. by W. S. Keys "The Application of the Acoustic Televiewer to the Characterization of Hydraulic Fracture in Geothermal Wells," Dept. of Energy DOE/AL/10563-T7, August 1980.

46. Roberston, A. M., 1970. "The Interpretation of Geologic Factors for Use in Slope Theory," Proceedings of the Symposium on the Theoretical Background to the Planning of Open Pit Mines with Special Reference to Slope Stability, (Johannesburg, Republic of South Africia), A. A. Balkema, Capetown, S. A., pp. 55-71.

47. Rouleau, A., J. E. Gale, 1970. "Statistical Characterization and Numerical Simulation of a Fracture System for Hydrogeothermal Purposes," International Groundwater Symposium on Groundwater Resources Utilization and Contaminant Hydrogeology, Montreal, Quebec, Canada, 1, pp. 188-196.

48. Seeburger, D. A., and Zoback, M. D., 1982. "The Distribution of Natural Fractures and Joints at Depth in Crystalline Rock," Journal of Geophysical Research, 87, B7, pp. 5,517-5,534.

49. Segall, P., and D. D. Pollard, 1983. "Joint Formation in Granitic Rock of the Sierra Nevada," Geological Society of American Bulletin, 94, pp. 563-575.

50. Sharp, J. C., and Y. N. T. Maini, 1972. "Fundamental Considerations on the hydraulic characteristics of joints in rocks," Proceedings Symposium on Percolation Through Fissured Rock, International Society for Rock Mechanics, Stuggart, No. T1-F.

51. Sledz, J. J., D. D. Huff, 1981. Computer Model for Determining Fracture Porosity and Permeability in the Conasauga Group, Oak Ridge National Laboratory, Tennessee, ORNL/TM-7695.

52. Soonawala, N. M., P. A. Brown, G. Larocque, 1982. Geology, Geophysics and Rock Properties Research for the Canadian Nuclear Waste Management Program Technical Record TR-152, Atomic Energy of Canada Limited.

53. Stetten, O., et al., 1975, "Recent Developments in the Interpretation of Data From Joint Surveys in Rock Masses," 6th Reg. Conf. for Africa on Soil Mech. and Found., 9/75, II, pp. 17-26.

54. Terzaghi, R. D., 1965. "Sources of Error in Joint Surveys," Geotechnique, 15, pp. 287-304.

55. Thorpe, R. K., 1980. "An Example of Rock Fracture Characterization for Modeling Purposes," Proceedings, Workshop on Numerical Modeling of Thermohydrological Flow in Fractured Rock Masses, LBL-11566, ONWI-24-Lawrence Berkeley Laboratory, Berkeley, California, pp. 37-42.

56. Thorpe, R., D. J. Watkins, W. E. Ralph, R. Hsu, 1980. Strength and Permeability Tests on Ultra-Larbe Stripa Granite Core, LBL-11203, SAC-31, UC-70, Berkeley, California.

57. Thorpe, R. K., 1983. Strength and Permeability of an Ultra-Large Specimen of Granitic Rock, LBL-16268.

58. Tsang, Y. W. and P. A. Witherspoon, 1981. Hydromechanical behavior of Deformable Rock Fracture Subject to Normal Stress, Journal of Geophysical Research, 86:810.

59. Tsang, Y. W., 1983. "Dependence of Fracture Mechanical and Fluid Flow Properties on Fracture Roughness and Sample Size," Journal of Geophysical Research, 88:B3.

60. Tsang, Y. W., 1983. Two Dimensional Fluid Flow Through a Rough Fracture, AGU H31C-03.

61. Ubbes, B., In Press., Summary Status Report, Test Facilities Task.

62. Wallis, P. F., and M. S. King., 1980. "Technical Note--Discontinuity Spacings in a Crystalline Rock," International Journal Rock Mechanics and Mineral Sciences and Geomechanics Abstracts, 17, pp. 63-66.

63. Wilson, C. R. and Witherspoon, P. A., 1976. "Flow Interference Effects at Fracture Intersections," Water Resources Research, 12, pp. 102-104.

64. Witherspoon, P. A., C. H. Amick, J. E. Gale, K. Iwai, 1979b. "Observations of a Potential Size Effect in Experimental Determination of the Hydraulic Properties of Fractures Water Resources Research, 15, 5.

65. Witherspoon, P. A., J. S. Y. Wang, K. Iwai, J. E. Gale, 1979a. "Validity of Cubic Law for Fluid Flow in a Deformable Rock Fracture." Technical Information Report 23, LBL-9557, SAC-23, UC-70, Lawrence Berkeley Laboratory, Berkeley, California.

66. Zanbak, C., 1977. "Statistical Interpretation of Discontinuity Contour Diagrams," International Journal of Rock Mechanics and Mining Sciences and Geomechanics Abstracts, 14, 3, pp. 111-120.